

UNCLASSIFIED

AD NUMBER	
AD369585	
CLASSIFICATION CHANGES	
TO:	unclassified
FROM:	confidential
LIMITATION CHANGES	
TO:	Approved for public release, distribution unlimited
FROM:	Distribution authorized to U.S. Gov't. agencies and their contractors; Administrative/Operational Use; FEB 1966. Other requests shall be referred to Air Force Rocket Propulsion Labs., AFSC, Edwards AFB, CA.
AUTHORITY	
AFRPL ltr, 7 May 1973; AFRPL ltr, 7 May 1973	

THIS PAGE IS UNCLASSIFIED

369585

CONFIDENTIAL

AFRPL-TR-65-257
(Unclassified Title)

HYPERGOLIC IGNITION AT REDUCED PRESSURES

A. D. Corbett
B. E. Dawson
T. F. Seamans
M. M. Vanpee

February, 1966

Air Force Rocket Propulsion Laboratory
Research and Technology Division
Air Force Systems Command
Edwards, California

DOWNGRADED AT 3-YEAR INTERVALS
DECLASSIFIED AFTER 12 YEARS
DOD DIRECTIVE 5200. 10

THIokol CHEMICAL CORPORATION
Reaction Motors Division
Denville, New Jersey

CONFIDENTIAL

AFRPL-TR-65-257

Although this document carries the classification of CONFIDENTIAL, only those pages marked CONFIDENTIAL contain classified information. All other material may be treated as UNCLASSIFIED.

SPECIAL NOTICES

This document contains information affecting the national defense of the United States within the meaning of the Espionage Laws (Title 18, U.S.C., sections 793 and 794). Transmission or revelation in any manner to any unauthorized person is prohibited by law.

Qualified users may obtain copies of this report from the Defense Documentation Center.

When U.S. Government drawings, specifications, or other data are used for any purpose other than a definitely related Government procurement operation, the Government thereby incurs no responsibility nor any obligation whatsoever, and the fact that the Government may have formulated, furnished, or in any way supplied the said drawings, specifications, or other data, is not to be regarded by implication or otherwise, or in any manner licensing the holder or any other person or corporation, or conveying any rights or permission to manufacture, use, or sell any patented invention that may in any way be related thereto.

Do not return this copy. When not needed, destroy in accordance with pertinent security regulations.

CONFIDENTIAL

AFRPL-TC 35-257

(Unclassified Title)

HYPERGCLIC IGNITION AT REDUCED PRESSURES

A. D. Corbett
B. E. Dawson
T. F. Seamans
M. M. Vanpee

February, 1966

Air Force Rocket Propulsion Laboratory
Research and Technology Division
Air Force Systems Command
Edwards, California

Air Force Systems Command Project 3058, Task 3058560

Contract No. AF04(611)-9946

Submitted by: *A. D. Corbett*
A. D. Corbett, Supervisor
Rocket Technology Section
Research Engineering Dept.

Approved by: *S. J. Tunkel*
S. J. Tunkel, Manager
Research Engineering Dept.

D. J. Mann
D. J. Mann
Director of Research

DOWNGRADED AT 3-YEAR INTERVALS
DECLASSIFIED AFTER 12 YEARS
DDI DIRECTIVE 5200.10

THIokol CHEMICAL CORPORATION
Reaction Motors Division
Denville, New Jersey

CONFIDENTIAL

CONFIDENTIAL

AFRPL-TR-65-257

(Unclassified Foreword)

FOREWORD

This is the Final Report - Part II covering the work performed by Thiokol Chemical Corporation, Reaction Motors Division, Denville, New Jersey under an extension to Air Force Contract AFG4(611)-9946. The internal report number is Report RMD 5801-F Part II. The work was administered under the direction of Mr. K. Rimer, Rocket Propulsion Laboratory, Edwards Air Force Base under the following project and task numbers:

Project No. 3058, Task No. 3058560
Air Force Program Structure No. 750 G

The Research effort reported herein was conducted during the period 15 April 1965 to 15 October 1965 on RMD Project 5801. The work previously performed under Part I of the program covering the period 1 May 1964 to 28 February 1965 is reported in AFRPL-TR-65-105.

Principal investigators of the effort described herein are Messrs. B. E. Dawson, T. F. Seamans, and Dr. M. Vanpee. Other contributors to the program were Messrs. E. Hornstein, R. Storms, and W. Sutton. Dr. Vito Agosta, Professor of Aerospace Engineering, Polytechnic Institute of Brooklyn, served as a consultant for the establishment of the vaporization model and contributed significantly to its development. The Project Leader was Mr. A. D. Corbett and the Program Manager was Mr. S. J. Tunkel.

This report contains no classified information extracted from other classified documents.

This technical report has been reviewed and is approved.

Mary M. Racovich
AF Contracting Officer
Directorate of Procurement

CONFIDENTIAL

(Unclassified Abstract)

ABSTRACT

By theoretical and experimental means, a mathematical model of hypergolic ignition in reaction control systems has been developed based on physical kinetics of droplet evaporation and chemical kinetics of ignition reactions. Reasonable agreement between theoretical and experimental ignition delays are obtained. The dominant reactions of N_2O_4 with the hydrazine fuels at reduced pressures are found to be thermal, gas phase reactions which are bimolecular and have low activation energies and pre-exponential factors. A pre-ignition reaction product was found which is a clear, yellow, viscous liquid with a very low vapor pressure. The "adduct" has the characteristics of a monopropellant and contains considerable energy. Its relation to pressure spiking during engine start transients is as yet undetermined. Of six additives tested, only furfuryl alcohol had a significant beneficial effect on the ignition characteristics of N_2O_4 /MMH.

The influence of thrust chamber design parameters on the ignition delay and pressure transients of Compound A with N_2H_4 , UDMH and MHF-5 and also gaseous F_2/H_2 was investigated. The results are reported. Very short ignition delays and smooth pressure transients were obtained with the F_2/H_2 combination regardless of chamber configuration. Also, short rise times to 90% steady-state chamber pressure resulted. However, a dependency on chamber L^* only exists.

Previous pages were blank, therefore not filmed.

AFRPL-TR-65-257

TABLE OF CONTENTS

	<u>Page No.</u>
I. INTRODUCTION	1
II. SUMMARY	4
III. TASK I - MEASUREMENT OF REACTION RATE	12
A. Development of Mathematical Model of Hypergolic Ignition	12
B. Thrust Chamber Pressurization Due to Propellant Vaporization	14
1. Theory	15
2. Results and Discussion	23
C. Reaction Kinetics	52
1. Theory of Thermal Explosions	53
2. Experimental Apparatus	58
3. Experimental Results	62
4. Discussion of Reaction Kinetics Results	77
5. Summary and Conclusions	89
D. Statement and Results of Mathematical Model of Hypergolic Ignition	90
1. Hypergolic Ignition Model	90
2. Results of Hypergolic Ignition Model and Comparison with Experiment	100
3. Pressure Spiking Considerations	103
IV. TASK II - EVALUATION OF ADDITIVES TO REDUCE ACTIVATION ENERGY	107
A. Fuel Additiv	107
B. Oxidizer Additives	108

TABLE OF CONTENTS (cont')

	<u>Page No.</u>
V. TASK III - THRUST CHAMBER DESIGN PARAMETER STUDY	110
A. Test Apparatus and Instrumentation	110
1. Experimental Facilities	110
2. Experimental Hardware	115
3. Instrumentation	122
B. Experimental Thrust Chamber Program	126
C. Experimental Results - Compound A/ Hydrazine-based Fuel Tests	127
1. Schlieren Characterization of Propellants	128
2. Thrust Chamber Tests - Compound A/N ₂ H ₄	132
3. Thrust Chamber Tests - Compound A/UDMH, Compound A/MHF-5	150
D. Experimental Results - Fluorine/Hydrogen Tests	159
VI. CONCLUSIONS	169
VII. RECOMMENDATIONS	173
REFERENCES	175

LIST OF FIGURES

<u>Figure No.</u>	<u>Title</u>	<u>Page No.</u>
1	General Concept of Ignition Delay Time Model	13
2	Calculated Chamber Pressure and Temperature History for CCl ₄	24
3	Fully Developed CCl ₄ Flow at Various Pressures	33
4	Fully Developed UDMH Flow at Various Pressures	36
5	Fully Developed UDMH Flow at Various Liquid Injection Velocities, Ambient Pressure = 140 mm Hg	38
6	Fully Developed UDMH Flow at Various Liquid Injection Velocities, Ambient Pressure = 1 mm Hg	39
7	Fully Developed N ₂ O ₄ Flow at Various Ambient Pressures - Liquid Injection Velocity = 110 ft/sec	40
8	Fully Developed N ₂ O ₄ Flow at Various Ambient Pressures - Liquid Injection Velocity = 11 ft/sec	41
9	Effect of Drop Size on Rate of Pressurization - CCl ₄	42
10	Effect of Accommodation Coefficient on Pressurization Rate - CCl ₄	44
11	Experimental and Theoretical Chamber Pressure Histories - CCl ₄	47
12	Schematic of Low Pressure Ignition Apparatus for Tasks I and II	59
13	Concentric Tube Reactor	61

LIST OF FIGURES

<u>Figure No.</u>	<u>Title</u>	<u>Page No.</u>
14	Axial Temperature Profiles, NO_2/MMH	70
15	Axial Temperature Profile in Flow Tube, NO_2/MMH	72
16	Axial Temperature Profile in Flow Tube, NO_2/UDMH	73
17	Infrared Absorption Spectrum of the Adduct Formed by NO_2/MMH Vapors at Sub-Ignition Pressure	76
18	Infrared Absorption Spectrum of the Adduct Formed by NO_2/UDMH Vapors at Sub-Ignition Pressure	76
19	Effect of Reactor Radius on Minimum Ignition Pressures	79
20	Effect of Equivalence Ratio on Minimum Ignition Pressure, NO_2/MMH	81
21	Effect of Equivalence Ratio on Minimum Ignition Pressure, NO_2/UDMH	82
22	Effect of Temperature on Minimum Ignition Pressures	83
23	Average Ignition Delay vs. Pressure for Unconfined Laminar Stream Tests (from Ref. 1)	92
24	Influence of Propellant Volatilities on Ignition Delay at One Atmosphere	94
25	Theoretical Ignition Delay - Pressure Curves for $\text{H}_2\text{O}_2/\text{UDMH}$	101
26	Comparison of Experimental and Theoretical Ignition Delays for Estimated Preignition Vapor Phase Composition and Temperature	102

LIST OF FIGURES

<u>Figure No.</u>	<u>Title</u>	<u>Page No.</u>
27	Theoretical Ignition Delay - Pressure Curves for N_2O_4 /MMH	104
28	Vacuum Pumps and Adsorption Column for Fluorinated Oxidizer Propellant Combinations	111
29	Schematic of Compound A/Hydrazine Propellant Systems	112
30	Schematic of Fluorine/Hydrogen Propellant Systems	113
31	Transparent Thrust Chamber Assembly	116
32	Exploded View of Transparent Thrust Chamber	116
33	Set of Nozzles for Same Design Chamber Pressure (75 psi) and Different Contraction Ratios (1.5 - 8)	117
34	Set of Nozzles for Same Contraction Ratio (3.5/1) and Different Design Chamber Pressures (20-200 psi)	117
35	Injectors for Compound A/ N_2H_4 - Type Propellants	120
36	Concentric Injector and Valves for F_2/H_2 Tests	121
37	Schematic of Thrust Chamber Test Setup	123
38	Schlieren Light Source and Oscilloscope Setup	125
39	Schlieren Camera Setup	125
40	Schlieren of Hydrazine Injection	130
41	Schlieren of Compound A Injection	130

LIST OF FIGURES

<u>Figure No.</u>	<u>Title</u>	<u>Page No.</u>
42	Effect of Chamber Configuration on Ignition Time - Compound A/Hydrazine	143
43	Effect of Chamber Configuration on Rise Time - Compound A/Hydrazine	144
44	Oscillograph Records of Compound A/N ₂ H ₄	146
45	Effect of Mixture Ratio on Ignition Time - Compound A/N ₂ H ₄ and Compound A/MHP-5	147
46	Effect of Propellant Leads on Ignition Time - Compound A/Hydrazine	149
47	Ignition Times - Compound A/Hydrazine Fuels	157
48	Time to 90% Pc - Compound A/Hydrazine Fuels	158
49	Effect of Valve Current on Ignition Time - F ₂ /H ₂ Chamber Tests	165
50	Effect of Chamber L* on Rise Time - F ₂ /H ₂ Chamber Tests	167
51	Oscillograph Records of F ₂ /H ₂ Tests	168

LIST OF TABLES

<u>Table No.</u>	<u>Title</u>	<u>Page No.</u>
I	Example of Condensation on a Cold Drop (CCl_4 #R)	25
II	Chamber Pressure and Temperature at $t = 10.0$ msec	29
III	Drop Sizes Used in the Computer Program to Represent the Injected Propellant Spray	43
IV	Summary of Calculated and Experimental Steady State Values for Thrust Chamber Pressurization by CCl_4	51
V	Minimum Ignition Pressures of NO_2 /MMH Vapors in Flow Reactors	64
VI	Minimum Ignition Pressures of NO_2 /UDMH Vapors in Flow Reactors	66
VII	Minimum Ignition Pressures of NO_2 /50-50 Vapors in Flow Reactors	68
VIII	Minimum Ignition Pressures of NO_2 / N_2H_4 Vapors in Flow Reactors	68
IX	Minimum Ignition Pressure in Free Jets	69
X	Analysis of Reaction Products of Pre-Ignition Reaction, NO_2 /MMH	75
XI	Effect of Reactor L/D on Minimum Ignition Pressures, NO_2 /MMH and NO_2 /UDMH	78
XII	Comparison of Reactivities of Various Hypergolic Combinations at 298°K	85
XIII	Summary of Experimentally Determined Kinetic Factors for Gas-Phase Ignition of NO_2 /Hydrazine Fuels	91
XIV	Effect of Fuel Additives on Ignition of NO_2 /MMH Mixtures	108

<u>Table No.</u>	<u>Title</u>	<u>Page No.</u>
XV	Task III Thrust Chamber Configurations	119
XVI	Schlieren Data-Unconfined Tests of Compound A, N_2H_4 , UDMH and MHF-5 Using Doublet Injector	129
XVII	Thrust Chamber Tests-Compound A/ N_2H_4 , Doublet Injector, O/F = 2.0	133
XVIII	Thrust Chamber Tests-Compound A/ N_2H_4 , Doublet Injector, Variable Mixture Ratio	136
XIX	Thrust Chamber Tests-Compound A/ N_2H_4 , Doublet Injector, Variable Leads	138
XX	Thrust Chamber Tests - Compound A/ N_2H_4 , Triplet Injector, O/F = 2.0	151
XXI	Thrust Chamber Tests - Compound A/UDMH, Doublet Injector, O/F = 2.0	151
XXII	Thrust Chamber Tests - Compound A/MHF-5, Doublet Injector	152
XXIII	Thrust Chamber Tests - Fluorine/Hydrogen, Concentric Injector, O/F = 8	160

NOMENCLATURE

A	Frequency factor, cc/mole-sec for bimolecular reaction
A*	Nozzle throat area, ft ²
A _c	Surface area of the thrust chamber, ft ² (Task I)
A _c /A _t	Contraction ratio (Task III)
A _d	Surface area of drop or drops, ft ²
c _a , c _b	Concentrations of reactants A and B, mole/cc
c _p	Specific heat, cal/gr-°C
c _{pl}	Heat capacity of the liquid, Btu/lb _m -°R
c _{pg}	Heat capacity of the vapor, Btu/lb _m -°R
C _p	Molar heat capacity, Btu/lb-mole-°R
C _i	Constant (pg. 18)
E, E _a	Energy of activation, cal/mole
$f = \frac{A}{Z}$	Steric factor
g _c	Dimensional factor, 32.2 lb _m -ft/lb _f -sec ²
h	Heat transfer coefficient, Btu/sec-ft ² -°R
G _{evap}	Mass of gas evaporated, lb _m
G _{ij}	Mass evaporated from one drop in the <u>i</u> th class of the <u>j</u> th ensemble during one time interval, lb _m
G _N	Total mass evaporated from all drops in the system during one time interval, lb _m
G _w	Mass of vapor condensed on chamber walls during one time interval, lb _m
i	Drop class, 1 ≤ i ≤ 3
j	Drop ensemble, 1 ≤ j ≤ N

k	Isentropic exponent
k	Boltzmann constant = 1.38×10^{-16} erg/ $^{\circ}$ K molecule
k_g	Thermal conductivity of vapor, Btu/sec-ft ² -($^{\circ}$ R/ft)
L^*	Characteristic length, in.
m	Partial order of reaction with respect to fuel
m_c	Mass of vapor in the thrust chamber, lb _m
M_f, M_{ox}	Molecular mass of fuel and oxidizer, gm/molecule
m_{ex}	Vapor mass efflux through the nozzle during one time interval, lb _m
M	Molecular weight, lb _m /lb-mole
n	Partial order of reaction with respect to oxidizer
N	Total order of reaction = $m + n$
N	Number of time intervals, time/ Δt_n
N_i	Number of drops in <u>ith</u> drop class
N_j	Number of drops in <u>jth</u> ensemble
N_{fp}	Time interval in which the temperature of a drop reaches the freezing point
N_o	Avagadro number = 6.024×10^{23} molecules/mole
N_x	Time interval in which the drop becomes frozen solid
P	Gas pressure, atm.
P_c	Chamber pressure, psia
P_g	Total pressure = $P_f + P_{ox}$
$P_g(T_g)$	Gas pressure in the thrust chamber, lb/ft ²
$P_v(T_d)$	Propellant vapor pressure corresponding to the drop temperature, lb/ft ²
$P_v(T_w)$	Propellant vapor pressure corresponding to the wall temperature, lb/ft ²
Pr	Prandtl Number, dimensionless

Q	Heat of reaction, cal/mole
Q_H	Total energy reaching the surface of all drops in the system in one time interval, Btu
qv_{ij}	Energy reaching the surface of the <u>i</u> th size drop of the <u>j</u> th ensemble in one time interval, Btu
r	Reactor radius, cm
r_f, r_{ox}	Molecular radii, cm
r_{ij}	Radius of drops in the <u>i</u> th class of the <u>j</u> th ensemble, ft
R	Universal gas constant, 1546 lb _f -ft/lb-mole °R = 1.987 cal/gr-mole °K
Re	Reynolds Number, dimensionless
t	Time, sec
T	Temperature, °K
T_d	Drop temperature, °R
T_g	Gas temperature, °R
T_o	Wall temperature, °K
U	Mean molecular velocity, cm/sec
U	Linear velocity, cm/sec
V	Volume
V_c	Chamber volume, ft ³
V_{drop}	Drop velocity (assumed constant and equal to liquid injection velocity), ft/sec
\dot{w}	Weight flow of propellant, lb/sec
W	Reaction velocity, mole/cc-sec
W_i	Injected mass of drops of <u>i</u> th class in one time, lb _m
W_j	Mass of liquid injected during one time interval, $W_j = \dot{w} \Delta t$, lb _m

X	Quality
X	Mole fraction
X_{ij}	Fraction of a drop that is frozen, $0 < X_{ij} < 1$
z	Constant (pg. 26)
Z	Collision frequency factor, cc/mole-sec
z	$z/(e^z - 1)$
α	Accommodation coefficient
α	Constant (pg. 98)
β	Ratio of partial pressures of oxidizer to fuel
δ	Critical factor for thermal explosion
δ	Non-dimensional constant (pg. 56)
Δt_M	Length of time interval, sec
g	Constant (pg. 98)
μ_g	Absolute gas viscosity, lb _m /ft-sec
ν	Kinematic viscosity, cm ² /sec
λ	Thermal conductivity, cal/sec-cm-°C
λ	Constant (pg. 98)
λ_o	Heat of vaporization, Btu/lb _m
λ_f	Heat of fusion, Btu/lb _m
λ_s	Heat of sublimation, Btu/lb _m
ρ	Density, gr/cc
ρ_l	Density of the liquid, lb _m /ft ³

APRPL-TR-85-257

σ	Geometric standard deviation
τ_{ign}	Calculated ignition delay time, sec
Φ	Constant (pg. 27)
ϕ	Equivalence ratio, $O/F_{stoich}/O/F_{actual}$
∇^2	Laplacien operator, cm^{-2}

IINTRODUCTION

Thiokol Chemical Corporation, Reaction Motors Division has been investigating the ignition characteristics at reduced pressures of a number of hypergols under Air Force Contract AF04(611)-9946. The Final Report - Part I covering the work performed during the initial ten-month program is contained in Report AFRPL-TR-65-105, dated July 1965. These studies included an investigation of hypergolic ignition characteristics in (a) an unconfined impinging stream apparatus and (b) 50-lb. thrust chambers at simulated altitudes for the purpose of determining attitude control engine design criteria to minimize ignition delays and to eliminate pressure spikes in the start transients.

In brief, the results of the initial ten-month program indicate that:

- 1) ignition delays of N_2O_4 /hydrazine-type fuels are strongly pressure dependent,
 - 2) impinging stream injector parameters - impingement angle and length, injection velocity, type of manifolding - have a negligible effect on ignition delays,
 - 3) for constant propellant flowrate, design chamber pressure, i.e. nozzle throat area, significantly affects ignition delay and rise time to steady state chamber pressure,
 - 4) for constant propellant flowrate and constant design chamber pressure (throat area) thrust chamber geometry - L^* and contraction ratio - has little effect on ignition delay and rise time,
 - 5) pressure spikes during start transients are of random occurrence and magnitude and are not affected appreciably by any of the engine design parameters studied (design chamber pressure, L^* , and contraction ratio),
- and 6) a more fundamental approach is needed to understand and then correct the ignition delay-pressure spiking

problem that exists with the H_2O_4 /hydrazine-type fuels combinations.

The reader is referred to the final report of the ten-month program (Ref. 1) for a detailed discussion of the above findings.

A six-months continuation program was undertaken subsequently for the purpose of constructing a fundamental mathematical model for the ignition of hypergolic propellants at reduced pressures in reaction control systems. The program was performed in three major tasks. The specific objectives of each task are described as follows:

Task I - Measurement of Reaction Rates

The objectives of this task are to measure the activation energy and order of reaction for the following propellant combinations and construct a mathematical model for ignition of these propellants at reduced pressures in altitude control engines.



Task II - Evaluation of Additives to Reduce Activation Energy

The objective of this task is to evaluate propellant additives for the reduction of activation energy requirements for $\text{N}_2\text{O}_4/\text{MMH}$ and $\text{N}_2\text{O}_4/50-50$ using the experimental apparatus developed for Task I above.

Task III - Thrust Chamber Design Parameter Study

The objective of this task is to evaluate the influence of thrust chamber design parameters on the ignition delays and start transients of Compound A/ N_3H_4 and gaseous F_2/H_2 . The specific parameters of interest are characteristic length, chamber pressure, contraction ratio, and propellant lead/lag. Tests were made at a thrust level of 70-lbs. over the range of parameters shown below:

AFRPL-TR-65-257

Characteristic length (L*)	5-50 in.
Chamber pressure	20-200 psia
Contraction ratio	1.5-8
Oxidizer lead	+2 to -2 msec
Thrust (nominal)	50 lbs.
Ambient pressure	< 0.2 psia

The results of the experimental and theoretical program are discussed in the following sections.

IISUMMARY

The objective of the program reported herein was to construct a fundamental mathematical model for the ignition of hypergolic propellants at reduced pressures. This program is a six-month extension of an initial ten-month program to establish attitude control engine design criteria which would minimize ignition delay and eliminate pressure spikes in the start transients with hypergolic propellants at reduced pressures. The results of the initial ten-month program are described in detail in Report AFRPL-TR-65-105. Results of the initial program indicated that the conventional injector and thrust chamber configuration parameters had little influence on ignition and that a more fundamental investigation of the pre-ignition reaction rates and chemical kinetics was required in order to develop a suitable model for ignition of hypergolic propellants at reduced pressures.

This report is the final report of the six-month extension program which was performed in three separate tasks in order to accomplish the objectives. The purpose of Task I was to measure the pre-ignition reaction rates for $\text{N}_2\text{O}_4/\text{UDMH}$, $\text{N}_2\text{O}_4/\text{MMH}$, $\text{N}_2\text{O}_4/\text{N}_2\text{H}_4$ and F_2/H_2 and incorporate these data into a fundamental mathematical model for the ignition of hypergolic propellants at reduced pressures in reaction control systems. The purpose of Task II was to evaluate selected additives for the reduction of activation energy requirements for $\text{N}_2\text{O}_4/\text{MMH}$ and $\text{N}_2\text{O}_4/50-50$. The purpose of Task III was to evaluate the influence of thrust chamber design parameters on the ignition delay and pressure transients of Compound A/ N_2H_4 and gaseous F_2/H_2 . The results of these tasks are summarized below.

The development of a mathematical model of hypergolic ignition in reaction control systems followed two paths: The determination of the pressure history in an engine due to propellant vaporization and the determination of the chemical kinetics of ignition reactions of the various hypergolic combinations. It is necessary to consider both parts of the problem since reaction times for the hydrazine-type fuels with nitrogen tetroxide at the pressure encountered during engine start-up are comparable to the times required for the pressure in the thrust chamber to reach levels at which ignition can occur. The hypergolic ignition model results from a merger of the two paths.

A computer program was developed for predicting chamber pressurization due to propellant vaporization taking into account the rate of propellant injection, the kinetics of propellant droplet evaporation and vapor condensation, vapor-drop heat transfer, drop residence time, thrust chamber geometry, and propellant vapor efflux through the nozzle. A three drop-size spray model is used to represent mathematically the actual propellant spray which forms in the thrust chamber. The principal quantities, whose time-dependent values are calculated, are:

- (a) mass evaporation from each spray drop
- (b) radius of each drop
- (c) temperature of each drop
- (d) fraction of each drop that is frozen
- (e) vapor mass flow through the nozzle
- (f) vapor mass condensing on the chamber walls
- (g) gas temperature

and (h) gas pressure.

Using carbon tetrachloride as the working fluid since its properties are well known, it was found that the vapor-drop system is non-adiabatic. Despite the short times involved in chamber pressurization due to propellant vaporization, heat addition to the vapor-drop system occurs when drops strike the chamber walls. Using a crude model to account for the heat addition to the vapor-drop system, agreement to within 10% was obtained between calculated and experimental curves of chamber pressurization.

The computer program permitted an evaluation to be made of two potential problem areas: the effect on chamber pressurization rates of accommodation coefficient and of spray drop sizes. Using two propellants individually (one, CCl_4 ; the other, hypothetical propellant differing only in its accommodation coefficient) it was found that the effect of accommodation coefficient on chamber pressurization is much less than linear. The direct effect of a low accommodation coefficient-decreased evaporation rate at a given drop

temperature - is offset to a great extent by the resulting slower cooling rate of the drop. Thus, the vapor pressure of the drop is higher than it otherwise would be and this results in relatively more vaporization. A 50% decrease in accommodation coefficient caused only a 10 to 15% decrease in chamber pressure at any time. Since accommodation coefficients are in general unknown and are extremely difficult to measure, it is fortunate their effect on chamber pressurization rates is small.

The effect of spray drop sizes on chamber pressurization was also found to be small. Two computer runs were made differing only in the initial values of radii of the three drop-size sprays. The mass-median drop in one case was 75 microns, in the other 50 microns. The resulting pressure curves differed by only 7%. Although the smaller drops mean a greater total drop surface area since there are more drops for a given flowrate, these smaller drops evaporatively cool at a faster rate which leads to less vaporization due to lower vapor pressure. Due to the uncertainties in actual drop sizes of propellant sprays, this finding, too, is fortunate.

Very short exposure photographs were taken of propellant streams injected into a low pressure environment. The photographs show not only that ambient pressure strongly affects the characteristics of the sprays but also that the breakup of the injected stream into drops occurs quickly at low ambient pressures, up to 1 1/2 msec depending on the propellant and injection velocity.

For the more volatile propellants such as N_2O_4 and Compound A, the calculated and experimental chamber pressurization curves indicate that a significant amount of time is required for the flow, once initiated, to build-up to the full flowrate. Appreciable "flashing" of the propellant within the injector volume slows the arrival of all-liquid flow at the injector face. The reduced mass flow causes a slower pressure rise in the chamber than would otherwise be the case. The computer program at present does not include expressions to account for transient flow upon propellant valve opening. With less volatile propellants, i.e., the hydrazine-type fuels, full flowrates are reached very quickly if fast-acting valves are used and injector volume is kept to a minimum.

The kinetic factors required in the hypergolic ignition model to describe the ignition reactions were obtained through an application of the theory of thermal explosions to experimentally measure ignition pressure limits. The overall order

of reaction was determined from the variation of ignition pressure limits with reactor size, the activation energy from the effect of initial temperature, and the partial reaction orders from composition effects. The pre-exponential factor was calculated in two ways: (1) from the theory of thermal explosions (steady-state approximation equation) using the experimentally determined values of overall reaction order, partial reaction orders and activation energy; and (2) from a measured axial temperature profile in the premixed reactant stream at low pressures. The good agreement between the two determinations of the pre-exponential factor substantiates the applicability of the theory of thermal explosions to the ignition reactions of the hydrazine-type fuels with nitrogen tetroxide. The reactions are found to be bimolecular with low activation energies (7.2 kcal/mole for UDMH and 5.2 kcal/mole for MMH) and low pre-exponential factors.

During the experimental determinations of the kinetic factors, the formation of a pre-ignition reaction product was observed for each of the four hydrazine-fuel combinations tested. The adducts formed at pressures below minimum ignition pressures, condensed on the walls of the reactor, and collected as a liquid at the base of the experimental apparatus. In general, the adducts are clear, yellow, viscous liquids with very low vapor pressures and are stable at room temperatures and pressures. Preliminary analyses of the adduct formed from premixed MMH and NO_2 vapors at 5 mm Hg indicate the adduct is a simple additive product which has the characteristics of a monopropellant and which contains considerable energy. Its role in relation to pressure spiking during start transients in reaction control systems is as yet undetermined.

The theoretically derived ignition delay equation (bimolecular ignition reaction) is:

$$\tau_{\text{ign}} = \frac{R^2 T_g^3}{P_g A Q E_a} \left(1 + \frac{1}{\beta} \right) \left(C_{pf} + \beta C_{pox} \right) e^{E_a / RT_g}$$

where $P_g = P_f + P_{ox}$ and $\beta = \frac{P_{ox}}{P_f}$ (see nomenclature for meaning of symbols)

The reactant partial pressures, p_f and P_{ox} , are obtained individually by the analysis for chamber pressurization due to propellant vaporization.

The above equation assumes that gas phase ignition reactions are the dominant reactions. The justification for the assumption comes from both experimental and theoretical results. Experimental ignition delays of several hydrazine fuels with N_2O_4 in an impinging stream apparatus indicate that fuel vaporization is the controlling process at one atmosphere ambient pressure, thereby implying gas phase reactions. Also, theoretical calculations show that the collision frequency between unlike gas molecules is 4000 times greater than the frequency of gas-drop surface collisions at comparable conditions.

Pressure-ignition delay curves, calculated by the above equation for N_2O_4 /UDMH and N_2O_4 /MMH, show the effects of both temperature and vapor phase composition on ignition delays. Ignition delays are decreased by about 22% per $10^\circ C$ increase in temperature. The optimum vapor phase composition for ignition is found to be the equimolecular mixture which, for UDMH, MMH and 50-50 with N_2O_4 , is markedly more fuel rich than typical mixture ratios for optimum performance.

A comparison between experimental and calculated engine ignition delays, estimating for the calculations the vapor composition and temperature, gives good agreement. To predict the vapor composition and temperature, it is necessary to include in the pressurization analysis expressions for the transient N_2O_4 flow upon propellant valve opening and for the heat transfer between thrust chamber walls and the evaporating vapor - drop system. Then, further verification of the model is needed.

Five fuel additives and one oxidizer additive were tested for their effects on ignition characteristics of N_2O_4 /MMH. The additives were tested in the apparatus used for the chemical kinetics study. This apparatus is well suited to additive screening. The five fuel additives tested were:

- furfuryl alcohol
- phenyl ether
- methyl butynol
- ethyl ether
- and benzene.

The additive concentrations were 10% by weight of the fuel.

Of the five additives only furfuryl alcohol caused a significant effect. The minimum ignition pressure of NO_2 /MMH was reduced by 25% with the additive.

CONFIDENTIAL

AFRPL-TR-65-257

(C) Compound R, $\text{FC}(\text{NF}_2)_3$, was tested as an oxidizer additive in amounts of 2 and 3% of NO_2 . This additive not only raised minimum ignition pressures but also made them very erratic. It was necessary to thoroughly wash the apparatus in order to obtain again the usual, very repeatable ignition pressure limits.

(U) Under Task III, thrust chamber tests were made with a variety of thrust chamber configurations (L^* , contraction ratio, design chamber pressure) to determine the effect of chamber design parameters on the ignition characteristics of Compound A with several hydrazine-type fuels and gaseous F_2/H_2 . The design chamber pressures selected for the tests were 20, 75 and 200 psia, each for a nominal thrust level of 50 lbs. Thrust chambers having L^* 's of 5, 10, 30 and 50 in. and nominal contraction ratios of 1.5, 3.5 and 8 were fabricated for each design chamber pressure (except for several combinations of parameters which resulted in impractical configurations) and tested at a nominal ambient pressure of 10 mm Hg. Transparent thrust chamber cylinders were used for visual and photographic observation of ignition characteristics. A simple, single-element doublet injector having minimum manifold volumes was used for most of the Compound A/hydrazine-type tests. A concentric tube injector consisting of a single axial orifice for the oxidizer and a concentric annulus for the fuel was used for the F_2/H_2 tests.

(C) The thrust chamber tests with Compound A as the oxidizer were made primarily with N_2H_4 as the fuel. In addition to the investigation of configuration effects, tests were made to determine the influence of mixture ratio and propellant leads on ignition characteristics. Additional tests also were made with UDMH and MHP-5 as the fuel for comparison purposes. MHP-5 is a classified mixed hydrazine fuel consisting of 26% hydrazine, 55% monomethyl hydrazine and 19% hydrazine nitrate. In general it was found that ignition delays with these propellants were very short and, contrary to the results of similar thrust chamber tests with N_2O_4 /hydrazine-type propellants (Ref. 1), were independent of pressure in the chamber prior to ignition. There was no correlation between chamber pressurization due to propellant vaporization (necessary for ignition of $\text{N}_2\text{O}_4/\text{N}_2\text{H}_4$ propellants) and ignition delay in these tests.

(C) Ignition delays and times to 90% of steady state chamber pressure were shortest with Compound A/UDMH. Ignition

CONFIDENTIAL

AFRPL-TR-65-257

(C)

occurred approximately 7-9 msec after application of the electrical signal to the propellant valves. This corresponds to the time at which both propellants first enter the chamber as a vapor-liquid mixture. Although Compound A and UDMH vapors initially enter the chamber at 3 msec, the concentrations are insufficient for ignition, except for several instances of weak, discontinuous, preignition reactions detected by faint light output in some tests with UDMH (and other fuels).

(C) Ignition with both N_2H_4 and MHF-5 occurred 10-14 msec after the start signal which corresponds quite closely with the times (10-12 msec) at which both the oxidizer and the fuels first enter in the liquid state. MHF-5 is first detected entering as a vapor-liquid mixture at about 7 msec after start. In the case of N_2H_4 , liquid injection in the liquid state is the first detectable indication of fuel entry. N_2H_4 enters as a discrete, cohesive stream with no evidence of vaporization even at the low ambient pressures. In contrast, injected streams of Compound A, UDMH and MHF-5 spread out and vaporize rapidly upon injection even after steady-state liquid flowrates have been established.

(C) Because of the lack of dependency upon pressure, ignition delay is not significantly influenced by thrust chamber configuration parameters (design chamber pressure, L^* , contraction ratio, etc.). Although configuration parameters also do not strongly influence the time to reach 90% of steady-state chamber pressure, there is a trend toward longer times with larger volume configurations as might be expected. Mixture ratio tests indicate slightly shorter ignition delays (1-2 msec) with fuel-rich mixture ratios than oxidizer-rich mixture ratios. Propellant lead tests with Compound A/ N_2H_4 indicate that ignition occurs rapidly upon injection of (liquid) hydrazine regardless of the state (vapor, mixture, or liquid) of the Compound A.

(C) Photographic and pressure instrumentation indicate that ignition occurs at the injector with these propellants and rapidly spreads to the nozzle end. Because of the short ignition delays, the start transients were smooth without evidence of the random, short duration, large amplitude spikes characteristic of the N_2O_4 /hydrazine-type propellants.

(U) Thrust chamber tests with gaseous F_2/H_2 also resulted in very short ignition delays and smooth pressure transients. Ignition generally occurred within 1 msec of injection of both

CONFIDENTIAL

propellants and was not significantly influenced by thrust chamber design parameters. As with Compound A/hydrazine-type propellants, ignition is not dependent upon chamber pressurization prior to ignition. Except for propellant lead tests in which one valve was deliberately delayed, ignition occurred before any detectable rise in chamber pressure due to propellant entry occurred. Ignition occurred at the injector end of the chamber and for configurations having long chamber lengths, delays up to about 0.8 msec were measured between start of pressure rise at the injector and nozzle ends corresponding to the spread of ignition through the chamber.

Rise times to 90% of steady-state chamber pressure were generally less than 7.5 msec, averaging about 6.5 msec for 50 in. L* configurations and about 4.5 msec for the 5 and 10 in. L* configurations. Contraction ratio or design chamber pressure had little effect on the rise time.

There was no indication of pressure spikes with F_2/H_2 in any of the tests.

III

TASK I - MEASUREMENT OF REACTION RATE

A. Development of Mathematical Model of Hypergolic Ignition

A mathematical model of hypergolic ignition in attitude control engines in space is desirable for several reasons. A model that takes into account the many processes involved can provide not only design information for minimizing ignition delays, but also it can give valuable insight into the pressure spiking problem by defining quantitatively the conditions from which pressure spikes result, i.e. the mass of the propellants in the chamber at ignition, the fraction of the propellants in the condensed phase, etc.

In the following sections, a mathematical model is described as well as the determinations of some of the quantities required by the model.

The general approach followed in developing the model is indicated in Figure 1. Since hypergolic ignition of N_2O_4 -type fuels is sensitive to pressure (Ref. 1), the pressure build-up in the chamber due to propellant vaporization must be determined. Also required is an expression of the dependency of hypergolic ignition delay on pressure, taking into account mixture ratio and the reactivity of the specific propellant combination. The intersection of the two curves in Figure 1 is taken to be the ignition delay time in the engine at space conditions. Ignition delay as used here is that time which elapses between initial entry of the propellants into the thrust chamber and ignition, i.e. emission of visible light accompanied by an increase in pressure. A total ignition delay time for a given attitude control system is obtained by adding to the above ignition delay period the time elapsed from valve signal to initial propellant entry. Some comments regarding the latter as well as the assumptions inherent in the ignition model indicated in Figure 1 will be given at the appropriate points in the following sections.

The determination of the chamber pressurization curve due to propellant vaporization will be discussed first. Subsequently, the chemical kinetics aspect of the mathematical model will be covered in detail.

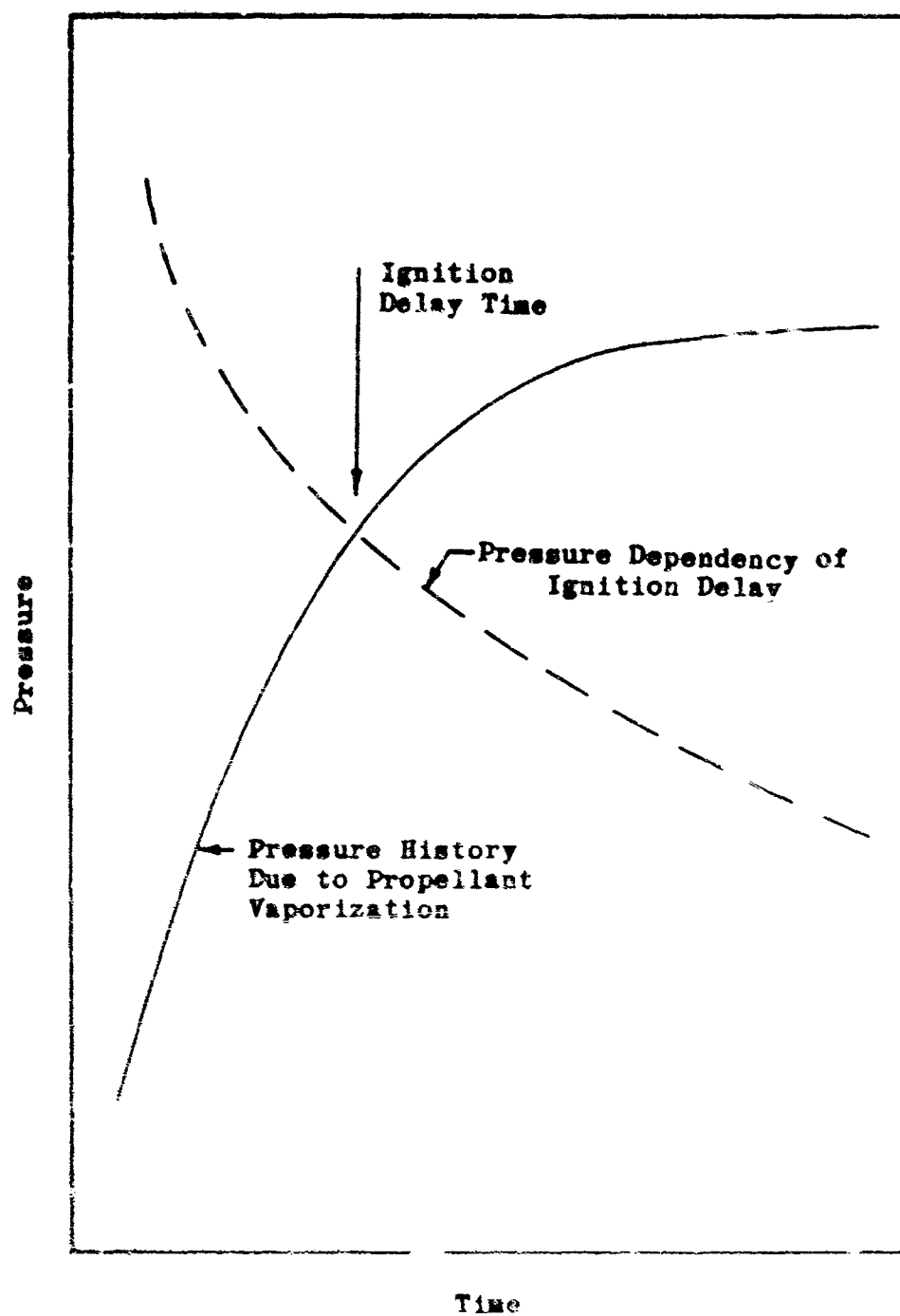


Figure 1. General Concept of Ignition Delay Time Model

B. Thrust Chamber Pressurization Due to Propellant Vaporization

The problem under consideration in this section can be described in general terms as follows. A propellant stream, issuing from an injector orifice into the low pressure environment of the thrust chamber, forms a spray consisting of a great many drops of various sizes. The drops undergo evaporation, decrease in size, and cool. Evaporative cooling can bring a drop's temperature to its freezing point. Subsequent vaporization occurs at constant temperature while the fraction of the drop that is frozen increases until the drop becomes completely frozen. Further evaporation can occur from the frozen drop (sublimation), the drop temperature resuming its decline.

The evaporated gas raises the pressure in the chamber. The pressure at any time is influenced by the chamber geometry and by the gas temperature, the latter in turn is related to the drop temperatures. Some vapors pass through the nozzle and, under certain conditions, vapors can condense on the thrust chamber walls.

It is necessary, therefore, to determine the following quantities, all as a function of time:

- a) the evaporation from each drop in the system
- b) the radius of each drop
- c) the temperature of each drop
- d) the fraction of each drop that is frozen
- e) mass flow through the nozzle
- f) mass of vapors that condense on the chamber walls
- g) gas temperature, and finally
- h) gas pressure.

The starting point of the analysis is the work of Agosta and Kraus reported in Ref. 2. The present work was performed in close cooperation with Dr. Agosta who served as consultant. For the present program, their analysis was modified somewhat and additional features were added to it. Their basic equations are reviewed first, and then the features that were added are discussed. Finally, comparisons between theoretical and experimental results are given.

The analysis takes into account the rate of propellant injection, propellant evaporation and condensation (assuming a Knudsen-Langmuir kinetic model), thrust chamber geometry, and propellant vapor efflux through the nozzle. In essence, the pressure in the chamber at any time is obtained from a mass balance on the system.

Steady state calculations are made in successive time intervals which are taken sufficiently short that all properties remain essentially constant during each time interval. The solution proceeds from known initial conditions to calculated new values of properties at the end of the first time interval. The new values are taken as initial conditions for the second time interval, etc. to completion.

1. Theory

a. Droplet Evaporation

The heart of the problem is droplet evaporation. Based on the kinetic theory of gases and the perfect gas law, the amount of evaporation occurring in a finite time interval is given by

$$G_{\text{evap}} = \left(P_v(T_d) - P_g(T_g) \right) \propto A_d \Delta t \sqrt{\frac{M g_c}{2\pi R T_d}} \quad (1)$$

The assumptions involved are:

1. The number of molecules leaving the liquid surface per unit time (when the ambient pressure is below the liquid vapor pressure) is the same as the number which impinge on the same surface when the liquid is in equilibrium with its vapor.
2. The gas evaporates at the same temperature as the liquid drop from which it is evolved.
3. The molecular weight of the vapor is the same as the molecular weight of the liquid, i.e. a non-dissociating propellant.

The propellant spray is represented mathematically by a three drop-size model. The three drop sizes are obtained by applying a logarithmicnormal distribution (with a specific

geometric standard deviation depending on the type of injector) to a given mass median drop size and then selecting three radii such that 30% of the weight flow is in drops of the smallest radius, 40% in the intermediate size drops, and 30% in the largest drops (Ref. 3). Thus there are three classes of drops, $1 \leq i \leq 3$.

The continuous processes involved in the vapor pressurization of the thrust chamber are treated mathematically as steady state processes in successive, very short time intervals. Consequently, in each time interval, a new ensemble of drops enters the thrust chamber. These undergo evaporation during the time interval as do the drop ensembles which entered the chamber in previous time intervals. Therefore, in the first time interval ($N = 1$), there is one drop ensemble ($j = 1$) which consists of three classes of drops ($1 \leq i \leq 3$). In the second time interval ($N = 2$) there is not only the first ensemble ($j = 1$) which continues to evaporate, but also a second ensemble ($j = 2$) which undergoes evaporation for the first time. This second ensemble also consists of three classes of drops. Therefore, there are six classes of drops to consider in the second time interval, nine in the third interval, twelve in the fourth interval, etc. Each class of drops has a unique radius, temperature and fraction of the individual drops that is frozen.

Each class of drops must be identified and this is done by i , j and N numbers which indicate the initial radius of the drops when the class first entered the thrust chamber, the time interval in which the class entered the thrust chamber (or, in other words, the number of intervals the class has been in the system) and the time interval in question. Thus the possible values of i , j and N are:

$$i = 1, 2 \text{ or } 3$$

$$j = 1, 2, 3 \text{ ---- } N$$

$$N = 1, 2, 3, 4, \text{ ----}$$

If $N = 500$, say, there are 500 drop ensembles (j -numbers) and each ensemble consists of 3 classes of drops (i -numbers). Therefore there are 1500 separate classes of drops to be accounted for in the 500th time interval, each class having a unique radius, temperature and quality X (see below).

From equation (1), the mass evaporated from a single drop in one time interval is given by:

$$G_{ij} = \left(P(T_{i,j})_{N-1} - P_2(T_2)_{N-1} \right) \propto (r_{i,j})^2_{N-1} \Delta t_N \sqrt{\frac{8\pi M g_s}{R T_{i,j} N-1}} \quad (2)$$

b. Total Evaporation During One Time Interval

To determine the total mass evaporated from all of the drops during one time interval, the total surface area of all of the drops in the system must be known. The total surface area depends, of course, on the number and radius of the drops in each class.

For a mass-median drop size, r_m , of 75 microns and a geometric standard deviation, σ , of 2.3 as given in Ref. 3 for an impinging stream injector, the initial radii of the three drop-size spray model are determined to be:

30% of injected mass in drops having $r_1 = 83 \times 10^{-6}$ ft

40% of injected mass in drops having $r_2 = 250 \times 10^{-6}$ ft

30% of injected mass in drops having $r_3 = 720 \times 10^{-6}$ ft

The number of drops in each of the three classes is obtained from

$$N_1 = \frac{W_1}{(4/3)\pi r_1^3 \rho_1} \quad \text{where } W_1 = .3 W_j \quad W_2 = .4 W_j \quad W_3 = .3 W_j \quad (3)$$

and $W_j = \dot{w} \Delta t$, the mass of propellant injected during one time interval.

The number of drops in each class is therefore:

$$\begin{aligned} N_1 &= 12.51 \times 10^{10} (W_j / \rho_1) \text{ for } r_1 = 83 \times 10^{-6} \text{ ft} \\ N_2 &= .61 \times 10^{10} (W_j / \rho_1) \text{ for } r_2 = 250 \times 10^{-6} \text{ ft} \\ N_3 &= .019 \times 10^{10} (W_j / \rho_1) \text{ for } r_3 = 720 \times 10^{-6} \text{ ft} \end{aligned} \quad (4)$$

The total number of drops injected in one time interval is

$$W_j = 13.14 \times 10^{10} (W_j / \rho_1). \quad (5)$$

The total surface area of the drops in the i^{th} class before evaporation begins is

$$A_{ij} = 4\pi r_i^2 N_i = 4\pi r_i^2 N_j (N_i / N_j) \quad (6a)$$

The total surface area of all the drops before evaporation is

$$A_j = \sum_{i=1}^3 A_{ij} = 4\pi N_j \left[r_1^2 \left(\frac{N_1}{N_j} \right) + r_2^2 \left(\frac{N_2}{N_j} \right) + r_3^2 \left(\frac{N_3}{N_j} \right) \right] \quad (6b)$$

The total evaporation occurring from all of the drops in the system in one time interval is obtained by expressing A_d of equation (1) by equations (6b), (5) and (4), giving

$$\begin{aligned} G_N &= \sum_{j=1}^N \sum_{i=1}^3 G_{ij} = \\ &= \sum_{j=1}^N \sum_{i=1}^3 C_i \left[P_v(T_{Lij})_{N-1} - P_v(T_2)_{N-1} \right] \frac{\alpha W_j (r_{Lij})_{N-1}^2 \Delta t_N}{\rho_1} \sqrt{\frac{M}{(T_{Lij})_{N-1}}} \end{aligned} \quad (7)$$

$$\text{where } C_1 = 4\pi \left(\frac{N_1}{N_j} \right) \left(\frac{r_1}{W_j} \right) \sqrt{\frac{3}{2\pi R}}$$

$$\text{or } C_1 = 2.09 \times 10^{10}$$

$$C_2 = 0.442 \times 10^{10}$$

$$C_3 = .0139 \times 10^{10}$$

$P_v(T_{dij})_{N-1}$ is the vapor pressure corresponding to the temperature of the i th size drop of the j th ensemble at the end of the $N-1$ time interval. The density of the liquid, ρ_l , is assumed constant.

c. Vapor Condensation on Chamber Walls

The mass of vapors condensing on the chamber walls is given by

$$G_w = [P_g(T_g)_{N-1} - P_v(T_w)] \propto A_c \Delta t_N \sqrt{\frac{M g_c}{2\pi R (T_g)_{N-1}}} \quad (8)$$

but with the constraint $0 \leq G_w < +\infty$. Condensation on the wall is considered only when $P_g(T_g) > P_v(T_w)$; that is, the condensation term cannot have a negative value thereby implying evaporation.

d. Vapor Flow Through Nozzle

The mass efflux through the nozzle during one time interval, for constant c_p and k for the gas, is given by

$$m_{noz} = (P_g)_{N-1} A^* \sqrt{\frac{k M g_c}{R (T_g)_{N-1}}} \left(\frac{2}{k+1} \right)^{\frac{k+1}{k-1}} \Delta t_N \quad (9)$$

e. Vapor Mass in Chamber

The mass of vapor in the chamber at the end of the N th time interval is obtained from the perfect gas law

$$(m_c)_N = \frac{V_c M}{R} \left(\frac{P_g}{T_g} \right)_N \quad (10)$$

f. Gas Temperature

The temperature of the gas in the chamber at the end of the N th time interval is obtained by taking a mass weighted average of the temperature, which includes the temperature of the gas generated due to evaporation during the time interval plus the temperature of the gas left from the previous time interval minus the temperature of the gas which condenses on the chamber walls and that which passes through the nozzle.

For a single specie system and a constant vapor heat capacity,

$$T_{gN} \sum_{j=1}^N \sum_{i=1}^2 G_{Lij} (T_{Lij})_{N-1} + (T_g)_{N-1} [(m_c)_{N-1} - (G_w)_N - (m_{noz})_N] \\ T_{gN} \sum_{j=1}^N \sum_{i=1}^2 G_{Lij} + (m_c)_{N-1} - (G_w)_N - (m_{noz})_N \quad (11)$$

g. Gas Pressure

A mass balance of the system yields the gas pressure in the chamber at the end of the N th time interval.

$$\left(\sum_{j=1}^N \sum_{i=1}^2 G_{Lij} \right)_N - (G_w)_N - (m_{noz})_N = (m_c)_N - (m_c)_{N-1} \quad (12)$$

The terms on the left hand side are given by equations (7), (8), and (9) while the right hand side is equation (10) evaluated at the end of the N and $N-1$ time intervals.

The gas pressure in the chamber at the end of the N th time interval, $(P_g)_N$, is given by:

$$\left[\left(\frac{P_g}{T_g} \right)_N - \left(\frac{P_g}{T_g} \right)_{N-1} \right] \frac{V_c M}{R} = \quad (13)$$

$$\sum_{j=1}^N \sum_{i=1}^2 C_i \left[R(T_{Lij})_{N-1} - P_g(T_g)_{N-1} \right] \frac{\alpha W_j (r_{Lij})_{N-1}^2 \Delta t_N}{A_i} \sqrt{\frac{M}{(T_{Lij})_{N-1}}}$$

$$- \left[P_g(T_g)_{N-1} - P_v(T_w) \right] \alpha A_c \Delta t_N \sqrt{\frac{M g_c}{2\pi R (T_g)_{N-1}}}$$

$$- (P_g)_{N-1} A^* \Delta t_N \sqrt{\frac{\kappa M g_c}{R (T_g)_{N-1}}} \left(\frac{2}{\kappa+1} \right)^{\frac{\kappa+1}{\kappa-1}}$$

Drop Radii

At the end of every time interval, new drop radii and drop temperatures must be calculated to account for the effect of evaporation during the time interval on the drop's size and temperature. A mass balance on the drop together with equation (2) yields the new drop radius:

$$(r_{li})_N = (r_{li})_{N-1} \left[1 - \frac{3 [P_v(T_{li})_{N-1} - P_s(T_s)_{N-1}] \alpha \Delta t_N}{\rho_l (r_{li})_{N-1} \sqrt{\frac{M g_c}{2 \pi R (T_{li})_{N-1}}}} \right]^{k_3} \quad (14)$$

1. Drop Temperature and "Qualities"

The new drop temperature is obtained from an energy balance on the drop.

$$(T_{li})_N = (T_{li})_{N-1} - \frac{3 [P_v(T_{li})_{N-1} - P_s(T_s)_{N-1}] \alpha (r_{li})_{N-1}^2 \lambda_e \Delta t_N}{\rho_l c_{pl} (r_{li})_N^3 \sqrt{\frac{M g_c}{2 \pi R (T_{li})_{N-1}}}} \quad (15)$$

Clearly the temperature within the drop is assumed to be uniform. The heat of vaporization, λ_e , the heat capacity of the liquid, c_{pl} , and the liquid density, ρ_l , are assumed constant. Values of these quantities corresponding to the mid-temperature of the range encountered are used.

At some point, an evaporatively cooling drop can arrive at its freezing point. Further evaporation of the drop occurs at constant temperature during which time the fraction of the drop that is frozen increases. Thus, equation (15) holds until the freezing point is reached. Once T_{dij} equals T_{fp} , then T_{dij} remains constant as the drop freezes. The fraction of the drop that freezes in one time interval due to evaporation is given by an energy balance on the drop.

$$G_{li} \lambda_s = X_{li} N \frac{4}{3} \pi \rho_l (r_{li})_N^3 \lambda_F \quad (16)$$

The solid fraction of the drop, that is its "quality", increases in successive intervals until the drop is frozen solid. The quality, X_{ij} , of a drop is given by

$$X_{ij} = \sum_{N=N_{FP}}^{N_x} \frac{3}{4} \frac{G_{Lj} \lambda_s}{\pi \rho_s (r_{Lj})^3 \lambda_F} \quad (17)$$

with the constraint that $0 < X_{ij} < 1$.

The summation over successive time intervals for the drop in question begins when the temperature of the drop, T_{dij} , reaches T_{FP} . The summation ends when the drop is completely frozen, i.e. $X_{ij} = 1$. G_{ij} in equation (17) is given by equation (2).

Once the drop is frozen solid, further evaporation (sublimation) causes the temperature of the drop to decrease. Equation (15), modified to reflect the solid state of the drop-let, becomes applicable again.

The above equations were programmed for a Control Data G-20 computer. The time intervals, Δt_N , used in the calculations ranged from 1 to 40 microseconds depending on the particular propellant and motor geometry under consideration. In general, the faster the pressure rise in the thrust chamber, the smaller the time interval required. The actual criterion for the length of the time interval is that the change in properties during each time interval, i.e. drop radius, drop temperature, etc., be kept small enough so that the properties can be considered constant during the time interval. New values are calculated at the end of each time interval and these are used for the next interval, etc. to completion of the calculation.

The equations are used to calculate in each time interval the gas pressure, the gas temperature, and a new radius and temperature for each drop in the system. Since the injected propellant stream is represented by three drop sizes, the number of classes of drops increases by three in each successive time interval. Each class of drops has a unique radius, temperature and drop "quality" X . In the 100th time interval, say, there are 300 drop radii, 300 drop temperatures, and 300 drop "qualities" to be accounted for. The changes in the values of each of these must be calculated to obtain the gas pressure at the end of the 101st time interval.

2. Results and Discussion

The preceding equations were solved to determine the pressure history in a thrust chamber due to vaporization of carbon tetrachloride. CCl_4 was selected because the many physical properties, especially accommodation coefficient, required in the computer program are known for this substance. Corresponding properties for modern propellants such as N_2O_4 and Compound A are often unknown at present or of obviously uncertain precision. Thus, the model for chamber pressurization due to propellant vaporization was developed and checked experimentally using CCl_4 as the working fluid. The vapor pressure of CCl_4 is very similar to that of the 50-50 blend of N_2H_4 -UDMH for the range of temperatures encountered.

a. Gas Temperature History

The initial calculations showed that the vapor temperature in the thrust chamber decreases initially as the chamber pressure increases but after a few milliseconds (depending on motor geometry and the propellant properties) the vapor temperature reaches a minimum and thereafter gradually rises until steady-state conditions are reached (Figure 2).

The initial cooling is the result of evaporation from drops which have already undergone some evaporative cooling. The minimum in the gas temperature history occurs because the evaporation from the coldest drops is more strongly diminished by the rising chamber pressure than the evaporation from the warmer (newer) drops. A point is reached at which the net production of cold vapors equals the net production of warm vapors and so the gas temperature remains unchanged.

The gas temperature subsequently increases gradually as a consequence of the rising gas pressure which first diminishes, then stops, and finally causes "negative evaporation" of the colder drops. The temperature inversion is of interest because it occurs generally during typical ignition delay times. The cooler gas temperatures would tend to lengthen ignition delays due to the effect of temperature on reaction rates.

b. Droplet Condensation

Condensation of the vapors was found to occur on drops which have undergone substantial evaporative cooling. The condensation results when the gas pressure in the chamber exceeds

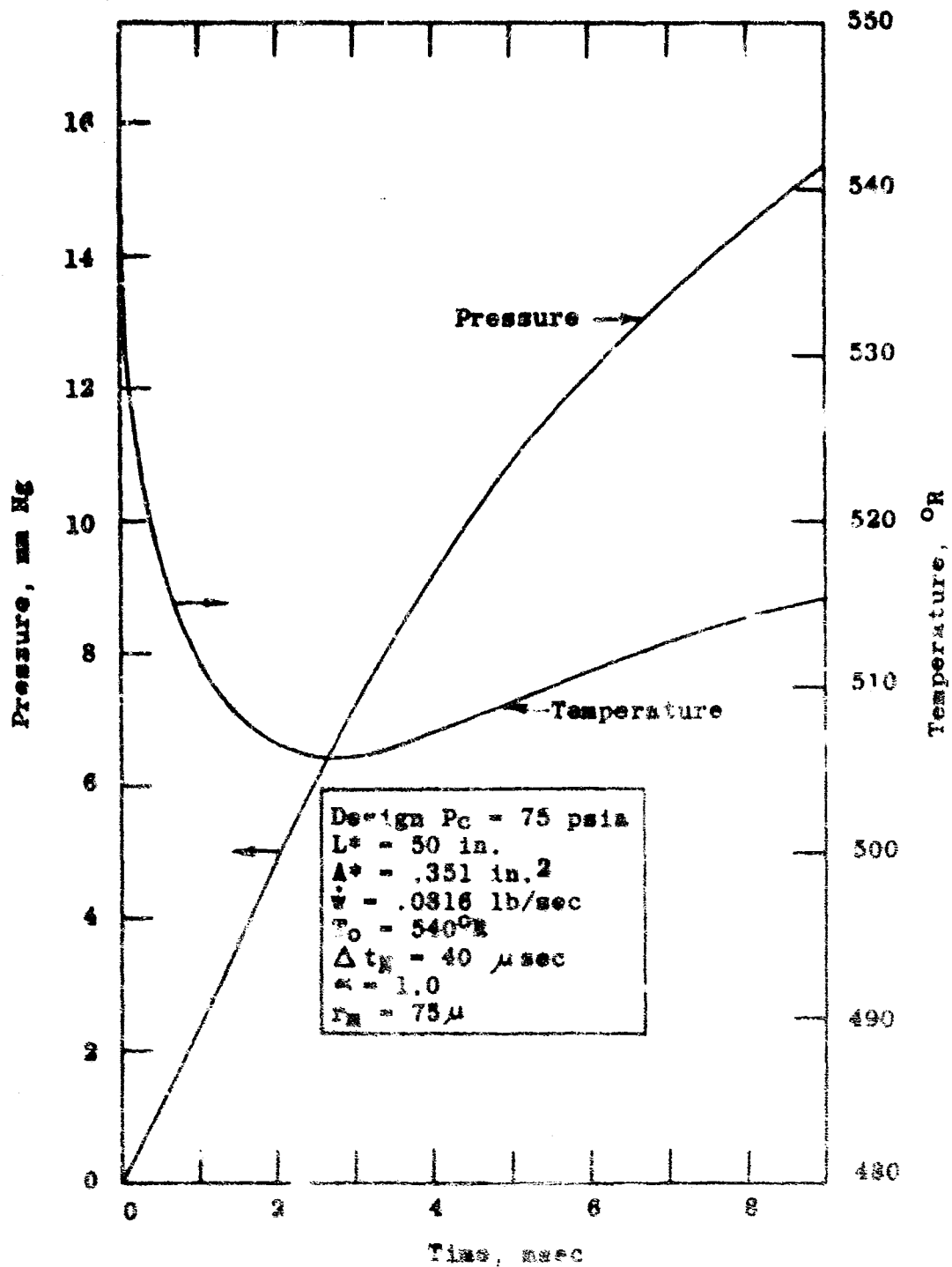


Figure 2. Calculated Chamber Pressure and Temperature History for CCl_4

the vapor pressure of the cold drop, see equation (1) or (2). An illustration of condensation on a cold drop is given in Table I.

TABLE I

EXAMPLE OF CONDENSATION ON A COLD DROP (CCl₄ #R)

<u>Time</u> msec	<u>Drop Radius</u> x 10 ⁻⁶ ft	<u>Drop Temp.</u> OR	<u>Drop V.P.</u> mmHg	<u>Chamber Pressure</u> mmHg
2.80	674.907	450.00*	8.291	6.804
3.20	674.550	450.00*	8.291	7.680
3.60	674.495	450.02	8.298	8.484
4.00	674.674	450.44	8.416	9.224
4.40	675.051	451.31	8.671	9.913

*Drop is partially frozen.

The drop under consideration in Table I had a radius of 720×10^{-6} ft when it entered the system which was at time zero. It is one of the $i = 3$ class of drops, the largest drops of the three drop-size spray model. After 2.80 msec, the drop radius has decreased to the value shown and its temperature has reached the freezing point. The drop is not frozen solid as yet but is only partially frozen. At this time the chamber pressure is still below the vapor pressure of the drop. During the next 0.40 msec, the drop continues to undergo evaporation (radius decreases further) since the gas pressure (column 5) is still less than the drop's vapor pressure (column 4). During this time the fraction of the drop that is frozen increases, the drop temperature remaining at the freezing point value.

At 3.60 msec, the chamber pressure has increased to a value greater than the drop's vapor pressure thereby causing condensation onto the drop. The drop's temperature has increased to 450.02°F indicating that the condensation energy absorbed by the drop not only melted the frozen fraction of the drop but also raised slightly the temperature of the all-liquid drop. Although the condensation increased the mass of the drop,

the net effect over the 0.40 msec period is a decreased radius due to the evaporation which occurred during the first part of the period, i.e. until the gas pressure equalled the drop's vapor pressure. During the next 0.40 msec period, that is at 4.00 msec, condensation on the drop continued (column 5 vs. column 4). The temperature of the liquid drop increased as did the size of the drop. Further condensation occurred during the last interval listed in the table as the gas pressure continued to be greater than the vapor pressure of the drop.

c. Vapor-Drop Energy Transfer

The possibility of heat transfer between the vapor and the drops is not accounted for by the equations given previously. In the case of CCl_4 , the temperature difference between the warm vapors and the coldest drops can be as much as 75°F . With such a driving force, one would expect the drops to be warmed and the vapors cooled to some extent.

The energy reaching the surface of a drop during one time interval is, according to ref. 3:

$$q_{v,u} \Delta t_N = 4\pi h (r_{Lj})_{N-1}^2 \sum \Delta t_N \left[(T_g)_{N-1} - (T_{dLj})_{N-1} \right] \quad (18)$$

$$\text{where } \sum = \frac{x}{e^x - 1}, \quad x = \frac{G_{Lj} c_{pg}}{4\pi h \Delta t_N (r_{Lj})_{N-1}^2} \quad (19)$$

$$h = \frac{k_g}{2 + (r_{Lj})_{N-1}} \left[2 + 0.5 \text{Pr}^{1/3} \text{Re}^{1/2} \right] \quad (20)$$

$$Pr = \left(\frac{c_p \mu}{K} \right)_g \quad (21)$$

$$\text{and } Re = \frac{2(r_{Lj})_{N-1} V_{d, \text{avg}} M(P_g)_{N-1}}{\mu_g R(T_g)_{N-1}} \quad \text{excluding drag effects.} \quad (22)$$

G_{1j} in equation (19) is given by equation (2).
An energy balance on the drop is then

$$G_{1j} \lambda_e = \frac{4}{3} \pi (r_{Lj})_N^3 \rho_L c_{pL} [(T_{dLj})_{N-1} - (T_{dLj})_N] + q_v \Delta t_N \quad (23)$$

from which the new drop temperature at the end of the time interval is

$$(T_{dLj})_N = (T_{dLj})_{N-1} \quad (24)$$

$$= \frac{3 [P_v(T_{dLj})_{N-1} - P_g(T_g)_{N-1}] \times (r_{Lj})_{N-1}^2 \lambda_e \Delta t_N}{\rho_L c_{pL} (r_{Lj})_N^3} \sqrt{\frac{M_{3c}}{12\pi R(T_{dLj})_{N-1}}} + \bar{\Phi}$$

$$\text{where } \bar{\Phi} = \frac{3h [(T_g)_{N-1} - (T_{dLj})_{N-1}] (r_{Lj})_{N-1}^2 \Delta t_N}{\rho_L c_{pL} (r_{Lj})_N^3} \quad (25)$$

Equations (24) and (25) are used in place of equation (15).

Inclusion of vapor-droplet heat transfer during the freezing period of a drop is achieved by modifying equation (17) giving:

$$X_{ij} = \sum_{N=N_{pp}}^{N_2} \left(\frac{3 G_{ij} \lambda_s}{4 \pi \rho_s (r_{ij})_N^3 \lambda_p} - \frac{c_{ps}}{\lambda_p} \Phi \right) \quad (26)$$

and Φ , Z and z , h , Pr , Re and G_{ij} are given by equations (25), (18), (20), (22) and (2) respectively.

The total energy reaching the surface of all drops in the system in one time interval is:

$$Q_N = \sum_{j=1}^N \sum_{i=1}^2 q_{v_{ij}} \Delta T_N N_i = \quad (27)$$

$$\sum_{j=1}^N \sum_{i=1}^2 4 \pi h (r_{ij})_N^2 \sum N_i \Delta T_N \left[(T_g)_{N-1} - (T_{d_{ij}})_{N-1} \right]$$

where N_i , the total number of drops in each class, is given by equation (4) and h and Z are given by equations (20) and (18), respectively. The energy Q_N comes from the gas in the chamber and therefore equation (11), the gas temperature equation, becomes

$$T_{g_N} = \frac{\sum_{j=1}^N \sum_{i=1}^2 G_{ij} (T_{d_{ij}})_{N-1} + (T_g)_{N-1} \left[(m_{ic})_{N-1} - (G_w)_N - (m_{noz})_N \right] - \frac{Q_N}{c_{pg}}}{\sum_{j=1}^N \sum_{i=1}^2 G_{ij} + (m_{ic})_{N-1} - (G_w)_N - (m_{noz})_N} \quad (28)$$

The effect of including vapor-droplet heat transfer on chamber pressure and temperature is slight as indicated in the first two lines of Table II.

TABLE II

CHAMBER PRESSURE AND TEMPERATURE AT $t = 10.0$ MSEC

P_g mmHg	T_g OR	
16.268	517	No heat transfer (CCl_4 #L)*
16.685	515	Heat transfer included (CCl_4 #R)
16.953	514	Heat transfer included, 5.00 msec residence time (CCl_4 #S)
17.160	513	Heat transfer included, 3.36 msec residence time (CCl_4 #T)

As expected, the gas temperature is lower when heat transfer to the cold drops is included. The change is small however. The higher gas pressure results from the drops which are slightly warmer due to the heat transfer and so the drops vaporize slightly more mass in succeeding time intervals. The increased mass of vapor more than offsets the gas temperature effect on chamber pressure, but the net change in the latter is small.

4. Drop Residence Time

The equations discussed to this point put no limit on the lifetime of the drops in the system. In reality, the lifetime of the drops is finite, the drops pass through the nozzle after some sort of residence time. Therefore, a residence time limitation was included in the program. The residence time used is defined simply as the average time required for a drop to travel from the injector to a chamber wall traveling at a constant velocity equal to the injection velocity.

* CCl_4 #L, #R, #S, etc. designate computer run numbers

Despite the short residence times to which the model leads, 1-1/2 to 5-1/2 msec typically depending on motor geometry and injection velocity, the effect on chamber pressure is very small. A comparison of the second and third lines of Table II shows the extent of the effect. An arbitrary reduction of the residence time from 5 to 3.36 msec (fourth line of Table II) shows again the smallness of the residence time effect.

Drop temperature histories show that once a drop has been in the system for one residence time period, its temperature is such that its vapor pressure is not very different from the gas pressure prevailing at that time. Thus, in accordance with equation (1) or (2), the amount of evaporation (or condensation) from that point onward is relatively small.

Table II shows that the residence time limitation causes a slightly higher chamber pressure and a slightly lower gas temperature. These effects result because some of the vapor condensation onto the cold drops is stopped. Thus, somewhat more gas at low temperatures is in the chamber than would otherwise be the case.

e. Effect of Drop Sizes

The initial radii of injected drops for the three drop-size spray model are derived from a given mass-median drop size as outlined previously. The mass-median drop size used initially in the calculations was 75 microns, based on the work of Priem and Heidman (Ref. 3) who cite investigations of the spray characteristics of liquid streams emerging into an environment in which the pressure was substantially above the vapor pressure of the liquid. At ambient pressures well below the vapor pressure of the liquid, one would expect additional dispersive forces to be operative resulting in smaller drops on the average.

A number of short duration (approx. 10 micro-second) exposures, with a magnification of 2X, was taken of streams of various propellants issuing from an injector orifice into a low pressure environment. Exposures were made at various pressures from one atmosphere to 1 mm Hg, using a General Radio Company High Speed Stroboscope, Type No. 1533-A, in the single pulse mode. A Bausch & Lomb 7-1/8" coated F/6.8 Proto VIIa lens permitted magnification of the object. The exposures were recorded on Polaroid, Type 57, 300 speed, 4 x 5 film. The streams are back-lighted, a diffuser being used between the stream and the light source. The direction of stream flow was vertically upward.

A strong effect of ambient pressure on the sprays resulting from CCl_4 liquid injection is shown in the pictures of Figure 3. At high ambient pressures, 100 mm Hg and above, the relatively low velocity stream is coherent for the two-inch stream length viewed. At 95 mm Hg, which is the vapor pressure of CCl_4 at 71°F , a vapor bubble in the stream appears to have "exploded". At somewhat lower ambient pressures, the "bubble explosions" are more numerous and liquid ligaments appear. At still lower pressures, the ligaments are smaller as are the drops on the average. At 10 and 1 mm Hg, the ligaments are short lived and many of the droplets approach the limit of resolution in the pictures which is about 50 microns in diameter.

Similar pictures for UDMH sprays at various ambient pressures are given in Figure 4. The liquid injection velocity of the streams in Figure 4 for UDMH is nearly the same as in Figure 3 for CCl_4 .

Obvious similarities exist between the UDMH streams and the CCl_4 streams. In both cases the streams are coherent at the high ambient pressures and "exploding bubbles" first appear when the ambient pressure is only slightly below the vapor pressure of the liquid (vapor pressure of UDMH at 71°F is 130 mm Hg). At lower pressures, slight differences are noted but these differences are in degree only. UDMH appears to form liquid ligaments more readily than CCl_4 ; and, on the average, the UDMH droplets at the lowest ambient pressures are somewhat smaller than the corresponding CCl_4 droplets. This is due, at least partially, to the greater evaporation rate of UDMH which results from its somewhat greater volatility.

The effect on spray characteristics of higher flowrates of UDMH through the same injector orifice is shown in Figure 5 for an ambient pressure of 140 mm Hg (slightly above the vapor pressure of UDMH) and in Figure 6 for an ambient pressure of 1 mm Hg. At the higher ambient pressure the higher flowrates, which give a higher injection velocity, lead to greater break-up of the stream. At the low ambient pressure, however, any differences between the sprays from the various flowrates are much less obvious. The degree of streaking in the pictures by the droplets increases with injection velocity but the drop sizes (width of streak) appear roughly similar in all four pictures. The distance to essentially complete stream break-up is affected only slightly by the injection velocity, or mass flowrate. Assuming the drops travel at a constant velocity equal to the injection velocity, break-up of the streams is complete in less than a millisecond.

For comparative purposes, similar spray pictures of N_2O_4 are reproduced from Ref. 1 in Figures 7 and 8. The mass flowrate is the same in all six pictures. The different injection velocities in the two figures are obtained by different injector orifice diameters. Again, the strong effect of ambient pressure is obvious. Since flowrate is constant in Figures 7 and 8, the effect of injection velocity alone on stream break-up time can be discerned. In the high velocity case, stream break-up is complete in $1/3$ msec at an ambient pressure of 100 mm Hg. In the low velocity case, the stream break-up time is about 1.5 msec at 40 mm Hg ambient pressure.

A complete, quantitative drop size distribution cannot be determined from the photographs; nevertheless semi-quantitative information can be gleaned by counting the resolved drops and measuring their diameters at successive sections of the spray.

Analysis of the pictures of the low pressure CCl_4 sprays indicates that the actual mass-median drop size is less than the 75 micron radius initially assumed for the sprays in the computer program. How much less could not be determined. Nevertheless, the effect of drop size on pressurization of a thrust chamber was determined by a calculation using smaller drop sizes. The mass-median drop size was arbitrarily reduced from the original 75 micron radius to a 50 micron radius. New radii for the three drop-size spray model used in the computer program were computed, again using the logarithmic-normal distribution, the same geometric standard deviation, and again selecting three radii such that 30% of the weight flow exists in drops of the smallest radius, 40% of the weight flow in drops of the intermediate radius and the remaining 30% in drops of the largest radius. The resulting radii are given in Table III together with the radii derived from the 75 micron mass-median drop size used initially.

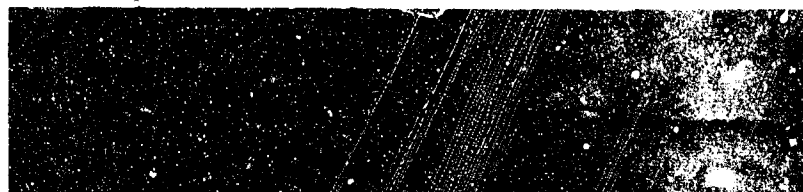
Computer calculations were made using each of the sets of radii in Table III to represent the spray. The calculated pressure curves for each case are given in Figure 9. As expected, the spray consisting of the smaller drops yields the higher pressures due to the increased surface area resulting from the greater number of drops. A compensating effect on chamber pressure, however, is that due to the higher mass fraction initially evaporated from the smaller drops, their temperature is lower in succeeding time intervals. The lower temperature causes a relatively lesser amount of evaporation in succeeding intervals. As a result, the surface area

For comparative purposes, similar spray pictures of N_2O_4 are reproduced from Ref. 1 in Figures 7 and 8. The mass flowrate is the same in all six pictures. The different injection velocities in the two figures are obtained by different injector orifice diameters. Again, the strong effect of ambient pressure is obvious. Since flowrate is constant in Figures 7 and 8, the effect of injection velocity alone on stream break-up time can be discerned. In the high velocity case, stream break-up is complete in $1/3$ msec at an ambient pressure of 100 mm Hg. In the low velocity case, the stream break-up time is about 1.5 msec at 40 mm Hg ambient pressure.

A complete, quantitative drop size distribution cannot be determined from the photographs; nevertheless semi-quantitative information can be gleaned by counting the resolved drops and measuring their diameters at successive sections of the spray.

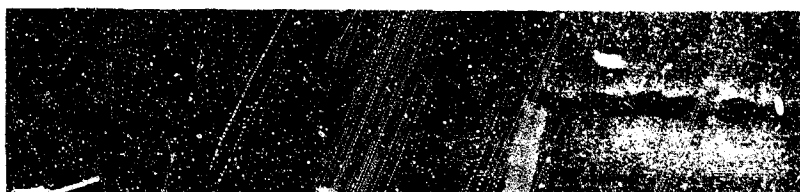
Analysis of the pictures of the low pressure CCl_4 sprays indicates that the actual mass-median drop size is less than the 75 micron radius initially assumed for the sprays in the computer program. How much less could not be determined. Nevertheless, the effect of drop size on pressurization of a thrust chamber was determined by a calculation using smaller drop sizes. The mass-median drop size was arbitrarily reduced from the original 75 micron radius to a 50 micron radius. New radii for the three drop-size spray model used in the computer program were computed, again using the logaritmiconormal distribution, the same geometric standard deviation, and again selecting three radii such that 30% of the weight flow exists in drops of the smallest radius, 40% of the weight flow in drops of the intermediate radius and the remaining 30% in drops of the largest radius. The resulting radii are given in Table III together with the radii derived from the 75 micron mass-median drop size used initially.

Computer calculations were made using each of the sets of radii in Table III to represent the spray. The calculated pressure curves for each case are given in Figure 9. As expected, the spray consisting of the smaller drops yields the higher pressures due to the increased surface area resulting from the greater number of drops. A compensating effect on chamber pressure, however, is that due to the higher mass fraction initially evaporated from the smaller drops, their temperature is lower in succeeding time intervals. The lower temperature causes a relatively lesser amount of evaporation in succeeding intervals. As a result, the surface area

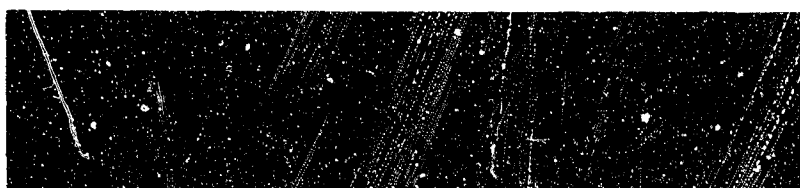


Ambient
Pressure,
mm Hg

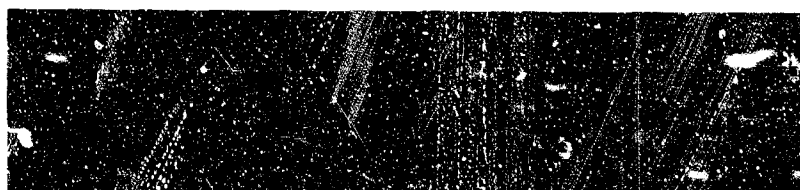
100



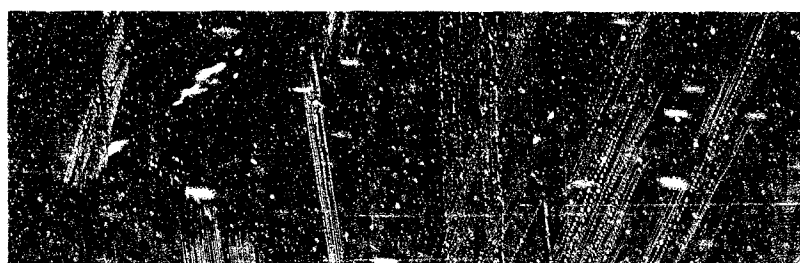
95



80

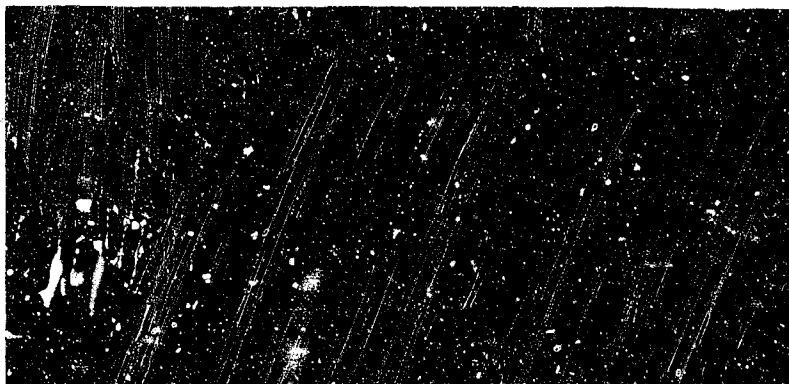


70



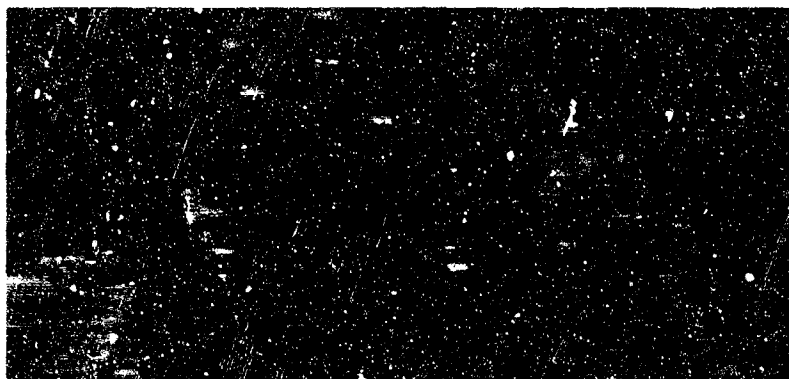
60

Figure 3a. Fully Developed CCl_4 Flow at Various Pressures. Liquid Injection Velocity = 30 ft/sec, Flowrate = 0.0071 lb/sec, Orifice = 0.021 in. dia. \times 0.042 in. long, Ambient Temperature, Magnification 2X.

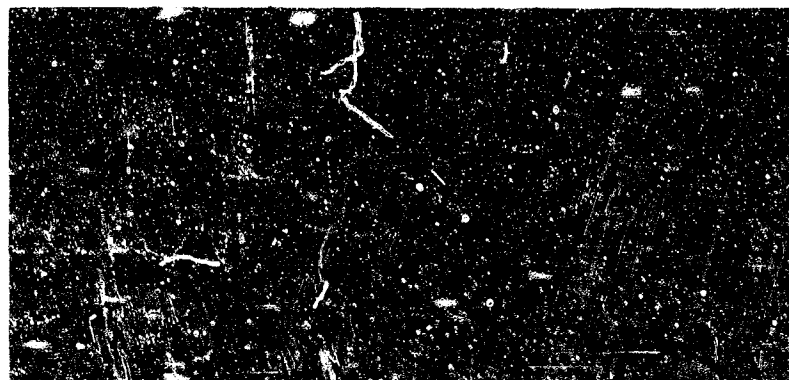


Ambient
Pressure,
mm Hg

30

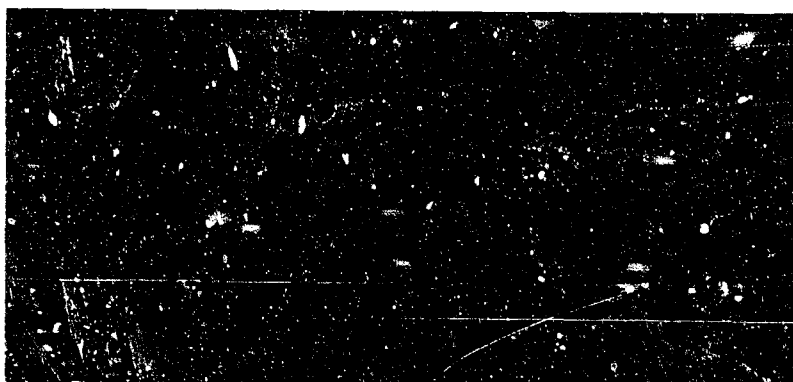


40



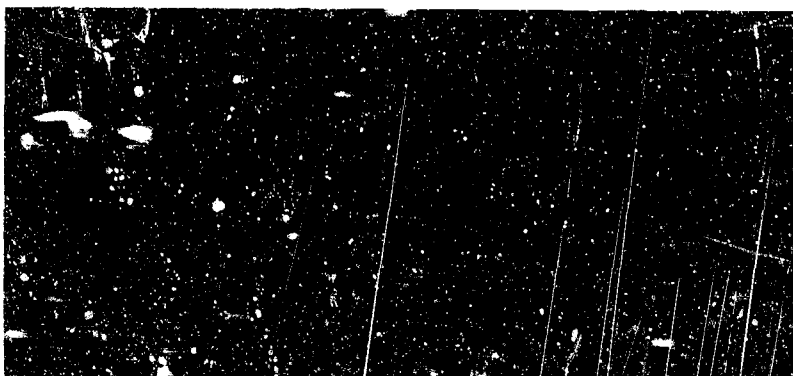
30

Figure 3b. Fully Developed CCl_4 Flow at Various Pressures. Liquid Injection Velocity = 30 ft/sec, Flowrate = 0.0071 lb/sec, Orifice = 0.021 in. dia. \pm 0.043 in. long, Ambient Temperature, Magnification 3X.

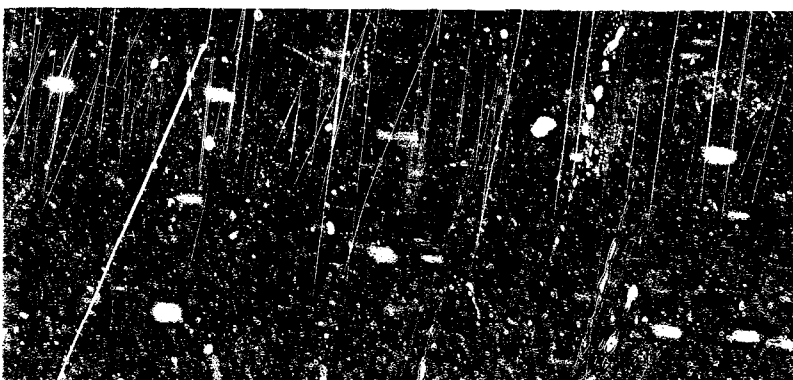


Ambient
Pressure,
mm Hg

20



10



1

Figure 3c Fully Developed CO_2 Flow at Various Pressures. Liquid Injection Velocity = 30 ft/sec, Flowrate = 0.0071 lb/sec, Orifice = 0.021 in. dia. x 0.042 in. long, Ambient Temperature, Magnification 2X.



Ambient
Pressure,
mm Hg
160



140



120



100

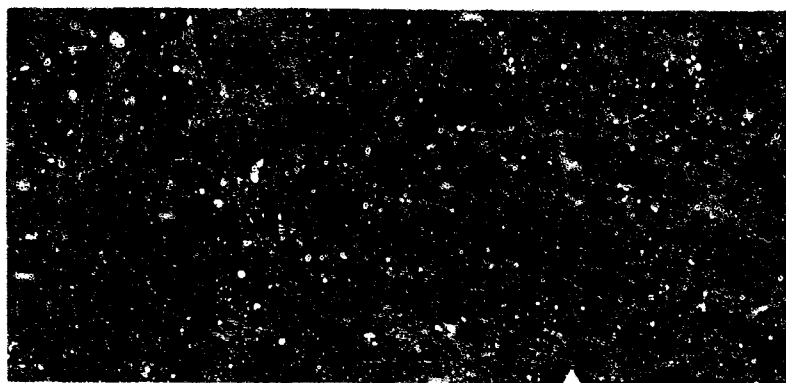


80



60

Figure 4a. Fully Developed UCMF Flow at Various Pressures. Liquid Injection Velocity = 40 ft/sec, Flowrate = 0.0055 lb/sec, Orifice = 0.021 in. dia. \pm 0.042 in. long, Ambient Temperature, Magnification 2X.



Ambient
Pressure,
in. Hg

40



20



Figure 4a. Fully Developed UMH Flow at Various Pressures. Liquid Injection Velocity = 40 ft/sec, Flowrate = 0.0055 lb/sec, Orifice = 0.021 in. dia x 0.042 in. long, Ambient Temperature, Magnification 2X.


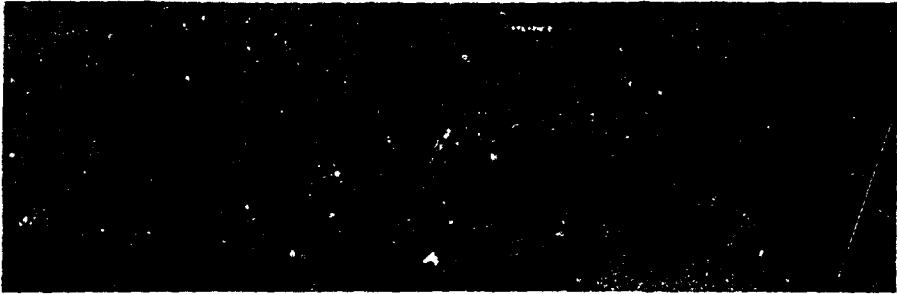

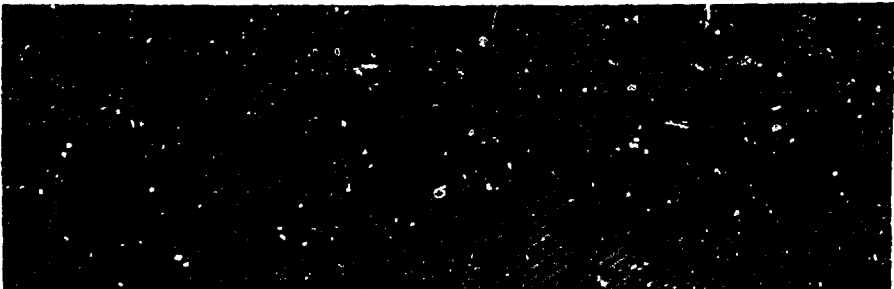
	Velocity, ft/sec	Flowrate lb/sec
	40	0.0055
	60	0.0083
	80	0.0110
	100	0.0138

Figure 5. Fully Developed UDMH Flow at Various Liquid Injection Velocities. Ambient Pressure = 140 mm Hg, Orifice = 0.021 in. dia. x 0.042 in. long, Ambient Temperature, Magnification 2X.

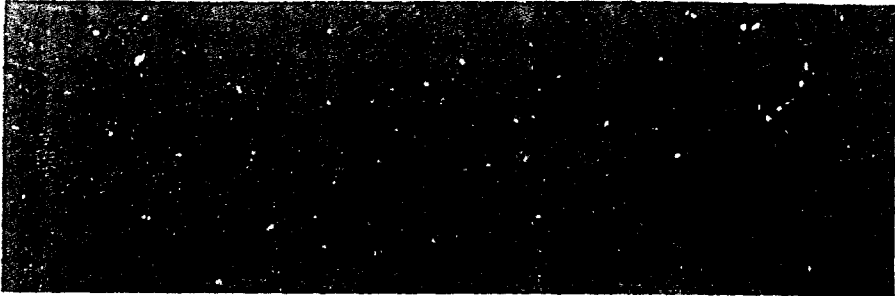
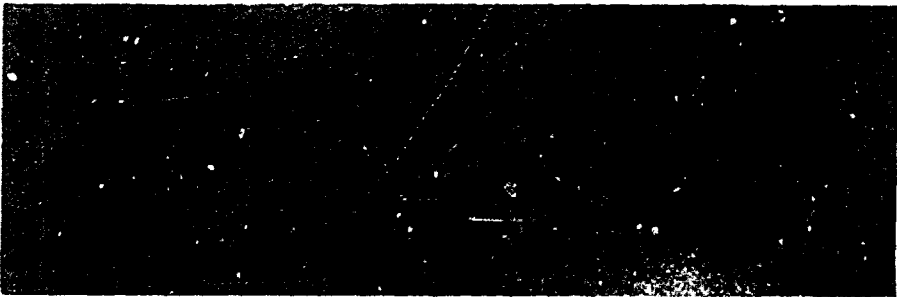
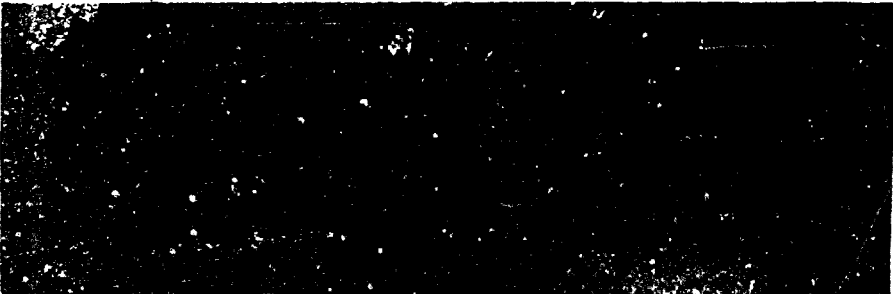
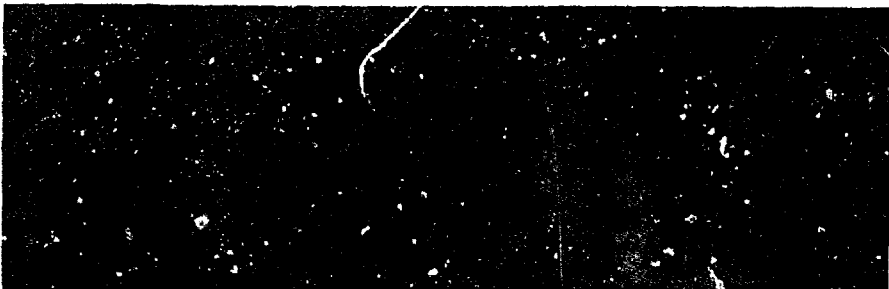
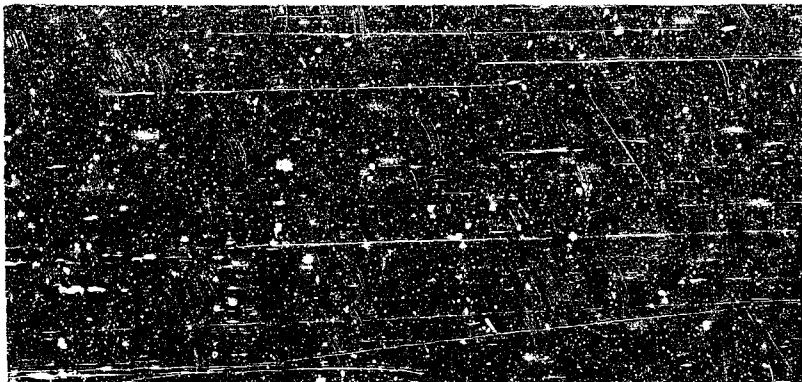
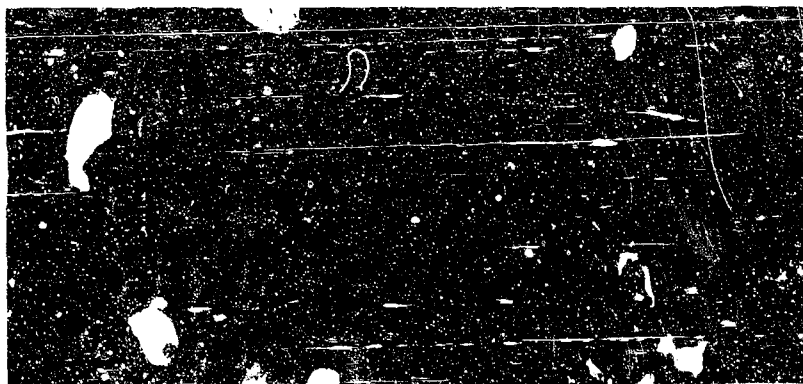
	Velocity, ft/sec	Flowrate lb/sec
	40	0.0055
	60	0.0083
	80	0.0110
	100	0.0138

Figure 6. Fully Developed UDMH Flow at Various Liquid Injection Velocities. Ambient Pressure = 1 mm Hg, Orifice = 0.021 in. dia. x 0.042 in. long, Ambient Temperature, Magnification 2X.



(a) 750 mm Hg

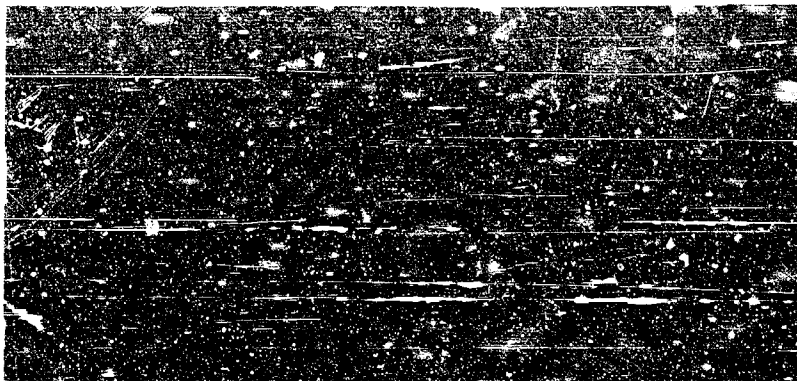


(b) 150 mm Hg

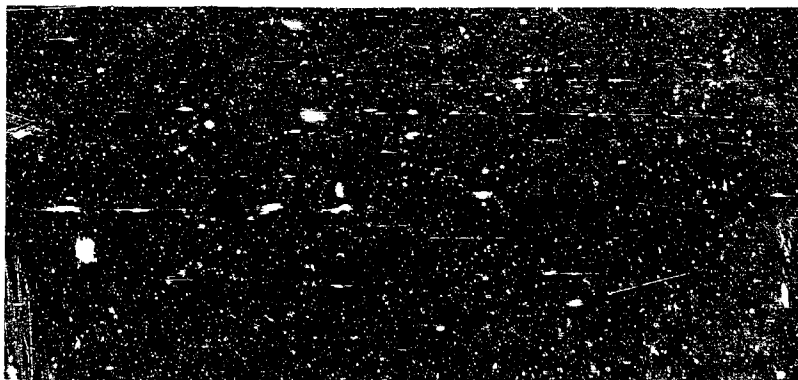


(c) 100 mm Hg

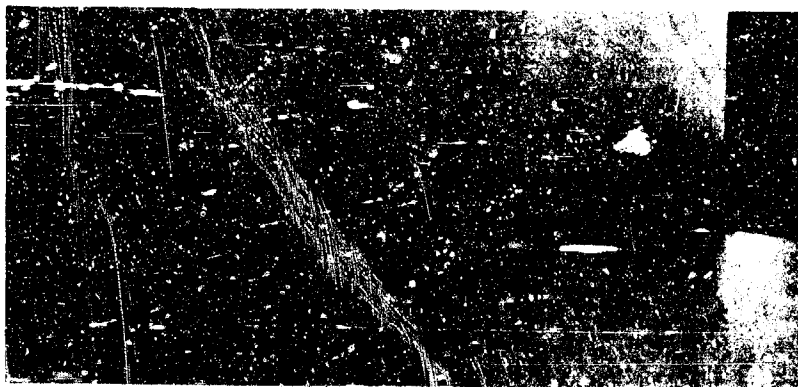
Figure 7. Fully Developed N_2O_4 Flow at Various Ambient Pressures. Liquid Injection Velocity = 110 ft/sec, Flowrate = 0.030 lb/sec, Orifice = 0.024 in. dia. x 0.048 in. long, Ambient Temperature, Magnification 1.8X.



(a) 750 mm Hg



(b) 100 mm Hg



(c) 40 mm Hg

Figure 8. Fully Developed N_2O_4 Flow at Various Ambient Pressures. Liquid Injection Velocity = 11 ft/sec, Flowrate = 0.030 lb/sec, Orifice = 0.073 in. dia. x 0.146 in. long, Ambient Temperature, Magnification 1.8X.

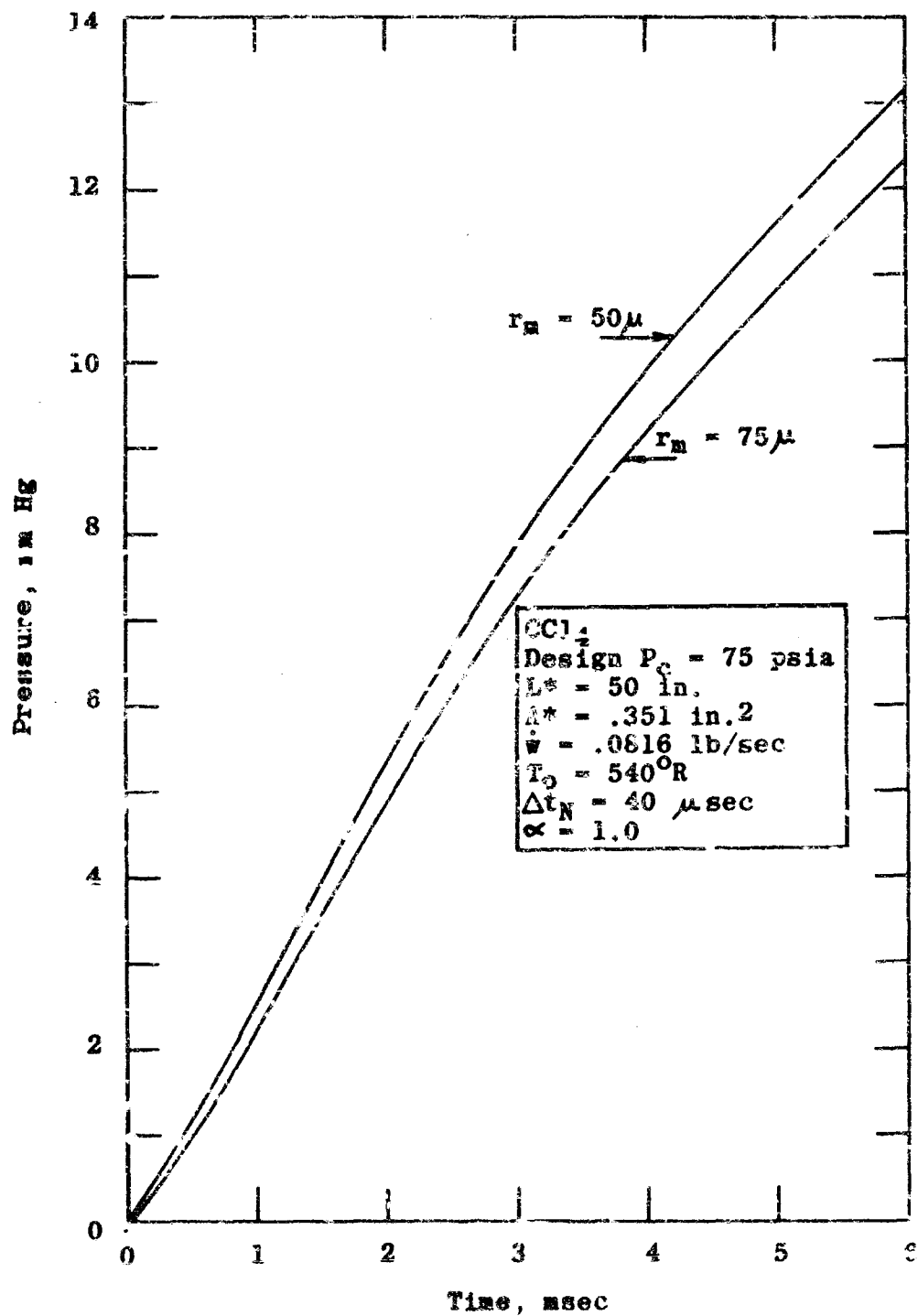


Figure 9. Effect of Drop Size on Rate of Pressurization - CCl₄

increase due to the smaller drop sizes is partially offset by somewhat lower drop temperatures. The net effect of the smaller drop sizes on chamber pressurization is rather small.

TABLE III

DROP SIZES USED IN THE COMPUTER PROGRAM
TO REPRESENT THE INJECTED PROPELLANT SPRAY

Mass-Median Drop Size microns	Radii		
	<u>i = 1</u>	<u>i = 2</u> micro feet	<u>i = 3</u>
75	83	250	720
50	58.3	171	384

Figure 9 shows that the absolute pressure difference between the two curves increases with pressure. However, the percentage pressure difference is found to be nearly constant beyond about 3 msec. The constant percentage increase in pressure is about 7% for the 30% reduction in mass-median drop size. Due to the uncertainties in actual drop sizes for propellant streams issuing into a low pressure environment, it is comforting to find that the influence of spray drop sizes on chamber pressurization is quite small.

f. Effect of Accommodation Coefficient

Oversimplified, the accommodation coefficient may be considered as a measure of the ease with which a molecule of a substance evaporates from or condenses on a liquid surface of that specie. The accommodation coefficient is unknown generally for modern hypergolic propellants as well as for many common liquids. Furthermore, it is a property extremely difficult to measure.

To determine the importance of accommodation coefficient on chamber pressurization, calculations were made with CCl_4 as propellant but with two values for its accommodation coefficient, α . The recognized value of unity for CCl_4 was used in one calculation and then it was arbitrarily reduced to one-half for a second calculation. All other inputs were kept the same in the two computer runs. The resulting chamber pressure curves are given in Figure 10.

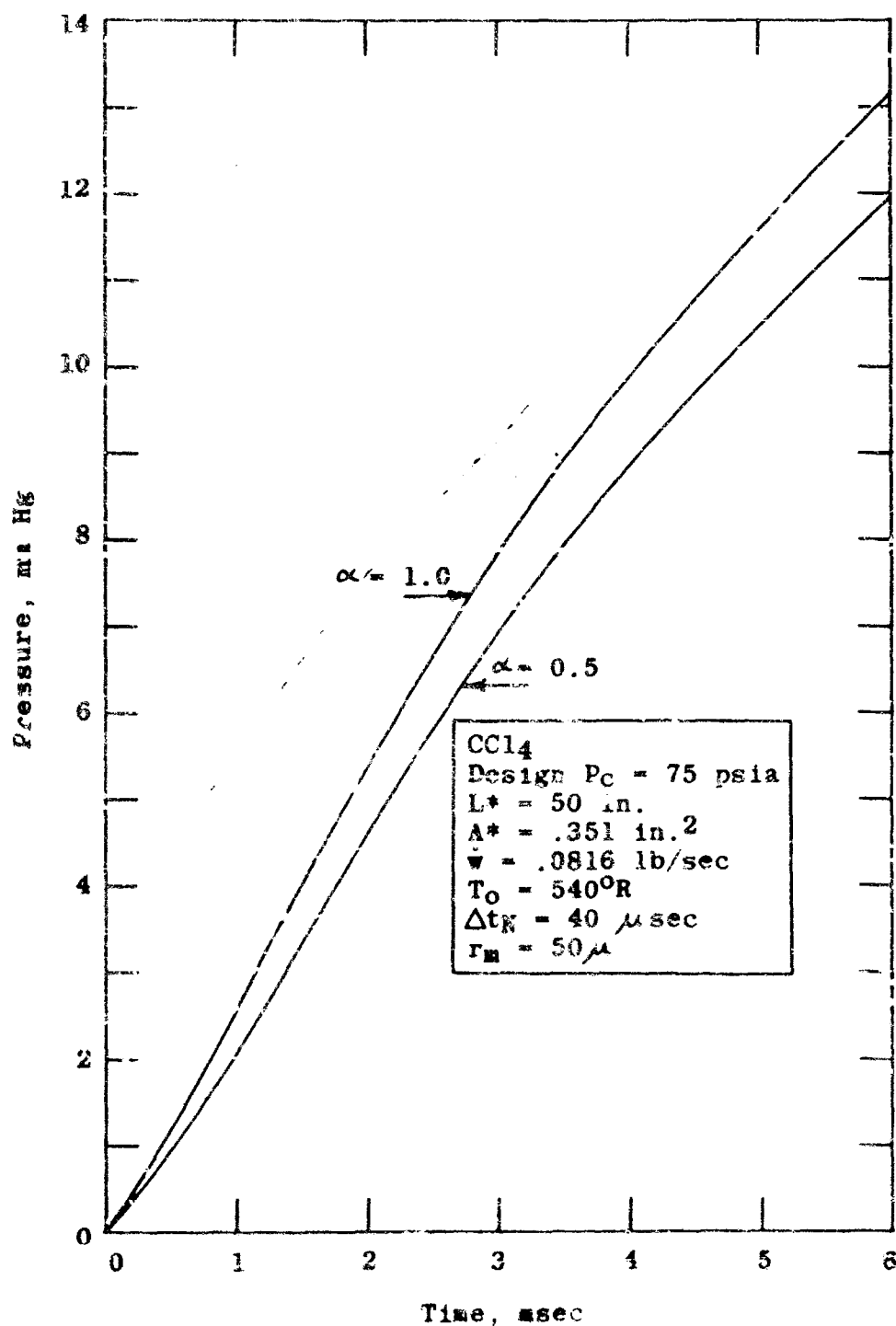


Figure 10. Effect of Accommodation Coefficient on Pressurization Rate - CCl₄

As in the case of the drop sizes, the effect of accommodation coefficient on chamber pressurization is quite small. Again, the absolute pressure difference increases with pressure; but, here, the percentage pressure difference gradually decreases as the chamber pressure increases. At 2 msec, the pressure corresponding to the lower accommodation coefficient ($\alpha = 0.5$) is almost 17% below the pressure for the $\alpha = 1.0$ case. The difference diminishes to about 11% at 4.00 msec, and to less than 10% at 6.00 msec for the 50% reduction in α .

Initially, the amount of vaporization of a given size drop when $\alpha = 1.0$ is twice that for $\alpha = 1/2$. This factor is not maintained, however, since the drop with the lower α is cooled to a lesser extent due to the lesser amount of evaporation. Thus, in the second time interval, the drop with $\alpha = 1/2$ is warmer than the drop with $\alpha = 1.0$ and therefore (by equation 1 or 2) the mass evaporated in the second time-interval by the drop with $\alpha = 1/2$ is more than one-half the mass evaporated by the $\alpha = 1.0$ drop. Consequently, the direct effect of a low accommodation coefficient is partially offset by the consequent slower drop-cooling rate. The net effect on chamber pressurization is much less than linear. Again, due to the considerable uncertainties in actual accommodation coefficients, it is fortunate that its effect on chamber pressurization is rather small.

g. Thrust Chamber Wall Effects

An experimental chamber pressurization curve was measured using high response Kistler piezoelectric pressure transducers. The experimental conditions are as follows (CCl₄ Test #16-19):

Propellant	CCl ₄
Design P ₀ , psia	200
A*, sq. in.	9.137
L*, inch	10.3
Contraction ratio	9.0
Injector	4-set doublet
Flow passage	Outside holes

Orifice diameter (4), inch	0.025
Flowrate, lb _m /sec	0.0816
Flow control	Cavitating venturi
Liquid injection velocity, ft/sec	60.7
Injector volume, cu. in.	0.0077
Initial system temperature, °R	530
Initial ambient pressure, mmHg	1

Carbon tetrachloride was used to check experimentally the theoretical chamber pressurization model because of its known accommodation coefficient and other properties required in the computer program. The CCl₄ mass flowrate is approximately one-half the total mass flow of N₂O₄/UDMH which generates 50 lbs. thrust in the same engine. Fast-acting electric venturi valves, which attach directly to the injector, were used (see Section VA2).

The experimental chamber pressure curve for CCl₄ is given in Figure 11 together with several calculated pressure curves based on the same engine and CCl₄ flow. The times for the experimental curve are measured from the first indication on the oscilloscope record of a pressure rise in the thrust chamber. The time from valve signal to propellant entry is obviously not included.

The drop sizes used in the calculations are those given in Table III for a mass-median drop size of 50 microns. The residence time limitation for the lifetime of the drops in the system is included in the computer runs as is heat transfer between the vapor and the drops. Also, the appropriate accommodation coefficient (unity) is used. The calculated pressure curve under these conditions is given in Figure 11a; it is labeled "no wall heating". For the first 1-1/2 msec, agreement between the calculated and experimental curves is considered satisfactory; beyond that time agreement is clearly inadequate.

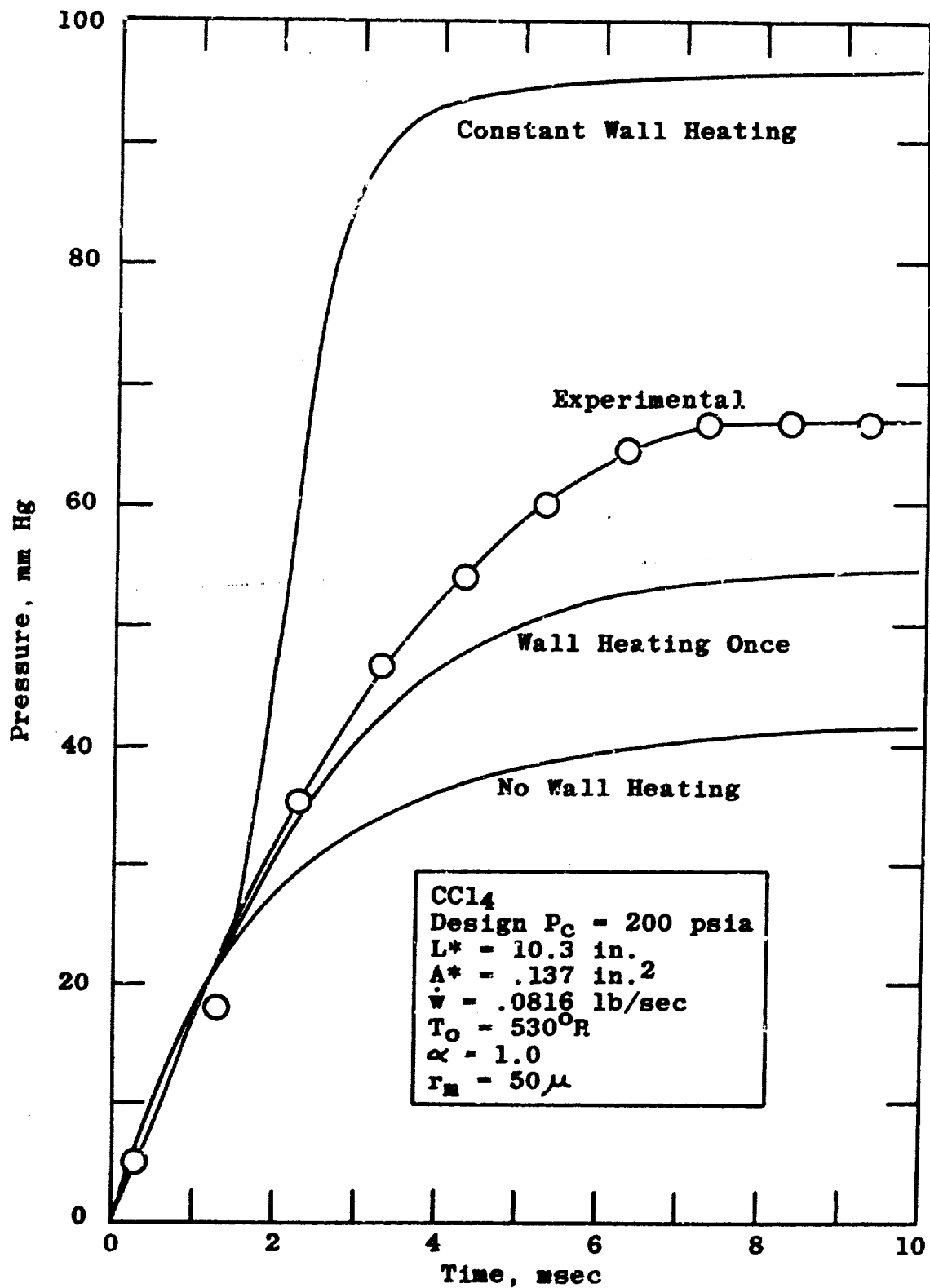


Figure 11a. Experimental and Theoretical Chamber Pressure Histories - CC14

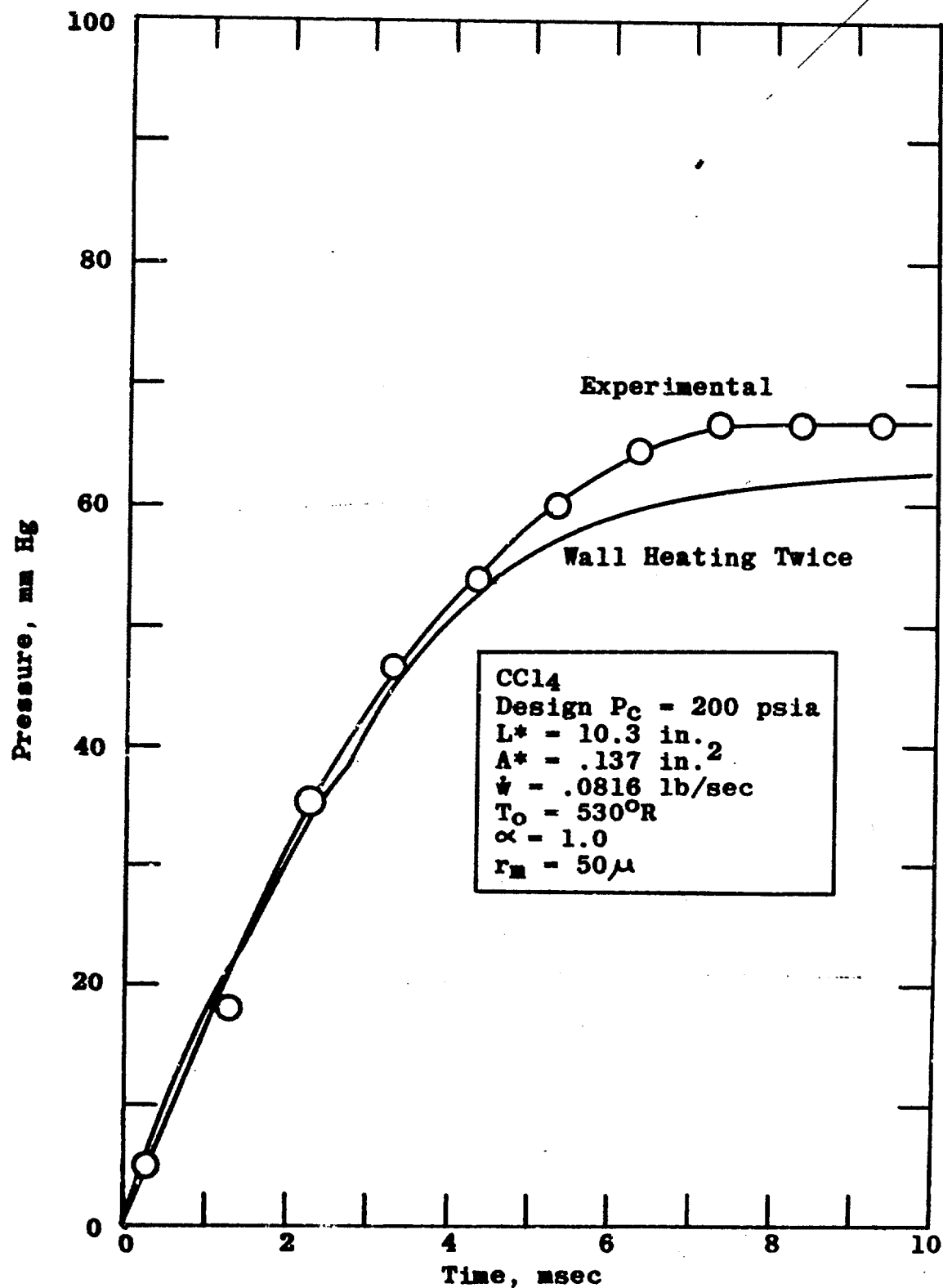


Figure 11b. Experimental and Theoretical Chamber Pressure Histories - CCl₄

According to the definition of residence time given previously (the average time for a drop traveling at the injection velocity to reach the chamber wall), the residence time for the case under consideration is 1.4 msec. Drops that have been in the system for this length of time have cooled substantially; in the present case, after 1.4 msec of flow, the temperature difference between the first drops that entered the system and the chamber wall ranges from 50 to 70°F for the three classes of drops. This driving force leads to heating of the drops when they impinge on the chamber walls, the extent of the heating depending on several factors. Two cases are considered.

In one case, the drops are brought immediately to the chamber wall temperature once they have been in the system for one residence time period. The drops then continue to undergo evaporation for a second residence time period, at the end of which the drops are made inactive. This model of heat addition to the drop-gas system crudely simulates the following. A drop undergoes evaporation during the time required for it to travel to the chamber wall. When the drop strikes the chamber wall, the drop is warmed to the wall temperature and then bounces off the wall back into the thrust chamber where it undergoes further evaporation. Evaporation continues for another residence time period, at which time the drop passes through the nozzle. The chamber wall is considered an infinite heat source and an infinite heat transfer rate from the wall to the drop is implied.

The chamber pressurization curve calculated for these conditions is given in Figure 11a and is labeled "wall heating once". This curve coincides initially with the "no wall heating" curve. Once the first drops to enter the system reach the chamber walls (1.4 msec), the two pressure curves begin to diverge because of the greater evaporation from the "heated" drops. The ensuing difference between the two calculated curves is a measure of the amount of heat added to the vapor-drop system by the chamber walls. Agreement between the experimental and calculated curves is improved substantially.

The second case of heat addition considered simulates drops sticking to the chamber walls rather than bouncing off the walls after being heated. In this case, the drops are again brought to the wall temperature once they strike the wall. But here the drop temperatures are maintained at the wall temperature while the drops undergo continued vaporization until their radii decrease to one-tenth their

initial values (99.9% of the mass of the original drop evaporates). However, since the vaporization is kinetically controlled, this case is not the same as assuming complete vaporization, as will be shown in the following section. In the calculation, the shape of the drop is maintained spherical, that is, although the drop sticks to the wall, the shape of the drop is not altered.

The chamber pressurization curve calculated for the condition of "constant wall heating" is also given in Figure 11a and is labeled as such. Clearly the experimental curve is surrounded by the two calculated cases of heat addition to the system. One concludes, therefore, that despite the rather short times involved during chamber pressurization due to propellant vaporization, the vapor-drop system is non-adiabatic. Additional experimental evidence verifies qualitatively this conclusion. With a Plexiglas chamber and stainless steel nozzle precooled with dry ice, the pressure in the chamber rose during the first residence time period only.

A calculation was made in which the drops were brought to the wall temperature twice, once after the first residence time period and again after a second residence time period. Evaporation continued for a third residence time period at the end of which the drops were made inactive. The calculated curve is given in Figure 11b together with the experimental curve given in Figure 11a. The good agreement between the curves (10%) is a measure of the amount of heat addition to the vapor-drop system and its time dependency. However, this model of heat addition is of course unrealistic since some splattering of the drops would result when they strike a wall, some of the liquid mass sticking to the wall and some bouncing off with very little heating.

h. Summary of Values-Steady State Pressure and Temperature

A comparison of steady state values calculated for CCl_4 according to various models of chamber pressurization is given in Table IV. An experimental value of the steady state chamber pressure resulting from CCl_4 vaporization in the engine under consideration is included also.

Best agreement with the experimental value of chamber pressure is obtained with the "wall heating twice" model given above.

TABLE IV
SUMMARY OF CALCULATED AND EXPERIMENTAL STEADY STATE
VALUES FOR THRUST CHAMBER PRESSURIZATION BY CCl_4

Model	Gas Pressure mmHg	$\frac{P_{\text{calc}} - P_{\text{exp}}}{P_{\text{exp}}}$ %	% of Flow Vaporized	Gas Temperature $^{\circ}\text{R}$	Condensed Phase Temperature $^{\circ}\text{R}$
Thermodynamic Phase Equilibrium	40.6	-39	6.5	499	499
Kinetic, no wall heating (CCl_4/Z)	42.4	-36	6.7	522	500*
Kinetic, wall heating once (CCl_4/ND)	54.9	-18	8.9	524	508*
Kinetic, wall heating twice (CCl_4/TT)	63.2	-5.4	10.1	526	514*
Experimental ($\text{CCl}_4/\text{I6-19}$)	66.8	---	10.7**	---	---
Kinetic, constant wall heating (CCl_4/EE)	95.9	+44	15.4	530	530*
Complete Vaporization:					
i. For $T_g = T_{\text{TP}}$	582	+770	100	450	all vapor
ii. For $T_g = T_{\text{wall}}$	631	+850	100	530	all vapor

* Approximate average for all active drops in the system

** Calculated from measured P_g assuming $T_g = 526^{\circ}\text{R}$

The lowest calculated value of steady state chamber pressure results from a model in which the temperature of the system (both vapor and condensed phases) is assumed to be that temperature which gives a vapor pressure equal to the gas pressure in the chamber. That is, phase equilibrium prevails in an adiabatic system. Equations 3 through 6 of Reference 1 were used.

If one assumes complete vaporization of the propellant, in effect a gaseous feed, very high steady state chamber pressures result, the values depending somewhat on the assumed temperature. This model is very different from the computer calculated case for constant wall heating of the drops, once they strike the chamber wall. The latter model is kinetically controlled which results, in the present case, in only 15% of the propellant flow being vaporized, as given in the table.

In summary, the model which best predicts thrust chamber pressurization due to propellant vaporization is the model discussed herein which is based on physical kinetics and a non-adiabatic system. For two principal reasons, however, the model as it presently exists is not complete. The first reason is that the heat addition aspect needs to be made general. Secondly, a comparison between experimental and calculated pressure curves for considerably more volatile propellants such as N_2O_4 and Compound A shows that a finite time is required for the flow, once initiated, to build up to the full flowrate. Substantial "flashing" of these propellants occurs within the injector volume upon propellant valve opening. Therefore, only vapors emerge from the injector initially, then a vapor-liquid mixture, and finally all-liquid flow is achieved. During the vapor and vapor-liquid periods of flow, the mass flowrate is substantially below the full, nominal flowrate. Consequently the pressure in the chamber rises more slowly than would be the case without the vapor and two-phase flow condition.

C. Reaction Kinetics

The prediction of ignition delays in hypergolic systems necessitates an accurate knowledge of the rate constants of the reaction leading to ignition. A first step toward this goal is the determination of the overall reaction rate as a function of the concentrations of reactants and temperature. A second step is to assess the exact mechanism of reaction.

This part of the report describes the progress which has been accomplished toward the solution of these two problems. It is organized as follows. First a background of thermal explosion theories with regard to their use for the determination of reaction kinetics is presented. These considerations are followed by a description of the experimental apparatus and procedure. A following section analyzes the experimental data and then the experimental results are discussed, including our present knowledge of a product that is formed by preignition reactions of N_2O_4/N_2H_4 -type fuels.

1. Theory of Thermal Explosions

Thermal explosions may be expected to develop in a reacting system whenever the heat liberated from exothermic reactions exceeds the rate of heat dissipation by conduction or by convection. Because of the exponential dependence of the reaction rate on temperature, the rate increases rapidly as the temperature rises until an explosion results.

The quantitative mathematical treatment of thermal explosions has been developed mainly by Semenov (Ref. 4), Todes (Ref. 5), Frank-Kamenetskii (Ref. 6), Rice (Ref. 7), Chambre (Ref. 8), and Thomas (Ref. 9, 10). The progress in the theory has consisted mainly of finding methods of integration of the differential heat equation which governs the process. A good review of the use of explosion limit phenomena for elucidation of reaction mechanism is given by W. Roth and D. Scheer (Ref. 11) in the Advances in Chemistry Series of the A.C.S.

Two questions are generally considered in the theory. The first is to find the so called critical conditions for ignition. This aspect of the theory does not consider the time variable. All one is concerned with is the minimum values of the parameters, (pressure, concentrations, temperature, characteristic length) above which an explosion develops. This problem is relatively simple and has been solved analytically for a number of configurations (slab, cylinder, and sphere). As will be seen, the critical conditions for ignition (or explosion limits) may serve to determine the global kinetic factors of the reaction.

The second question concerns the time interval which elapses prior to the development of a thermal explosion. This problem is more complex and analytical solutions are known only for the case of a reaction of zero order. A numerical solution

has been given by Rice (Ref. 7) in the case of a first order reaction. No attempt to treat the case of reactions of higher order has ever been made.

In the following, we will be concerned only with the explosion limits. We will discuss their use for the establishment of reaction kinetics.

a. Explosion Limits

Let us consider a reactive mixture contained in a closed vessel of constant wall temperature T_0 . In this case the transfer of heat is only by conduction as convection currents are assumed to be negligible. The appropriate equation for thermal balance between the heat generated by the chemical reaction and heat conducted away is then:

$$\lambda \nabla^2 T = -QW \quad (29)$$

where

- λ - thermal conductivity of mixture ($\text{cal sec}^{-1}\text{cm}^{-1}\text{K}^{-1}$)
- T - gas temperature ($^{\circ}\text{K}$)
- Q - heat of reaction (cal mole^{-1})
- W - reaction velocity ($\text{mole sec}^{-1}\text{cm}^{-3}$)
- ∇^2 - Laplacien operator (cm^{-2})

We have now to find a solution of (29) under the given boundary conditions. As long as such a solution exists, the system is stable. The value of the parameters at which such a solution becomes impossible is then taken as a condition of inflammation. For a wide class of reactions, one may write the Arrhenius reaction rate expression as

$$W(c_a, c_b, T) = A c_a^m c_b^n \exp\left(-\frac{E}{RT}\right) \quad (30)$$

where c_a and c_b are concentrations of reactants A and B, respectively. E is the energy of activation (cal mole^{-1}) and A is the so-called frequency factor. As a first approximation

we will consider A as constant*. The symbols m and n are the partial orders relative to A and B , respectively. By definition the total order of reaction, N , is $N = m + n$.

Substituting expression (30) for W in equation (29) the thermal balance equation becomes:

$$\nabla^2 T = -\frac{Q}{\lambda} A c_a^m c_b^n \exp\left(\frac{-E}{RT}\right) \quad (31)$$

Analytical solutions of equation (31) can be found if the two following approximations are made.

1) The exponent in the term $e^{-E/RT}$ is expanded as first proposed by Todes in a power series $(T-T_0)/T_0$ (where T_0 is the wall temperature) and powers higher than one are neglected. The following expression results:

$$\frac{-E}{RT} = \frac{-E}{RT_0} \left[1 - \frac{T-T_0}{T_0} \right]$$

It is worthwhile to note, since the expansion is valid only for values of T/T_0 close to unity, that Todes approximation implies $RT_0/E \ll 1$.

2) The concentrations of reactants are assumed to vary only slightly during the induction period so that the effective concentration of A and B at the ignition point may be approximated with the initial concentrations c_{a0} and c_{b0} , respectively.

Under the above assumptions it has been shown first by Frank-Kamenetskii that the criterion for thermal ignition is:

$$\delta = \frac{Q}{\lambda} \frac{E}{RT_0^2} r^2 c_{a0}^m c_{b0}^n A \exp\left(-\frac{E}{RT_0}\right) \quad (32)$$

* Strictly speaking A is only constant in the case of a reaction of the first order. When the order of reaction is superior to one, A is a weak function of temperature.

Expressing c_{a0} and c_{b0} in terms of total pressure, P , and initial mole fractions X_{a0} and X_{b0} of A and B,

$$c_{a0} = \frac{n_{a0}}{V} = \frac{P_{a0}}{RT_0} = X_{a0} \frac{P}{RT_0} \quad \text{and} \quad c_{b0} = X_{b0} \frac{P}{RT_0}$$

where

n_{a0} = initial moles of A in the vessel

V = volume of vessel

P_{a0} = partial pressure of A

P_{b0} = partial pressure of B

Substituting these values of c_{a0} and c_{b0} in (32) gives:

$$\delta = \frac{Q}{\lambda} \frac{E}{RT_0^2} r^2 X_{a0}^m X_{b0}^n \left(\frac{P}{RT_0} \right)^N A \exp \left(-\frac{E}{RT_0} \right) \quad (33)$$

In this expression r is a characteristic length and δ is a non-dimensional constant. The numerical value of δ depends on the geometry of the vessel and has the value of 1, 2 and 3.32 in the case of a slab, cylinder and sphere, respectively.

b. Determination of Reaction Kinetics from Explosion Limits

Equation (33) is the basic equation used for the determination of reaction kinetics from explosion limits data. In the following sections three categories of explosion limit data, depending on the parameter which is maintained constant, are considered.

1. Overall Order of Reaction, N

If the temperature and composition of the mixture are maintained constant and the vessel diameter is varied, equation (33) can be written in the form

$$P^N r^2 = \frac{T_0^{N+2} R^{N+1} \delta \lambda \exp\left(\frac{E}{RT_0}\right)}{E Q A X_{a0}^m X_{b0}^n} = \text{constant}$$

(34)

$$\text{or } \ln P = -\frac{2}{N} \ln r + \text{constant}$$

Thus, a plot of $\ln P$ vs $\ln r$ yields a straight line from whose slope one can determine N , the overall order of reaction.

ii. Partial Orders of Reaction, n and m

If the temperature and reactor size are maintained constant and the composition is varied, equation (33) can be written as

$$P^N = \frac{\text{constant}}{X_{a0}^m X_{b0}^n}$$

$$\text{with constant} = \frac{T_0^{N+2} R^{N+1} \delta \lambda \exp\left(\frac{E}{RT_0}\right)}{E Q A r^2}$$

It can easily be shown that the pressure limit has a minimum for a value of X_{a0} equal to $\frac{m}{n}$, allowing a determination of the partial orders m and n if the total order of reaction, N , is known.

iii. Activation Energy, E

If the composition and the reactor size are maintained constant and the initial temperature, T_0 , is varied, equation (33) can be written as

$$\ln\left(\frac{P}{T_0^{1+N/2}}\right) = \frac{E}{NRT_0} + \frac{1}{N} \ln \frac{\delta \lambda R^{N+1}}{E Q A r^2 X_{a0}^m X_{b0}^n}$$

Thus, a plot of $\ln \left(P/T_0^{1+2/N} \right)$ vs. $\frac{1}{T_0}$ gives with a good approximation a straight line with slope equal to $\frac{E}{R}$. This permits a determination of the activation energy, E , if the overall order of reaction, N , is known.

To summarize, the overall order of reaction N can be obtained from the effect of vessel size on ignition pressure limits. Also, the composition effect allows a determination of the partial orders relative to each reactant. Finally, the effect of temperature allows a determination of the activation energy.

2. Experimental Apparatus

The considerable reactivity of N_2O_4 with the hydrazine-type fuels requires that an experimental technique be used that slows the ignition reaction to a point which permits valid measurements to be made. Several techniques are possible: low temperatures, considerable dilution by an inert substance, or low pressures. The latter was chosen for several reasons. Since the reactions of interest are gas phase reactions, low temperatures are ruled out. Dilution by an inert substance is undesirable in general for kinetic investigations due to possible "third-body" effects, or influence, on reaction mechanisms. The low pressure technique was adopted so that the desired gas-phase reactions of the undiluted reactants could be studied at temperatures within the range encountered during the start-up of operational reaction control systems.

The apparatus used for the determination of the kinetic factors required in the mathematical model is shown schematically in Figure 12. It consists of vaporizing and flow metering sections, a flow reactor and a low pressure housing with observation windows and instrumentation.

a. Vaporization of Propellants

1. Fuels: Since the substances studied are liquids at room temperature, whereas vapor is desired, it is necessary to provide a means for vaporizing the propellants. All four hydrazine-type fuels investigated, N_2H_4 , MMH, UDMH, and 50-50, are hazardous and could give rise to explosive decomposition when vapors are in contact with metal. Therefore, an all glass vaporization system was used. The liquid was vaporized in a glass coil heated at $90^\circ C$, and was allowed to expand in a 1 liter flask maintained at the same temperature.

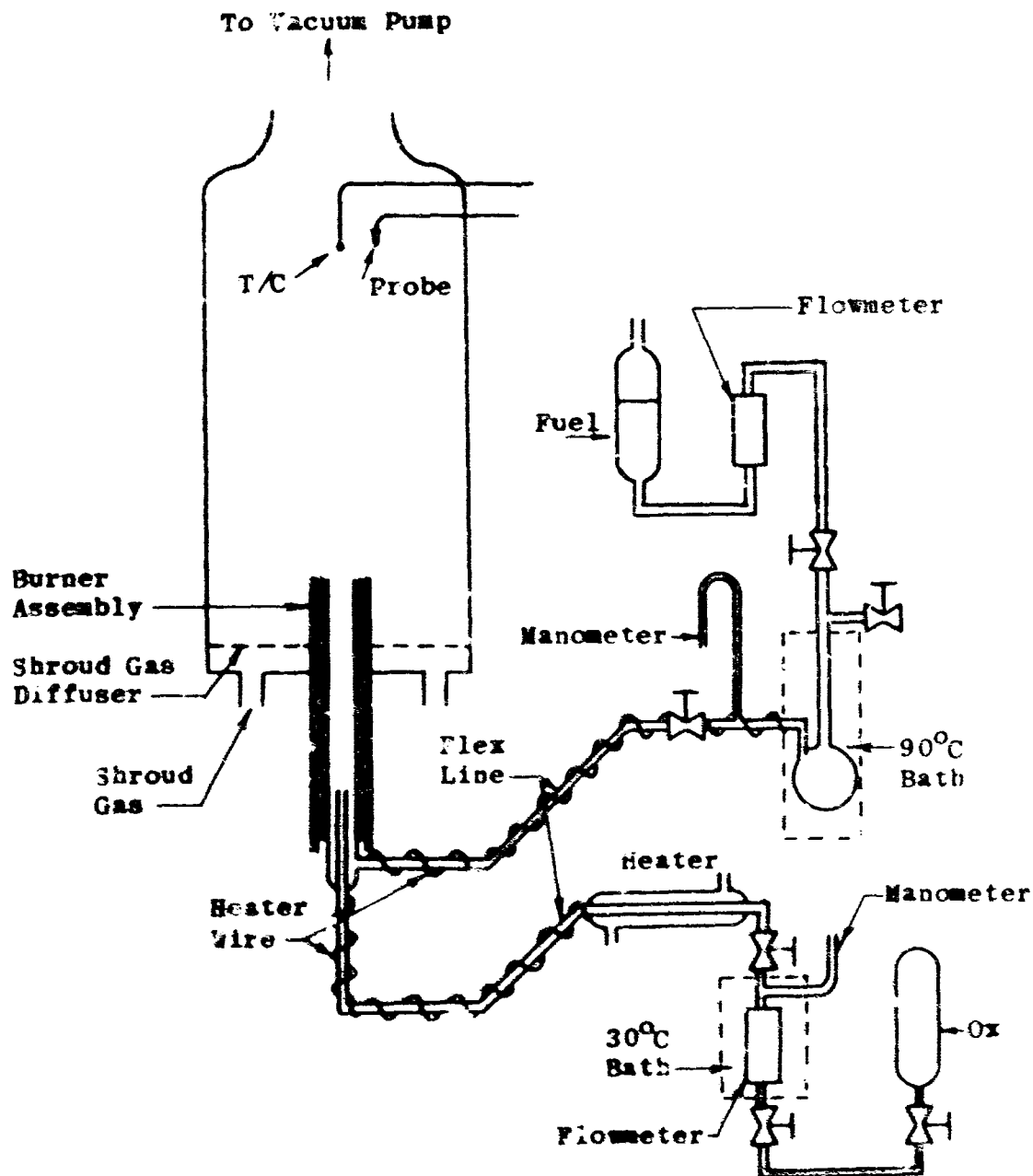


Figure 13. Schematic of Low Pressure Ignition Apparatus for Tasks I and II

The pressure in the vaporizer was monitored by a mercury manometer as shown in Figure 12. The vapors were then admitted to an all-glass, heated line connected to the flow reactor.

11. N_2O_4 : Gaseous N_2O_4 was taken directly from a cylinder immersed in a constant temperature bath at $30^\circ C$. The vapor pressure at this temperature is a little above 1 atmosphere. The heat source was sufficient to maintain steady flow conditions up to 0.2 gr /sec. This flow was adequate for the purpose of the experiments.

b. Flowrating Systems

1. Fuel: The hydrazines were flow rated in the liquid phase with calibrated rotameters prior to entering the vaporizer described above. Each of the fuels was calibrated individually. It took, in general, a few minutes before steady flow conditions were reached in the whole flow system. Stabilized flows were established in each test before data were taken.

11. N_2O_4 : Nitrogen tetroxide was flow rated in the gaseous form at a pressure slightly below ambient (800 mm Hg). The rotameter was maintained at constant temperature slightly above ambient, $30^\circ C$. Under these conditions the vapors are a mixture of N_2O_4 and NO_2 . Therefore, the flowrator was calibrated in terms of mass flow by collecting the vapors in a condenser at liquid nitrogen temperature and weighing the mass collected during a measured time period.

c. The Flow Reactor

The flow reactor shown schematically in Figure 12 was a pyrex tube open at one end to the ambient atmosphere of the low pressure housing described below. The standard flow tube in which most of the experiments have been conducted had a diameter of 4.7 cm and a mixing length of 51 cm. Two other diameters of 2.2 cm and 6.6 cm also were used. The flow tube was located in an insulated housing and could be heated electrically over its entire length up to temperatures of $300^\circ C$. Before entering the flow tube, the reactants were preheated to the reactor temperature and were premixed in a small section whose diameter is approximately 1/3 that of the reactor.

d. Concentric Tube Arrangement

Some ignition experiments were performed using the concentric tube arrangement shown in Figure 13. The concentric tube arrangement differed from the flow reactor discussed

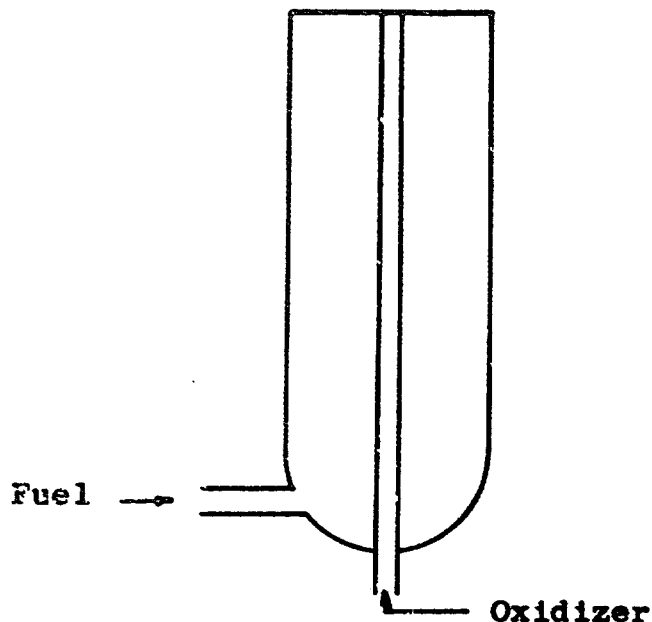


Figure 13. Concentric Tube Reactor

above in that the exits of the inner and outer tubes were in the same plane and mixing took place in the vacuum tank. These experiments were not intended for reaction kinetic study but were performed in order to compare the hypergolicity of the N_2O_4 /hydrazines combinations with the F_2/H_2 system on the same scale. The oxidizer was fed through the inner tube (1.2 cm in diameter) and emerged as a free jet in a concentric flow of fuel (4.7 cm in diameter).

e. Low Pressure Housing

The low pressure housing was made of stainless steel for corrosion resistance. It is a cylinder three feet high and 12 inches in diameter. The reaction tube and insulated housing are mounted in a stainless steel tube which is water cooled to prevent heat transfer to the surrounding shroud gas. The reactor assembly is installed through the lower flange of the low pressure vessel by means of a vacuum feed-through and can be moved up and down automatically. The pressure in the low pressure vessel is regulated both by a throttle valve in the connecting line to the high capacity pump and by an appropriate bleed of shroud air or nitrogen which has the additional function of diluting the corrosive gases.

f. Temperature Measurements

The temperature in the flow tube or in the exhaust stream is measured by means of Pt - Pt/Rh thermocouples made of wires of 0.2 mm in diameter. In one experiment the thermocouple bead was covered with a coat of SiO_2 to prevent the possibility of catalytic effects. As the readings did not differ from those obtained with the bare thermocouple it is concluded that no catalytic surface heating of the thermocouple took place and that the thermocouple, coated or uncoated, indicated the true temperature of the gas. Subsequently, most experiments were performed with an uncoated thermocouple.

g. Gas Sampling

The sampling probe was made of a pyrex tube, 0.8 cm in diameter, which had been drawn at the extremity to reduce its diameter. The diameter of the throat was 0.2 mm. As it was not intended to quench the reactions, the throat diameter was not of critical importance. The gases were withdrawn into a pre-evacuated vessel and were later analyzed mass-spectroscopically.

3. Experimental Results

a. Ignition Limits

1. Flow Reactor: The procedures for the flow reactor tests are as follows. The apparatus was first evacuated. Then a bleed of nitrogen of about 1 cfm was admitted into the pressure vessel and by adjusting the throttling valve in the vacuum line a pressure of about 0.5 mm Hg was maintained in the vessel. Gaseous fuel and oxidizer were then allowed to flow into the reactor. When steady flow conditions were reached the ambient pressure in the chamber was gradually raised by bleeding air into the vacuum line through an auxiliary valve. Ignition occurred at some minimum pressure and was observed visually. It was somewhat difficult to distinguish if ignition occurred in the tube or in the free jet. However, the occurrence of ignition was unmistakable as it resulted in a visible flame either anchored at the open end of the reaction tube or flashing back and forth in the tube.

All experimental data obtained with the hydrazine-type fuels are reported in Tables V, VI, VII, and VIII. Minimum ignition pressures for the vapor-mixtures of

NO₂/MMH, NO₂/UDMH, NO₂/50-50 and NO₂/N₂H₄ are given in the respective tables. The important parameters from a kinetic point of view are, as discussed above, the equivalence ratio ϕ , the initial temperature of the reactor, T_0 , and the reactor diameter. These are listed respectively in Columns I, II, and III. Column IV gives the length-to-diameter ratio (L/D), and Column V, the mean flow velocity of the gas in the reactor. The minimum ignition pressures are reported in Column VI. The order in which the data are reported in each table has been organized so as to show the effect of the individual parameters listed above.

ii. Concentric Flows

Minimum ignition pressures using the concentric flow arrangement of Figure 13 were obtained for NO₂/MMH and for F₂/H₂. The procedure with NO₂/MMH was similar to that used for the determination of the ignition limit in the flow tube arrangement. First, the desired flows were established with a low ambient pressure in the low pressure housing. Then the pressure was gradually raised until ignition occurred. The result of the ignition was a diffusion flame which burned at the exit of the inner tube.

With F₂/H₂ the experiments were performed in the large tank used in Task III of the program. The flows of H₂ and F₂ were metered by means of calibrated orifices in a manner similar to that described for the impinging stream tests. The control valves were preset for a running time of 1 second. Each experiment was conducted with a given pressure in the tank. The limit of ignition was found by trial and error. Here again the ignition resulted in a diffusion flame anchored at the open end of the inner tube. The minimum ignition pressures with the pertinent flow parameters are given in Table IX. It is seen that under similar flow conditions F₂/H₂ has an ignition pressure lower than that of NO₂/MMH.

b. Temperature Profiles

A typical longitudinal profile taken along the center line in the 4.7 cm diameter tube with a flow of 3.2 meters/sec of stoichiometric NO₂/MMH at 5.1 mm Hg is shown in Figure 14. The figure also shows profiles taken without flow in the reaction tube, one (Curve I) immediately before, and another (Curve III) immediately after the experiment. The data shows clearly that a low temperature reaction with heat evolution is taking place before ignition and corroborates, therefore, the general

TABLE V

MINIMUM IGNITION PRESSURES OF NO₂/MMH VAPORS
IN FLOW REACTORS

ϕ	T ₀ °K	D cm	L/D	U m/sec	P mmHg	P _{avg.} mm Hg
0.25	298	4.7	4.76	-----	>11	
0.5				----- 2.29	>10 6.00	6.0
1.0				0.96 1.50 3.18	5.56 5.35 5.05	5.32
2.0				1.72 2.29 3.79	4.00 4.50 5.45	4.65
2.5				1.84 2.47 3.89	4.15 4.65 6.05	4.60
3.0				1.85 2.43	4.55 5.20	4.87
4.0				2.07 2.78	4.80 5.35	5.07
5.0				2.34 3.05	4.90 5.66	5.28
1.0	404	4.7	4.76	4.95 5.80 8.06 9.66 12.1 15.7	2.2 2.5 2.7 3.0 3.0 3.6	2.83
1.0	298	4.7	10.8	0.88 1.48 2.75 3.57 5.05 6.44	6.1 5.6 5.85 6.0 5.3 5.3	5.67
2.5				2.64 3.48 5.10	2.9 3.3 4.5	3.57

TABLE V (continued)

ϕ	T_{01}	D cm	L/D	U m/sec	P mm Hg	P _{avg.} mm Hg
1.0	293	6.6	4.8	0.45 0.94 2.17 3.82 4.71	6.0 4.35 3.60 3.55 3.6	4.22
2.5				1.69 2.20 3.75	2.30 2.65 3.10	2.68
1.0	298	6.6	9.5	0.46 1.21 2.63 4.05 4.85	5.85 3.37 3.10 3.35 3.50	3.83
2.5				1.94 2.64 3.94	2.0 2.2 2.95	2.38
1.0	298	2.2	11.5	2.16 3.25 6.49 7.82 9.41	11.3 11.3 11.3 12.5 13.0	11.9
2.5				4.54 5.80 9.54	7.7 8.9 11.0	9.2
1	298	2.2	30	3.56 7.20	10.3 10.2	10.25
2.5				5.29 7.28 12.5	6.6 7.2 8.4	7.4
0.5 0.75 1.0 1.5 2.0 3.0				5.25 6.44 8.33 10.03 10.05 -----	14.0 11.4 8.6 7.3 7.3 >16.0	

NOTES: $\phi = \frac{(F/O) \text{ Actual}}{(F/O) \text{ Stoich. volume}} = \text{Equivalence Ratio}$

T_0 = Initial wall temperature of flow reactor

D = Diameter of reactor

L = Length of reactor

U = Initial gas velocity

TABLE VI

MINIMUM IGNITION PRESSURES OF NO₂/UDMH VAPORS IN FLOW
REACTORS

ϕ	T _{OK}	D cm	L/D	U m/sec	P mm Hg	P _{avg.} mm Hg
0.25	298	4.7	4.76	3.98 4.23 6.40 5.85	5.1 4.8 5.4 5.9	5.3
0.5				2.98 4.67 8.31	4.4 4.6 4.4	4.5
1.00				2.39 4.78 6.60 7.50 11.61	3.0 3.0 2.9 3.1 3.5	3.1
1.50				4.38 4.20	2.4 2.5	2.45
2.00				3.44 6.89	2.5 2.5	2.5
3.00				2.91 4.01 7.72	2.3 2.5 2.6	2.67
4.00				3.33 4.59	2.3 2.5	2.4
5.00				3.44 4.59	2.5 2.5	2.5
6.00				3.68 4.95	2.6 2.9	2.75
7.00				5.09	3.1	
1.00	341	4.7	4.76	5.13 6.44 8.64 10.95 13.69 17.21	1.6 1.7 1.9 2.0 2.0 2.7	1.98

TABLE VI (continued)

ϕ	T_{OK}	D cm	L/D	U m/sec	P mm Hg	P _{avg.} mm Hg
1.00	403	4.7	4.76	19.4 23.6 24.9	1.0 1.1 1.3	1.2
1.00	298	4.7	10.8	2.17 3.54 4.78 5.62 7.71	3.3 2.7 3.0 3.4 3.1	2.9
3.00				4.18 6.27 10.03	1.6 1.6 2.0	1.73
4.00				4.78 6.37 8.25	1.6 1.8 1.9	1.76
1.00	298	2.2	11.5	6.33 9.77 12.7 16.3 18.9	6.9 6.7 6.9 6.7 7.2	6.9
4.0				13.2 17.8	5.3 5.9	5.6

TABLE VII

MINIMUM IGNITION PRESSURES OF $\text{NO}_2/50-50$ VAPORS IN FLOW REACTORS

ϕ	T_o °K	D cm	L/D	U m/sec	P mm Hg	P _{avg.} mm Hg
1.0	298	4.7	10.8	2.30 2.77 3.68 6.54 7.16 8.01	3.6 4.0 4.5 3.35 3.85 4.3	3.93
2.26				3.62 5.46 6.24 6.20	2.0 2.1 2.45 3.7	2.56
1.0	298	2.2	11.5	6.49 9.45 12.2	7.8 8.0 8.3	8.03
2.26				10.3 11.3 13.6	5.1 6.2 7.7	6.33

TABLE VIII

MINIMUM IGNITION PRESSURES OF $\text{NO}_2/\text{N}_2\text{H}_4$ VAPORS IN FLOW REACTORS

ϕ	T_o °K	D cm	L/D	U m/sec	P mm Hg	P _{avg.} mm Hg
0.75	298	4.7	10.8	2.29	11.7	10.43
1.0				1.61 2.18 2.71	9.5 10.5 11.3	
2.0				1.64	10.5	

TABLE IX
MINIMUM IGNITION PRESSURE IN FREE JETS

Type	Oxidizer Flow cm ³ /sec STP	Fuel Flow cm ³ /sec STP	Jet Velocity cm/sec OTP	Ignition Pressure mm Hg
NO ₂ in MMH	12	24	520	15.3
F ₂ in H ₂	50	300	7500	12.0
F ₂ in H ₂	25	300	3750	11.5

Diameter inner tube - 1.2 cm

Diameter outer tube - 4.7 cm

STP - Standard Temperature and Pressure

OTP - Operating Temperature and Pressure

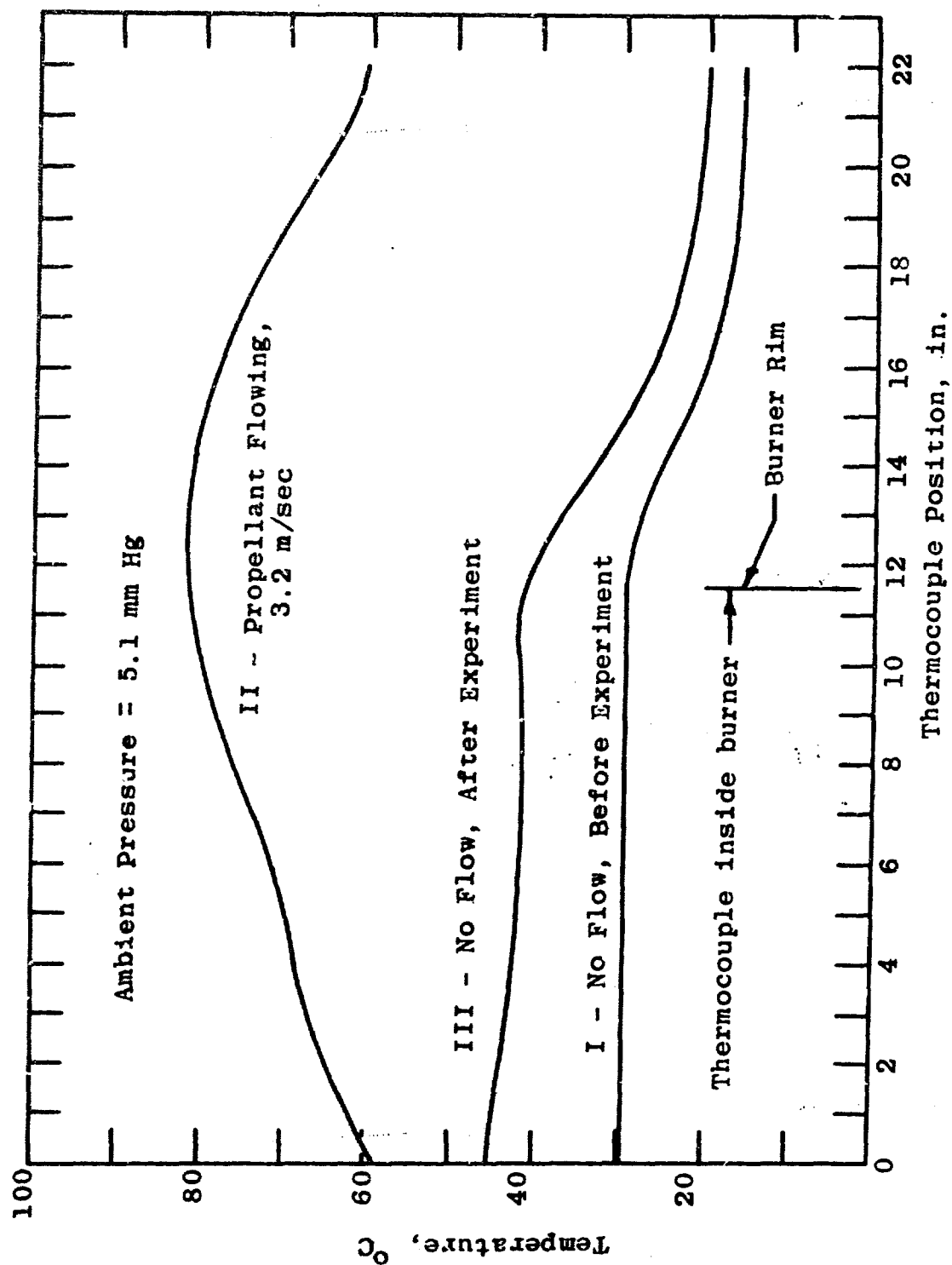


Figure 14. Axial Temperature Profiles,
NO₂/MMH

picture of thermal ignition which is postulated in this work. However, some experimental difficulties for the quantitative study of the reaction kinetics are apparent. Namely, a gradual increase of the wall temperature is taking place during the run as can be seen by the comparison of the profiles taken without flow before and after the experiment. Secondly, during the time needed to take the profile with the traversing mechanism (2 to 4 minutes) a condensate of low vapor pressure was observed on the walls of the tube and also on the thermocouple. The importance of this condensate or adduct will be discussed further later in this report. False readings of temperature were a very likely possibility under these conditions.

In order to eliminate these eventual causes of error, it was, therefore, decided to take the temperature point by point allowing only a minimum running time so that the wall temperature during the run would have changed only by a negligible amount. Such a technique was used to determine the temperature profile in the tube just prior to ignition. With the thermocouple located at a fixed position in the flow tube, the desired propellant flow rates were established at a low ambient pressure (~ 1 mm Hg) in the stainless steel vacuum tank. Ambient pressure then was increased gradually until ignition occurred. The temperature rise was recorded as a function of time and the maximum temperature reached just prior to ignition was noted.

The results of these experiments are reported in Figures 15 and 16 which give the temperature profiles obtained with stoichiometric NO_2/MMH and NO_2/UDMH , respectively. It should be noted that the temperature rises immediately from the mixing point and that it reaches a maximum. Such behavior indicates that the reaction starts immediately without any induction period. This point is of importance with regard to the mechanism of reaction as it tends to indicate a pure thermal mechanism, without chain branching.

c. Analysis of Reaction Products

The analyses reported herein refer to the products of the low temperature reaction occurring prior to ignition. No analyses of the end products of the explosive reaction were performed.

1. Gas Phase

The probe was located at the center line and exit plane of the 4.7 cm tube of $L/D = 10$. Only the

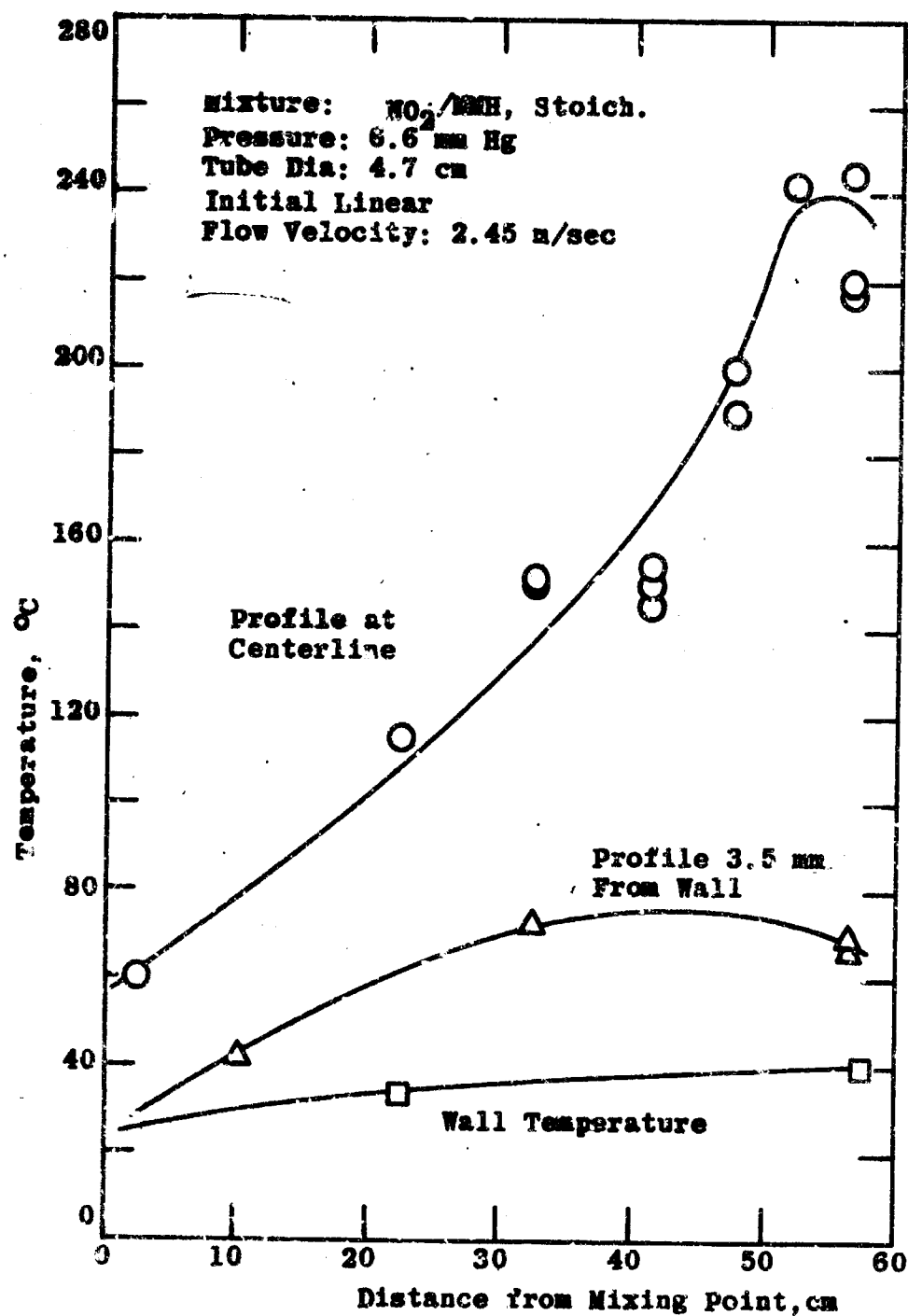


Figure 15. Axial Temperature Profile in Flow Tube, NO_2/MMH

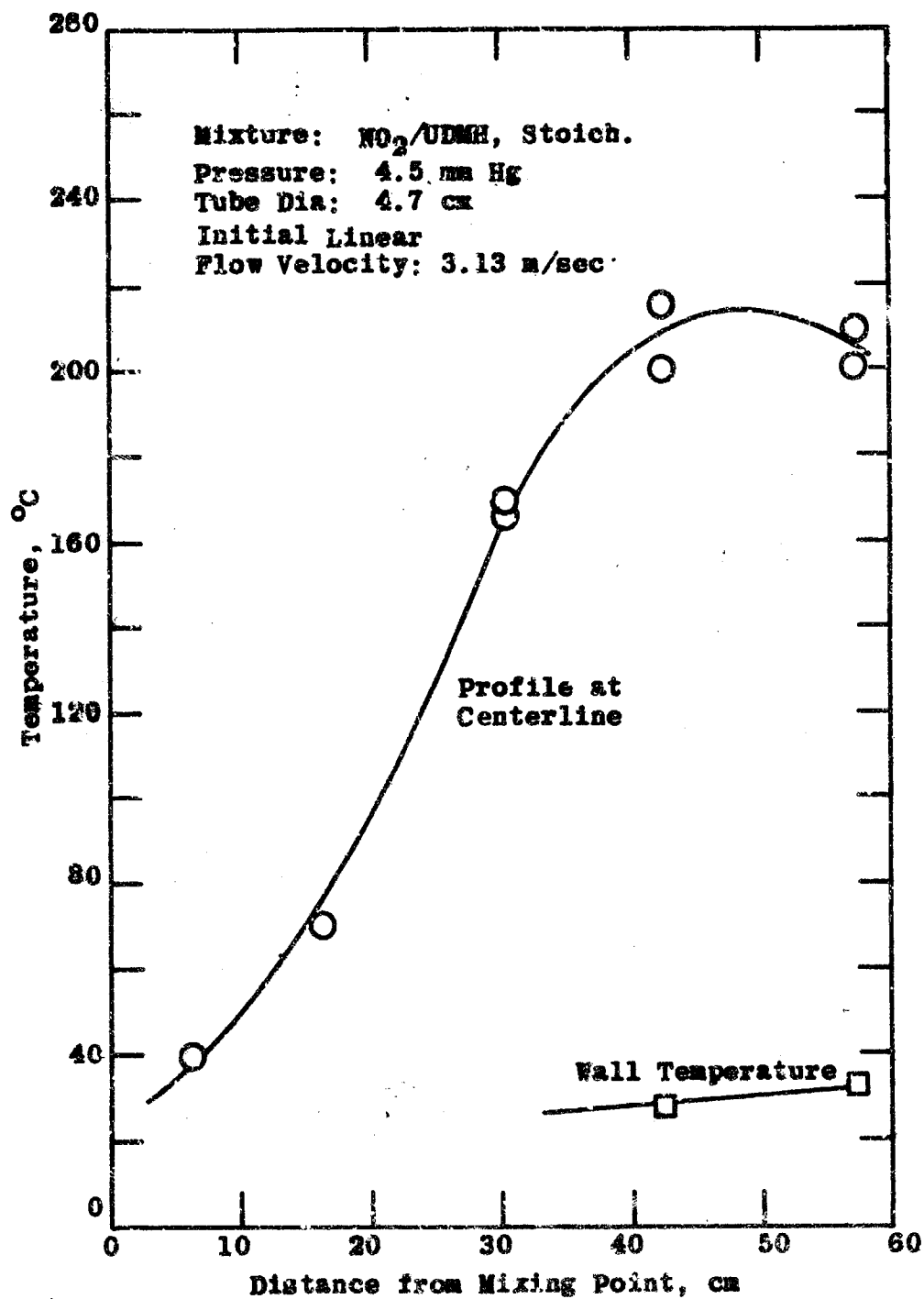


Figure 16. Axial Temperature Profile in Flow Tube, NO_2/UDMH

stoichiometric NO_2/MMH was investigated at pre-ignition pressures ($< 5 \text{ mm Hg}$). A shroud of helium gas was used in order to eliminate any doubt concerning the origin of N_2 in case this gas would have been present in the reaction products. The result of the mass spectrometric analysis are given in Table X. It is seen that only 2% of CO_2 appears in the pre-ignition reaction products. No nitrogen was found and no trace of MMH could be detected. It must be noted that the composition reported cannot by any means represent the exact composition of the exhaust gases as the reaction was not quenched, and in reality, continued in the sampling container. The analysis is revelant, however, in the sense that no nitrogen or hydrogen was formed and that only CO_2 appeared as an end product but in rather small amounts.

ii. Condensate

Upon mixing, the vapors of the hydrazines with NO_2 give a large amount of smoke. This has been reported by others previously. In our apparatus the liquid droplets condensed further on the walls and collected finally as a viscous yellow liquid at the base of the flow tube (placed vertically). The amount of condensate was the greatest in the case of NO_2/MMH and amounted to more than 20% by weight of the initial reactants in some experiments.

Results of the elemental analyses of the condensate are given in Table X for MMH and UDMH as fuels. The elemental analyses agree reasonably well with additive compounds of formula $\text{MMH}\cdot\text{NO}_2$ and $\text{UDMH}\cdot\text{NO}_2$.

The infrared absorption spectra, Figures 17 and 18, show the presence of nitrate and amine groups. No free MMH or UDMH was detected.

d. Thermochemical Data for Condensate

Some preliminary thermochemical data for the MMH adduct was also obtained. The heat of combustion with oxygen, as determined from limited bomb calorimetric tests, is 3090 cal/gr. This gives a heat of formation of the adduct of $\Delta H_f = -0.8 \text{ kcal/gr}$ based on the elemental analysis.

TABLE X
ANALYSIS OF REACTION PRODUCTS OF PRE-IGNITION
REACTION, NO_2/MMH

<u>GASEOUS PRODUCT OF STOICHIOMETRIC NO_2/MMH</u> <u>AT 5 mm Hg</u>	
N_2O_4	98%
CO_2	2%
Helium	Trace
MMH	None

<u>ELEMENTAL ANALYSIS OF CONDENSATE</u> <u>NO_2/MMH</u>	
Carbon	14.6%
Hydrogen	8.4%
Nitrogen	46.4%
Oxygen (by difference)	30.9%

<u>NO_2/UDMH</u>	
Carbon	23.0%
Hydrogen	9.1%
Nitrogen	26.8%
Oxygen (by difference)	41.1%

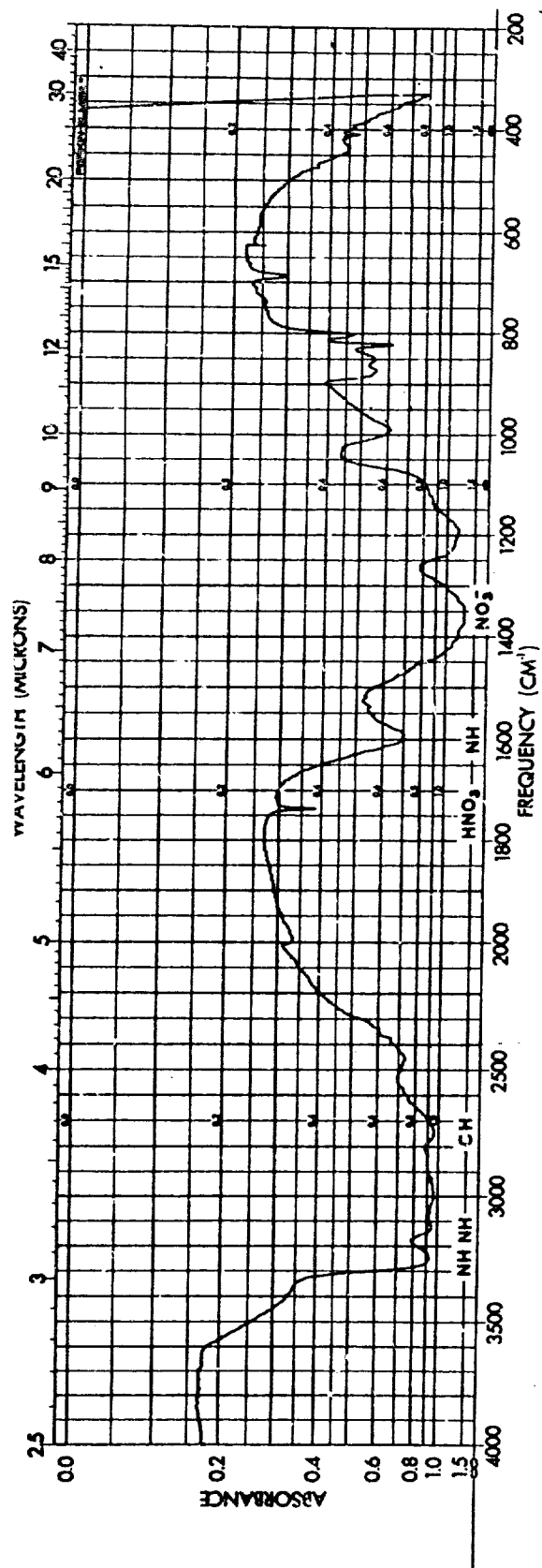


Figure 17. Infrared Absorption Spectrum of the Adduct Formed by NO₂/MMH Vapors at Sub-Ignition Pressure (RMD Spectrum No. 17368)

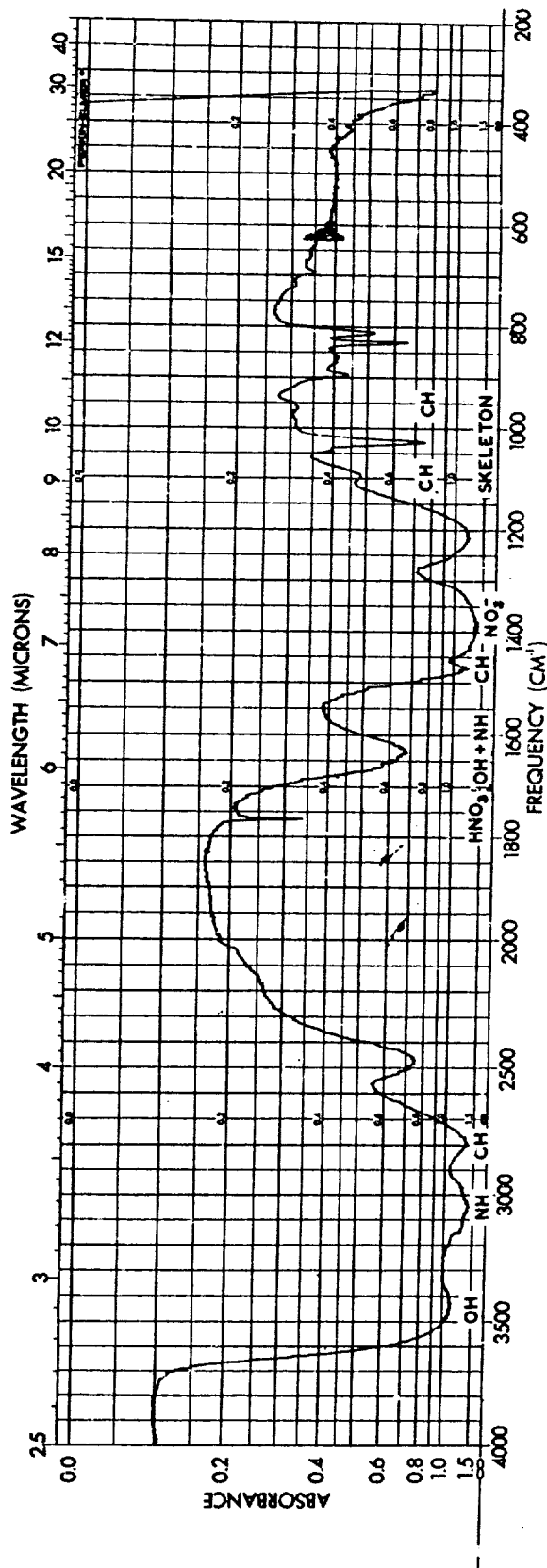


Figure 18. Infrared Absorption Spectrum of the Adduct Formed by NO₂/UDMH Vapors at Sub-Ignition Pressure (RMD Spectrum No. 17492)

4. Discussion of Reaction Kinetics Results

a. Ignition Limits

i. Effect of Flow Velocity

Each set of data consists of pressure limits for a number of flow velocities, all other parameters being maintained constant. It will be seen that the minimum ignition pressure has a tendency to increase with flow velocity within the limit of the flow rates investigated. This is a normal effect as it is known (Ref. 1) that there is an upper flow velocity limit called blow off limit above which no stable flame can be maintained in the stream. The important point is that in approaching this limit the ignition pressure does not vary drastically with the stream velocity. This is especially true for the stoichiometric mixtures. However, for the fuel rich mixture the velocity effect is somewhat greater.

ii. Effect of L/D

Disregarding as a first approximation the effect of velocity, mean values of pressure limits over the velocity ranges investigated may be computed. These values are listed in Column VII of Tables V to VIII. This averaging procedure is used to determine the effect of L/D on the minimum ignition pressures. In Table XI, the mean values of the pressure limits which are tabulated as functions of L/D and the equivalence ratio are compared where possible. Three sets of data exist for NO_2/MMH and one for NO_2/UDMH . It will be seen first that no appreciable effect of L/D can be detected for the stoichiometric mixture ($\phi = 1$). For rich mixtures, however, the minimum ignition pressure increases when L/D decreases.

iii. Effect of Reactor Size

The fact that L/D and velocity effects are negligible for stoichiometric mixtures makes it now possible to determine the true effect of diameter on the explosion limits. This is important since it permits the total order of reaction, N , to be deduced from these data. Since the L/D has only a slight effect for $\phi = 1$, it is possible to average again the pressure limit values of the two L/D's for each reactor size. The resulting averages are plotted in Figure 19 as $\ln P$ vs. $\ln r$. In the case of NO_2/MMH , for which three data points are available, a straight line is obtained with a slope indicating an order of

TABLE XI

EFFECT OF REACTOR L/D ON MINIMUM IGNITION PRESSURES,
 NO_2/MMH and NO_2/UDMH

6.6 cm Tube, MMH

ϕ \ L/D	4.8	9.5	
1	4.22	3.83	avg. = 4.02
2.5	2.68	2.38	

4.7 cm Tube, MMH

ϕ \ L/D	4.76	10.8	
1	5.33	5.67	avg. = 5.50
2.5	4.60	3.57	

4.7 cm Tube, UDMH

ϕ \ L/D	4.76	10.8	
1	3.1	2.9	avg. = 3.0
3	2.47	1.73	
4	2.4	1.76	

2.2 cm Tube, MMH

ϕ \ L/D	11.5	30	
1	11.9	10.25	avg. = 11.08
2.5	9.2	7.4	

Note: Minimum ignition
 pressure units
 are mm Hg

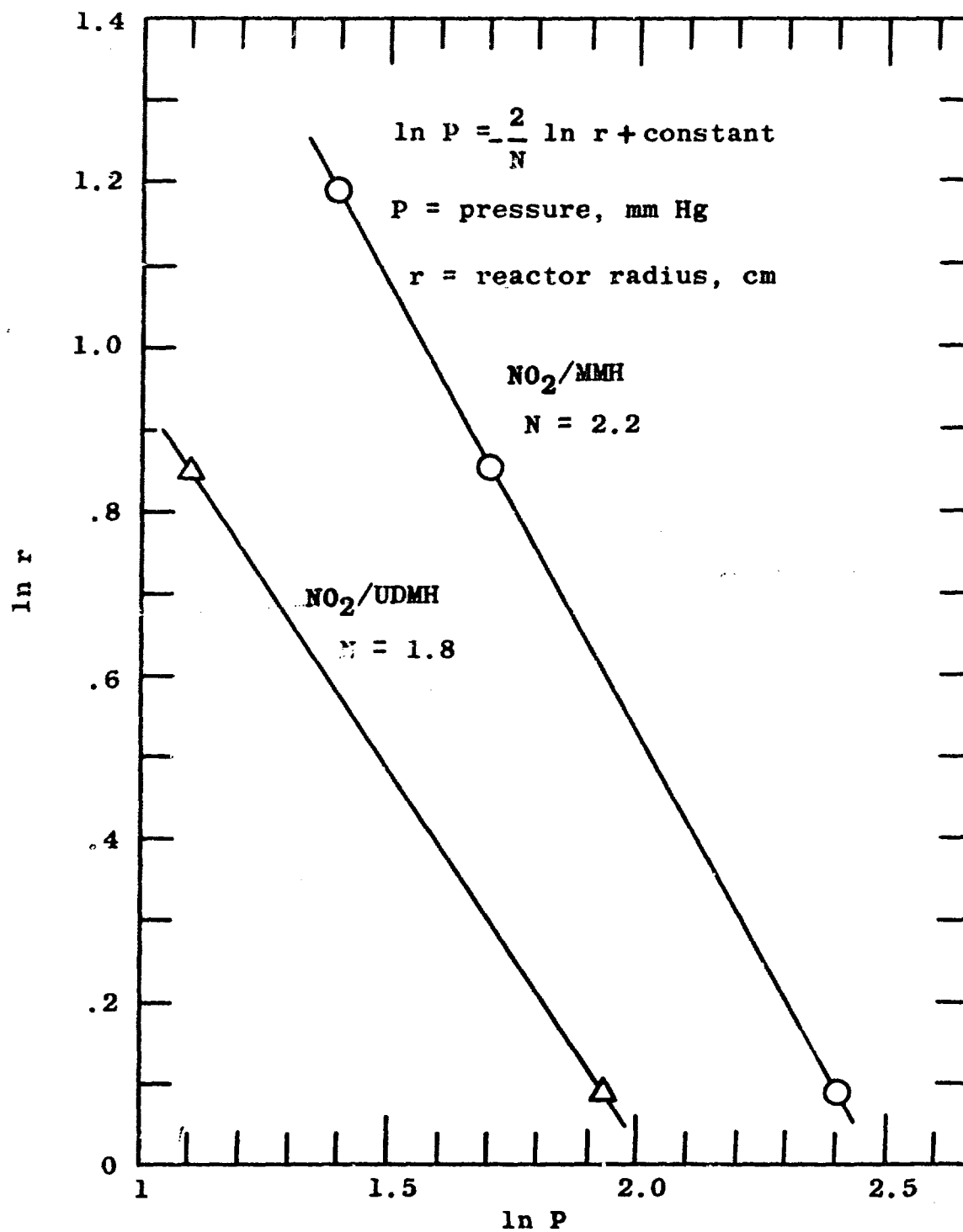


Figure 19. Effect of Reactor Radius on Minimum Ignition Pressures

reaction close to 2. For NO_2/UDMH and $\text{NO}_2/50-50$, only two data points exist but the lines joining the two points indicate again an order of reaction close to two.

iv. Effect of Equivalence Ratio

For the NO_2/MMH mixtures two sets of data are available, one taken in the 4.7 cm tube with an L/D of 4.76 and the other taken in the 2.2 cm tube with an L/D of 30. Using the averaging procedure described above, the minimum ignition pressures are plotted in Figure 20 against the equivalence ratio. In both cases the minimum is found on the fuel rich side. It is somewhat difficult to define exactly this minimum because the curves are quite flat but it can be estimated at about $\phi = 2.5$, i.e., the equimolecular mixture $\text{NO}_2 + \text{CH}_3\text{N}_2\text{H}_3$. In the case of NO_2/UDMH as indicated in Figure 21, it seems again that the minimum is close to the equimolecular composition, which is $\phi = 4$. Thus, for these two combinations the data indicate partial orders of reaction close to 1 relative to fuel and oxidizer.

No complete set of data are available for $\text{NO}_2/50-50$ and $\text{NO}_2/\text{N}_2\text{H}_4$. The only statement which can be made regarding these combinations at the present time is that the equimolecular mixtures ignite somewhat easier than the other mixture ratios tested.

v. Effect of Temperature

The effect of initial temperature was investigated for NO_2/MMH and NO_2/UDMH . The measurements were made using the 4.7 cm tube of L/D = 4.76. Averaging again the minimum ignition pressures over the velocity ranges investigated, the results are shown in Figure 22 in a plot of $\ln P/T_0^2$ against $1/T_0$. The three experimental points for NO_2/UDMH fall on a straight line whose slope corresponds to an energy of activation of $E = 7.2$ kcal/mole. Two points only were taken for NO_2/MMH . The slope of the line indicates an energy of activation of 5.2 kcal/mole. The temperature effect for $\text{NO}_2/50-50$ and $\text{NO}_2/\text{N}_2\text{H}_4$ was not investigated.

vi. Comparison of Reactivities of Hypergolic Combinations

This comparison is best given by the pressure limits obtained for the stoichiometric mixtures in the 4.7 cm reactor of L/D = 10. The comparison is shown in

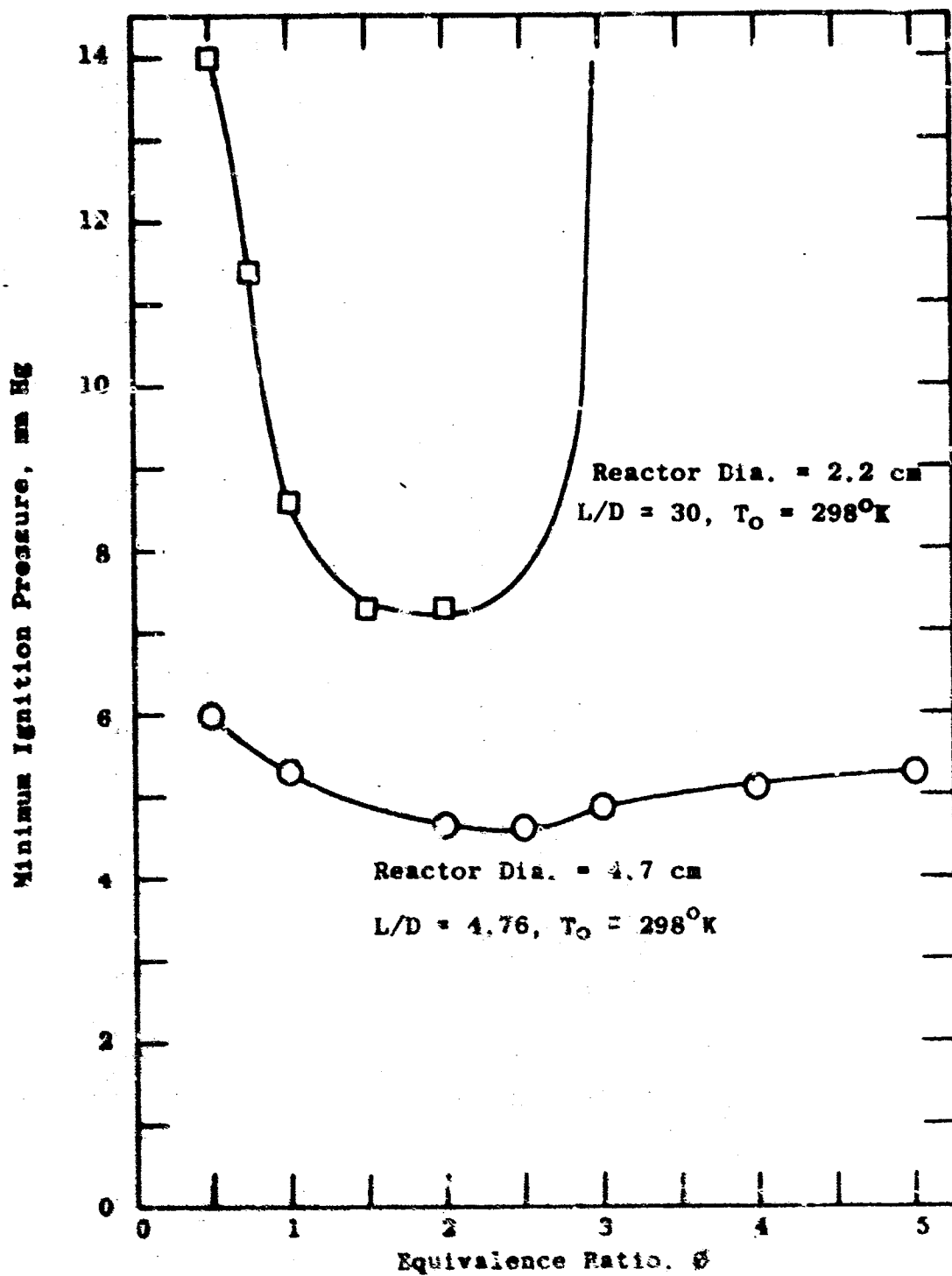


Figure 20. Effect of Equivalence Ratio on Minimum Ignition Pressure, NO_2/MMH

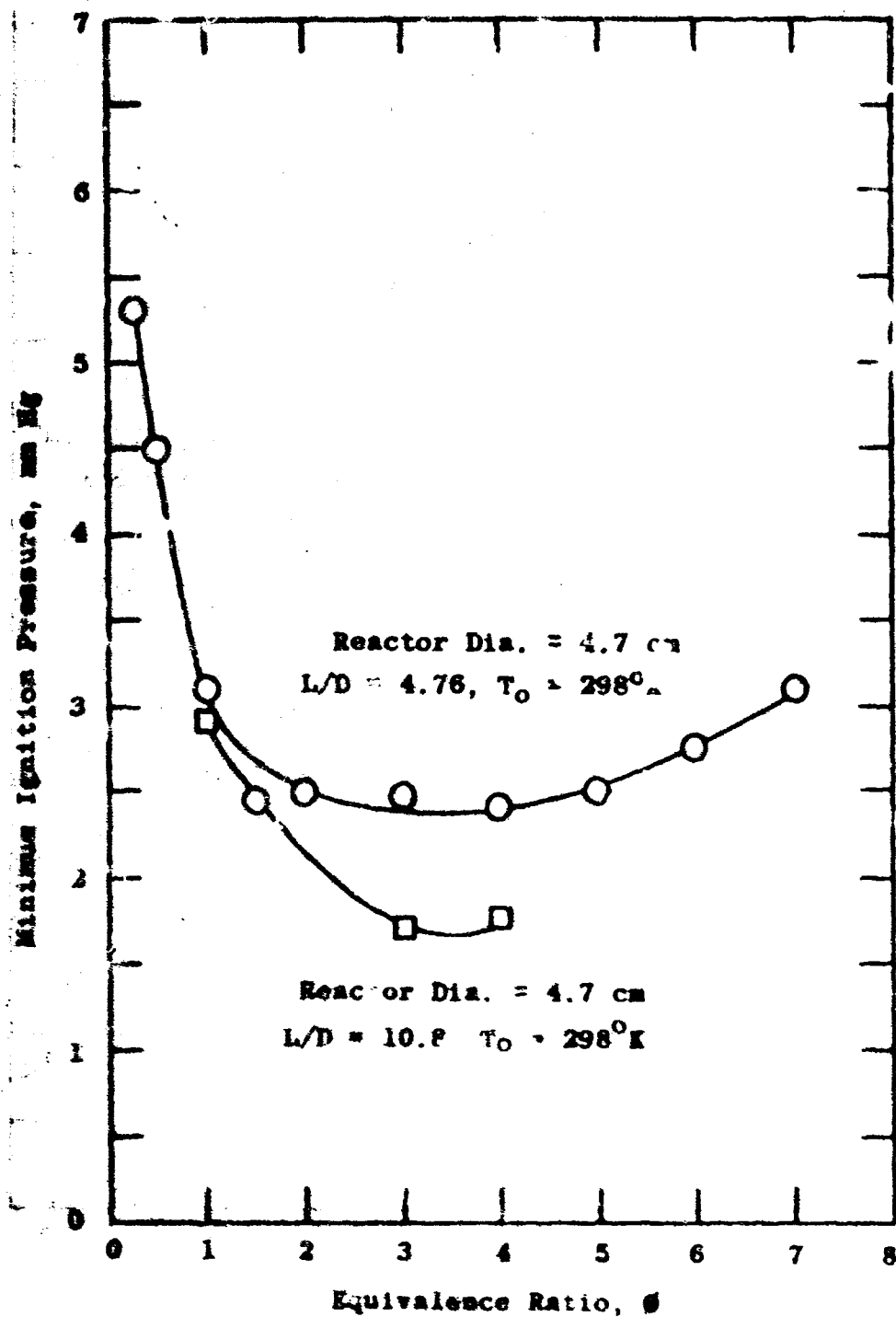


Figure 21. Effect of Equivalence Ratio on Minimum Ignition Pressure, $NO_2/UDMH$

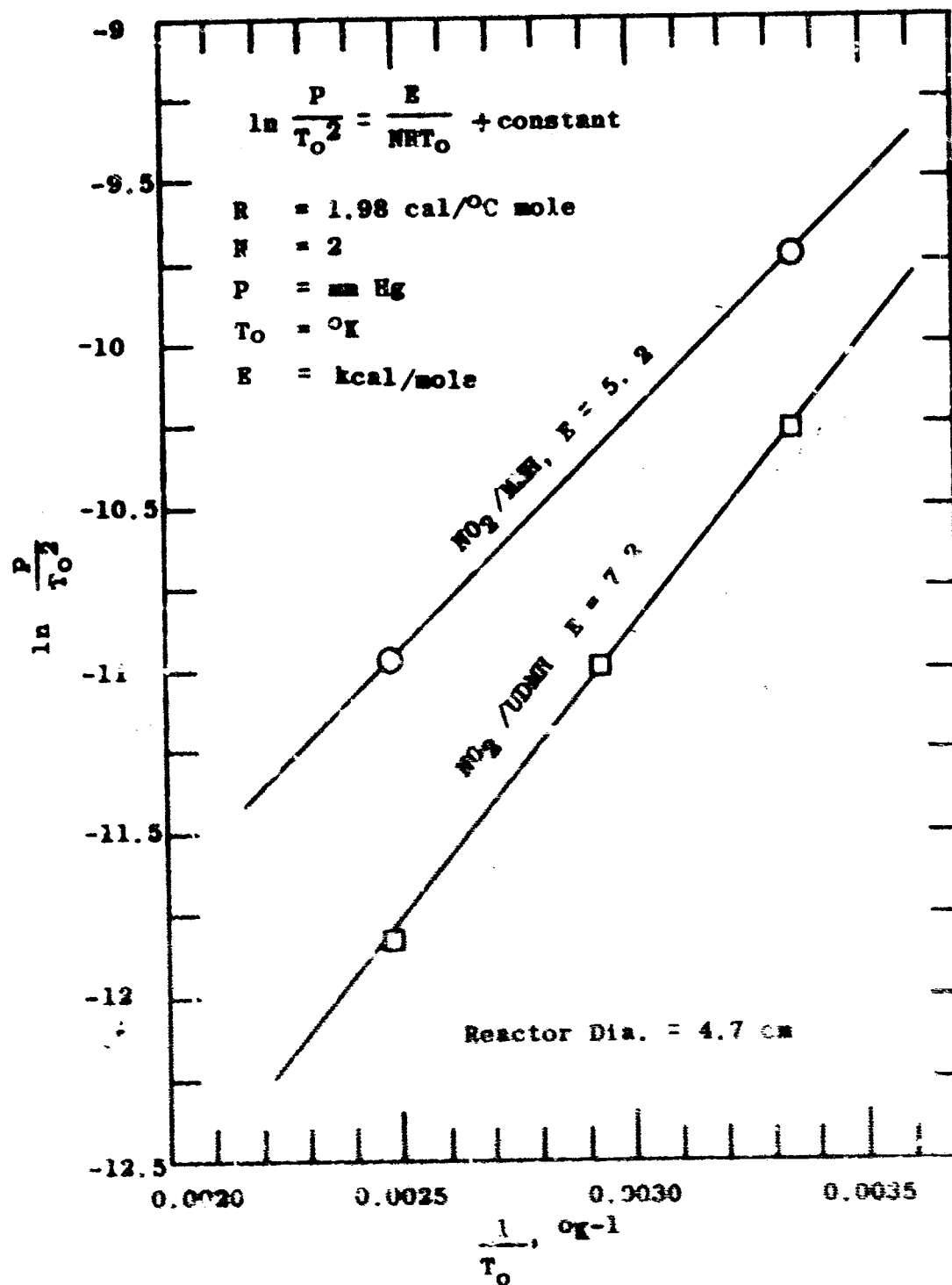


Figure 22. Effect of Temperature on Minimum Ignition Pressures

Table XII which includes also the concentric flow tests. The following order of reactivity is indicated: $\text{NO}_2/\text{UDMH} > \text{NO}_2/50-50 > \text{NO}_2/\text{MMH} > \text{NO}_2/\text{N}_2\text{H}_4$.

b. Determination of the Heat Release Factor (AQ)

So far the analyses of the experimental data on explosion limits has permitted us to establish the overall kinetics of the reaction. The total order of reaction for the two systems completely investigated (NO_2/MMH and NO_2/UDMH) has been found to be close to 2 and their partial orders relative to fuel and oxidizer, close to 1. It is now possible to write the rate expression for reaction rate in the form:

$$W = A c_1 c_2 \exp \left(- \frac{E}{RT} \right)$$

where c_1 and c_2 represent the concentrations of fuel and oxidizer, respectively. Substituting this expression into equation (32), the Frank-Kamenetskii criterion for thermal ignition becomes:

$$\delta = \frac{Q}{\lambda} \frac{E}{RT_0^2} r^2 c_1 c_2 A \exp \left(- \frac{E}{RT_0} \right) \quad (35)$$

In this expression all quantities are known from the explosion limits data with the exception of A and Q . It is thus possible to calculate the product AQ . This calculation will be performed in detail for the case of NO_2/MMH . The explosion limit is taken as 5.5 mm Hg which is the mean value obtained for the stoichiometric mixture at $T_0 = 298^\circ\text{K}$ in the tube of 4.7 cm diameter. Taking for E the value of 5.2 kcal/mole and taking for λ a value of 4×10^{-3} cal sec $^{-1}$ cm $^{-1}$ degree $^{-1}$, the following data are known:

$$\delta = 2$$

$$T_0 = 298^\circ\text{K}$$

$$r = 2.35 \text{ cm}$$

$$c_1 = 0.84 \times 10^{-7} \text{ mole/cc}$$

$$c_2 = 2.1 \times 10^{-7} \text{ mole/cc}$$

TABLE XII
COMPARISON OF REACTIVITIES OF VARIOUS
HYPERGOLIC COMBINATIONS AT
298°K

COMBINATION (stoichiometric)	MINIMUM IGNITION PRESSURE, mm Hg	
	4.7 cm Tube	Free Jet
NO ₂ /UDMH	3	
NO ₂ /50-50	3.9	
NO ₂ /MMH	5.5	15
NO ₂ /N ₂ H ₄	10.4	
F ₂ /H ₂		12

*Reactivity is inversely proportional to
ignition pressure.

$$\lambda = 4 \times 10^{-5} \text{ cal/sec-cm-}^{\circ}\text{C}$$

$$E = 5.2 \times 10^3 \text{ cal/mole}$$

Substituting these values into equation (35), the product AQ becomes:

$$AQ = 1.7 \times 10^{14} \frac{\text{cal cc}}{\text{mole}^2 \text{ sec}}$$

The product AQ may also be evaluated using a quite different method. Considering the temperature profile at the center line, as shown in Figure 15, it is noted that the first part of the curve is quite linear. In this region it might be assumed as a first approximation that heat losses by conduction to the wall are negligible. This is certainly true in the central region of the tube before the boundary layer is fully developed. Taking for the kinematic viscosity the value of $\nu = 13.3 \text{ cm}^2\text{sec}^{-1}$ and for the initial linear velocity the value of $U_0 = 245 \text{ cm/sec}$, it is found that the boundary layer merges in the center at a distance of 16.3 cm from the origin. For the central, initial portion of the tube the heat equation can be written in the form

$$\rho c_p U \frac{\partial T}{\partial x} = WQ = AQ c_1 c_2 \exp\left(-\frac{E}{RT}\right) \quad (36)$$

with ρ - density, c_p - specific heat and U - velocity at the center line

Applying this equation at $x = 10 \text{ cm}$ from the origin and taking into account the pressure and composition of the mixture, it is found that:

$$\frac{\partial T}{\partial x} = 2.4^{\circ}\text{C/cm}$$

$$U = 375 \text{ cm/sec}$$

$$T = 347^{\circ}\text{K}$$

$$c_1 = 0.79 \times 10^{-7} \text{ mole/cm}^3$$

$$c_2 = 1.99 \times 10^{-7} \text{ mole/cm}^3$$

$$c_p = 0.24 \text{ cal/gr-}^{\circ}\text{C}$$

$$\rho = 1.4 \times 10^{-5} \text{ gr/cm}^3$$

These values, substituted into equation (36), give

$$AQ = 3.4 \times 10^{14} \frac{\text{cal cc}}{\text{mole}^2 \text{ sec.}}$$

Considering the uncertainties in the values of c_p and λ , the agreement between the two methods must be considered as very satisfactory. It should be noted that the value from the temperature profile method is preferred as it is more direct and is independent of the approximations involved in the theory of thermal explosions.

c. Pre-ignition Gas Phase Reaction Mechanism

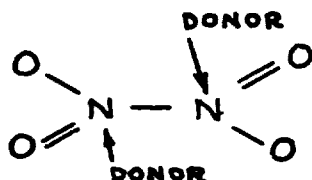
In defining a scheme of reaction for the processes leading to hypergolic ignition in the gaseous mixtures of the hydrazines with nitrogen dioxide the following facts have to be accounted for:

- (a) A low temperature reaction with heat generation takes place in the gaseous mixture prior to ignition.
- (b) The energy of activation of this reaction is low and of the order of 5 to 10 kcal per mole.
- (c) The total order of reaction, N , is close to 2 and the partial orders relative to fuel and oxidizer are close to unity.
- (d) The reaction starts without any apparent induction period.
- (e) Chemical additives tested have in general no other influence than the small influence expected from a diluent.
- (f) A liquid condensate of low vapor pressure and showing a 1/1, F/O molecular composition is formed prior to ignition.

The fact that no induction period is observed and that chemical additives have in general no influence on the rate of reaction leads first to the conclusion that the low temperature reactions

are not of the chain type. Further, the order of reaction and the adduct formation point toward a molecular association reaction between fuel and oxidizer. It is difficult at present to decide whether this association reaction is a necessary step or only a side reaction in the mechanism leading to ignition. However, we will venture to propose the following physical picture as a working hypothesis.

When fuel and oxidizer come into contact, they first form an adduct which further dimerizes to form the condensate of low vapor pressure. These steps are accompanied by a significant heat evolution. The heat liberated is only a fraction (10%) of the total heat liberated by the explosive reaction but it is sufficient to bring the mixture to a temperature level where decomposition and explosive chain reactions are initiated. It is well known that nitrogen tetroxide forms addition compounds with most organic compounds that are able to donate electrons. Electron donors usually form a 2:1 compound which may be represented as



It is well possible that the condensate isolated from the NO_2/MMH reaction could be a compound of this type as the elemental analysis gave C, H and N in the proportions of 14.6, 8.1 and 46.4 which is in reasonable agreement with the theoretical values of 14.5, 8.25, and 47.3 for a compound of the formula $(\text{CH}_3\text{N}_2\text{H}_3 \cdot \text{NO}_2)_2$.

Some interesting conclusions concerning the mechanisms of reaction might further be drawn by considering the results of the thermochemical data. The data were obtained from only a limited number of tests and certainly require verification. Nevertheless, we will use the existing preliminary information. From the determined heat of formation

$$\Delta H_{fo} = -0.8 \text{ Kcal/gram}$$

and the known heats of formation

$$\Delta H_{fo} = 23.2 \text{ Kcal/mole for MMH(g)}$$

and $\Delta H_{fo} = 7.9 \text{ Kcal/mole for NO}_2(\text{g})$

we find for the reaction, assuming the adduct is $(\text{CH}_3\text{N}_2\text{H}_3\text{NO}_2)_2$,



Assuming that this reaction is the dominant exothermic process in the low temperature regime prior to ignition, the value of Q appearing in the heat equation (36) and (35) might be identified with $-\Delta H = 105 \text{ kcal}$. Thus taking $3.4 \times 10^{14} \text{ cal cc mole}^{-2}\text{sec}^{-1}$ for the value of AQ , we find for the frequency factor of the bimolecular association reaction

$$A = 0.3 \times 10^{10} \text{ cc mole}^{-1}\text{sec}^{-1}$$

Such a value is substantially lower than the collision frequency, Z , which for moderate size molecules is of the order of $Z = 5 \times 10^{14} \text{ cc mole}^{-1}\text{sec}^{-1}$. Thus, only one efficient collision occurs for every 50,000 collisions between the reactant molecules and the steric factor $f = A/Z$ has a value of 6×10^{-6} . In most bimolecular reactions of free radicals with molecules, $0.1 < f < 1$. However, certain additional reactions, for instance at double bonds, have low f values ($10^{-3} - 10^{-5}$). Furthermore, it has been found that molecular association reactions have in general low A values. For instance, Kistiakowsky and Stouffer (Ref. 12) found for the A -factors of the association of hydrogen bromide and hydrogen chloride with 2-methyl propane values of $10^{10.2}$ and $10^{11} \text{ mole}^{-1}\text{cc-sec}^{-1}$ which are fairly close to the value obtained for the reaction between NO_2 and MMH from the preliminary thermochemical data on the adduct.

5. Summary and Conclusions

The analysis of the experimental data on explosion limits has permitted us to establish the overall kinetics of the low temperature reactions leading to ignition of the two systems NO_2/MMH and NO_2/UDMH . The total order of reaction for these two systems is close to 2 and the partial orders relative to fuel and oxidizer are close to unity. The energies of activation are 5.2 and 7.2 kcal/mole for NO_2/MMH and NO_2/UDMH , respectively. Partial data for the systems $\text{NO}_2/50-50$ and $\text{NO}_2/\text{N}_2\text{H}_4$ have been obtained. The total order of reaction for $\text{NO}_2/50-50$ has been found to be close to 2. The minimum ignition pressure for $\text{NO}_2/\text{N}_2\text{H}_4$ has been determined in the case of the stoichiometric mixture, which is also the equimolecular mixture, and indicates a reactivity less than those of the other hydrazines.

The formation of an adduct of low vapor pressure and of near 1/1 molecular composition relative to fuel and oxidizer has been observed and analyzed in the case of NO_2/MMH and NO_2/UDMH . A condensate was also observed in the case of $\text{NO}_2/50-50$ but it was not analyzed. Both its appearance and quantity formed are similar to the NO_2/MMH adduct. A considerably lesser amount of the NO_2/UDMH adduct collected in the liquid state at the base of the burner assembly.

A synoptic representation of these conclusions is given in Table XIII.

D. Statement and Results of Mathematical Model of Hypergolic Ignition

In this section, the results of Sections B and C on chemical kinetics and chamber pressurization due to propellant vaporization are combined into a mathematical model of hypergolic ignition in reaction control systems at space conditions. The model and the assumptions involved are discussed first. Subsequently, calculated ignition delays are given and compared to experimentally measured values. Finally, overpressures which occur during engine start-up transients are considered.

1. Hypergolic Ignition Model

a. Dominant Ignition Reactions

It is assumed in the mathematical model that the dominant ignition reactions are gas-phase reactions. Some experimental justification for this assumption comes from the work of the preceding ten-month program reported in Ref. 1. Figure 31 of that reference is a log-log plot of average ignition delays vs. pressure for a number of hypergols tested in an unconfined impinging stream apparatus (i.e. impinging stream injectors without thrust chambers). Curves for the $\text{N}_2\text{O}_4/\text{hydrazine-type}$ fuels combinations are reproduced in Figure 23 of the present report.

Essentially, the curves as drawn simply connect the averaged data points at each pressure by straight lines. However, in the pressure range from 150 to 60 mm Hg, the three data points for $\text{N}_2\text{O}_4/\text{UDMH}$, $\text{N}_2\text{O}_4/\text{MMH}$ and $\text{N}_2\text{O}_4/\text{MHF-5}$ (a mixed hydrazine fuel) fall on single straight lines. This linearity is found despite the fact that the greatest data scatter was observed in this pressure range (see Ref. 1). $\text{N}_2\text{O}_4/50-50$ shows a nearly linear relationship in the log-log plot in this pressure range.

TABLE XIII
SUMMARY OF EXPERIMENTALLY DETERMINED KINETIC FACTORS FOR GAS-PHASE
IGNITION OF NO₂/HYDRAZINE FUELS

FUEL	PARTIAL ORDER, n		TOTAL ORDER, N	ENERGY OF ACTIVATION, E kcal/mole	HEAT RELEASE FACTOR, AQ cal cm ³ /mole ² sec	FREQUENCY FACTOR, A cm ³ /mole sec
	FUEL	OXIDIZER				
UDMH	1.0	1.2	2.2	7.2	3.2×10^{16}	
MMH	0.9	0.9	1.8	5.2	3.4×10^{14}	0.3×10^{10}
50/50	~1	~1	~2			
N ₂ H ₄	~N/2	~N/2				

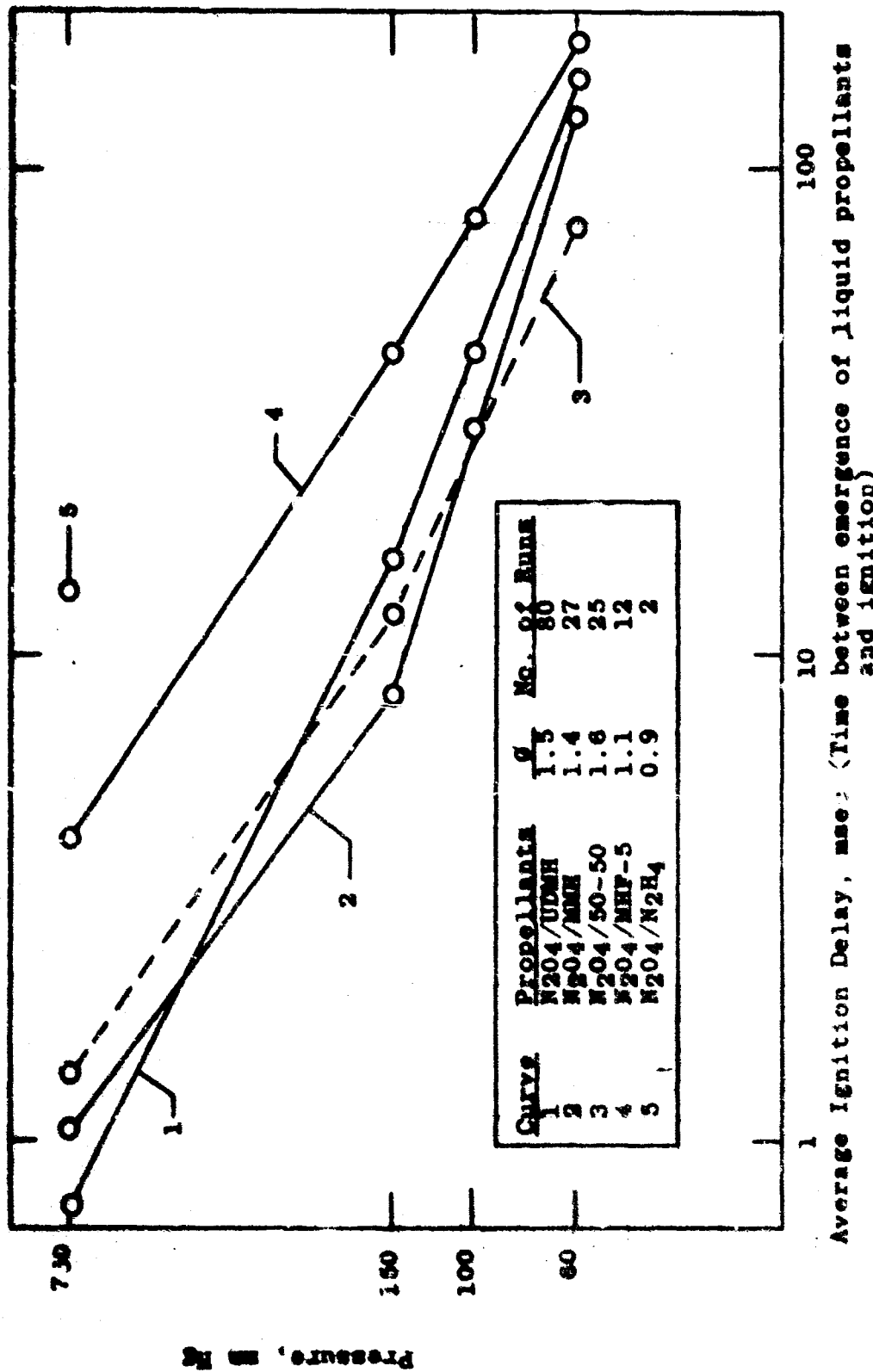


Figure 23. Average Ignition Delay vs. Pressure for Unconfined Impinging Stream Tests (from Ref. 1)

The fairly high degree of linearity in the 150 to 60 mm Hg pressure range suggests that a common process is rate controlling in this range. Since the delays at one atmosphere are longer in every case than those to be expected from an extrapolation of the straight-line low pressure curves, a different controlling process is indicated for the ignitions at high pressure.

The results of the nearly 150 tests made with these hypergolic combinations using various impinging stream injector configurations (injection velocities, impingement angles, impingement lengths and type of manifolding) show that mixing processes are not controlling at any pressure investigated. Neither the controlling process at one atmosphere, nor the one at lower pressures is propellant mixing.

Figure 24 is a log-log plot of average ignition delays at one atmosphere vs. relative volatilities of the five hypergolic combinations. Relative volatility as used here is simply the ratio of the vapor pressures of oxidizer to fuel. The figure shows that the greater the discrepancy between fuel and oxidizer volatilities the longer the ignition delay at one atmosphere. Two observations are suggested by the simple correlation of Figure 24. Since the oxidizer is the same for the five combinations, the abscissa of the figure is effectively the reciprocal of the vapor pressure of the fuel. The ignition delays of these hypergols, then, are seen to depend on the vapor pressure of the fuel. The figure indicates, therefore, that fuel vaporization is controlling at one atmosphere. Then, since fuel vaporization is controlling, the dominant ignition reactions, even at one atmosphere, must be gas-phase reactions.

At reduced ambient pressures, no correlation exists between ignition delay and relative volatility. Consequently, the controlling process at low pressures is not propellant vaporization, a result compatible with the curves of Figure 23. Since, as stated above, mixing processes are not controlling at low pressures, one concludes that gas-phase chemical kinetics is. The success of the mathematical model, which assumes that gas-phase chemical kinetics is controlling, supports the conclusion.

Further support comes from a comparison between the number of gas-drop collisions and the number of gas-gas collisions. Due to the large differences between the volatilities of N_2O_4 and the hydrazine fuels, we will consider the possibility of reactions resulting from collisions of gaseous NO_2 molecules

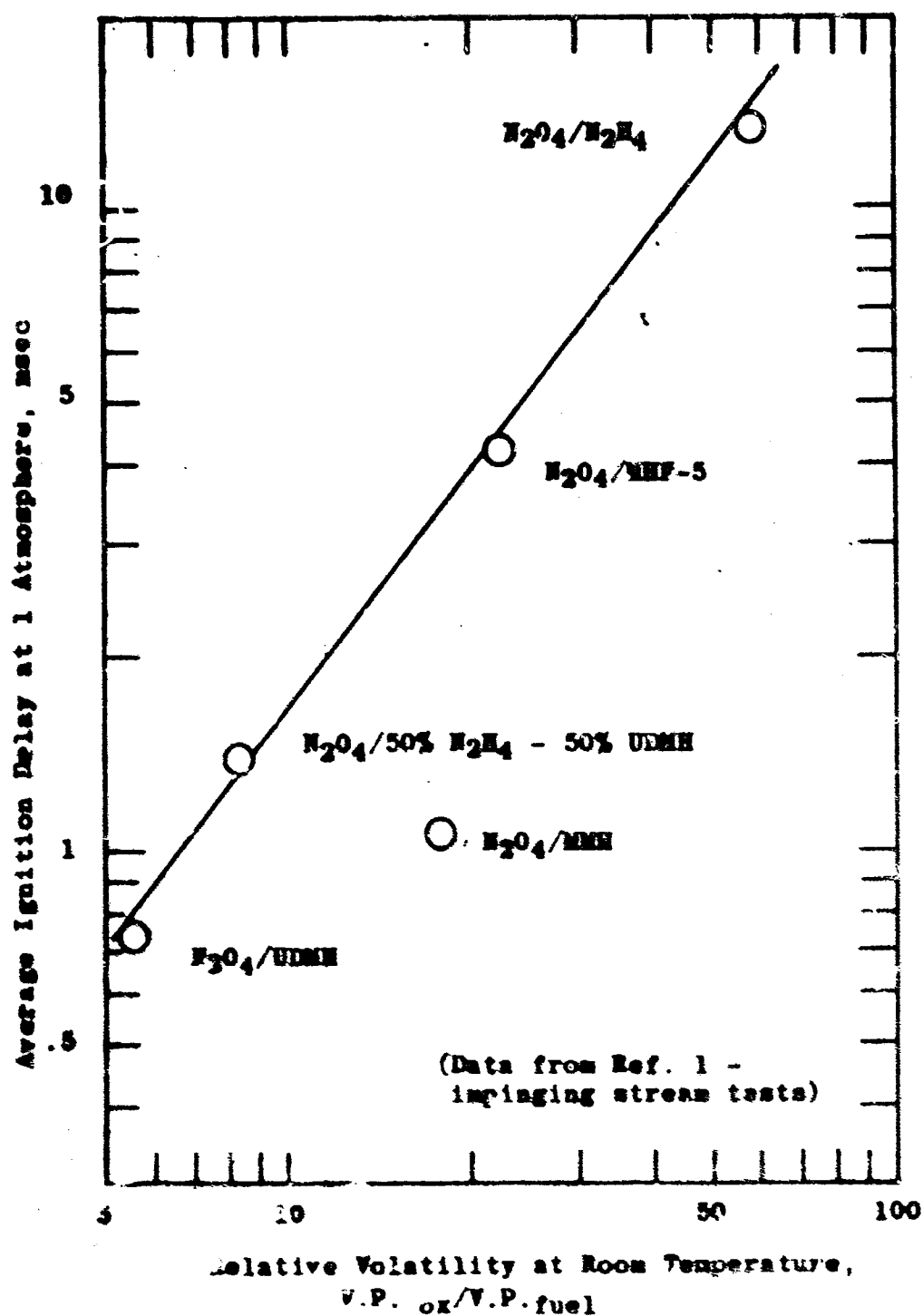


Figure 24. Influence of Propellant Volatilities
on Ignition Delay at One Atmosphere

with drops of MMH (gas-drop collisions), for example. The frequency of these collisions will be compared to the frequency of gaseous NO_2 -gaseous MMH collisions (gas-gas collisions).

Making use of computer run CCl₄ #R, for which $\dot{w} = 0.0816 \text{ lb}_m/\text{sec}$, $\Delta t_n = 4 \times 10^{-5} \text{ sec}$, $T_0 = 540^\circ\text{F}$, $V_c = 1.015 \times 10^{-2} \text{ ft}^3$, and $r_m = 75 \text{ microns}$ (see Table III for initial radii of the three drop size spray model), we first calculate the total droplet surface area per unit chamber volume. We select a time of 0.800 msec for which $P_g = 1.74 \text{ mm Hg}$, $T_g = 513^\circ\text{F} = 285^\circ\text{K}$ and the approximate average radii of all the drops in the system in each class are

$$\bar{r}_1 = 77 \times 10^{-6} \text{ ft} \quad (\text{range of actual } r_1\text{'s: } 83 \times 10^{-6} \text{ to } 75 \times 10^{-6} \text{ ft})$$

$$\bar{r}_2 = 236 \times 10^{-6} \text{ ft} \quad (\text{range of actual } r_2\text{'s: } 250 \times 10^{-6} \text{ to } 333 \times 10^{-6} \text{ ft})$$

$$\text{and } \bar{r}_3 = 705 \times 10^{-6} \text{ ft} \quad (\text{range of actual } r_3\text{'s: } 720 \times 10^{-6} \text{ to } 687 \times 10^{-6} \text{ ft})$$

By equations (3), (4) and (6a) and noting that 20 ensembles have undergone evaporation during the 0.800 msec period (time/ $\Delta t_n = 20$), we obtain the total surface area of the drops in each class. Dividing the resulting areas by the chamber volume gives the surface areas per unit volume for each of the three aggregate drop classes:

$$\text{Total } A_1/V_c = 1.98 \times 10^{-2} \text{ cm}^2/\text{cc} \text{ for } \bar{r}_1 = 77 \times 10^{-6} \text{ ft}$$

$$\text{Total } A_2/V_c = 0.91 \times 10^{-2} \text{ cm}^2/\text{cc} \text{ for } \bar{r}_2 = 236 \times 10^{-6} \text{ ft}$$

$$\text{and Total } A_3/V_c = 0.26 \times 10^{-2} \text{ cm}^2/\text{cc} \text{ for } \bar{r}_3 = 705 \times 10^{-6} \text{ ft}$$

The total drop surface area per cc is therefore $3.15 \times 10^{-2} \text{ cm}^2/\text{cc}$.

The concentration of gas molecules at 0.800 msec when $P_g = 1.74 \text{ mm Hg}$ and $T_g = 285^\circ\text{K}$ (above) is

$$\text{molecular concentration} = c = \frac{nN_0}{V} = \frac{P_g N_0}{RT_g}$$

$$5.90 \times 10^{18} \text{ gas molecules/cc} \quad (37)$$

$$\text{where } N_0 = \text{Avogadro number} = 6.024 \times 10^{23} \text{ molecules/mole}$$

By the kinetic theory of gases, the number of collisions per unit time between gas molecules and a surface of unit area is

$$Z_{\text{gas-surface}} = \frac{c \bar{u}}{4} = c \left(\frac{RT_g}{2\pi M} \right)^{1/2} \quad (38)$$

where c is molecular concentration and \bar{u} is mean molecular velocity.

Multiplying eq. (38) by the total drop surface area per cc as determined above, and taking into account the fact that the vapor molecules are CCl_4 , we obtain, for $T = 285^\circ\text{K}$:

$$Z_{\text{gas-drop}} = 9.2 \times 10^{18} \text{ gas-drop collisions/cc-sec} \quad (39)$$

Equation (39) is the number of CCl_4 gas-drop collisions per unit time per unit volume at 0.800 msec of the computer calculation.

We assume now that the vapor molecules are NO_2 and the drops are MMH. To account for the difference in molecular weights of CCl_4 and NO_2 (see eq. 38), eq. (39) is multiplied by $(M_{\text{CCl}_4}/M_{\text{NO}_2})^{1/2}$. Also, since the number of drops in each class is inversely proportional to density (see eq. 4), eq. (39) is multiplied also by $(\rho_{\text{CCl}_4}/\rho_{\text{MMH}})$. The result gives the frequency of collisions between the NO_2 molecules and MMH drops and is

$$Z_{\text{NO}_2 \text{ gas-MMH drops}} = 3.1 \times 10^{19} \text{ gas-drop collisions/cc-sec} \quad (40)$$

for $P_g = 1.74 \text{ mm Hg}$ and $T_g = 285^\circ\text{K}$

From the kinetic theory of gases, the total gas-gas collisions between unlike molecules per unit volume and per unit time is given by

$$Z_{\text{gas-gas}} = c_f c_{ox} (r_f + r_{ox})^2 \left[8\pi kT_g \left(\frac{1}{m_f} + \frac{1}{m_{ox}} \right) \right]^{1/2} \quad (41)$$

(41)

4100000000

where c_f and c_{ox} are molecular concentrations of fuel and oxidizer

r_f and r_{ox} are molecular radii

k = Boltzmann constant = 1.38×10^{-16} erg/°K molecule

and m_f and m_{ox} are molecular masses.

For $r_{MMH} = 4 \times 10^{-8}$ cm, $r_{NO_2} = 3 \times 10^{-8}$ cm, and $T = 285^\circ K$, we obtain

$$Z_{\text{gas-gas}} = 7.88 \times 10^{-10} c_f c_{ox} \text{ gas-gas collisions/cc-sec} \quad (42)$$

As a "worst case", we assume the molecular concentrations of gaseous MMH and NO_2 are in proportion to their vapor pressures at the temperature of interest ($285^\circ K$), $c_{NO_2}/c_{MMH} = 21$. Since the total molecular concentration is 5.90×10^{16} (eq. 37), the total gas-gas collisions between unlike molecules is

$$Z_{\text{gas-gas}} = 1.2 \times 10^{23} \text{ gas-gas collision/cc-sec} \quad (43)$$

This is the second of two collision frequencies sought. The results are summarized as follows:

Type of Collision	Gas Press. mm Hg	Gas Composition	Gas Temp. °K	Collision Frequency, Z molecules/cc-sec	Pressure Dependency of Z (constant A_d)
Gas-Drop	1.74	All NO_2	285	3.1×10^{19}	p
Gas-Gas	1.74	$\beta = 21$	285	1.2×10^{23}	p^2

The frequency of the gas-gas collisions is about 4000 times greater than the gas-drop collisions at the low pressure of the calculations. At higher pressures the discrepancy would be greater, as seen from equations (41) and (38) for a constant drop surface area. Of course, not every collision between oxidizer and fuel (whether gaseous or liquid) results in reaction. However, if the activation energies and steric factors are even roughly similar for the two cases, the gas phase reactions would be dominant.

b. Ignition Delay Time

The analytical expressions yielding ignition delays in an engine are based on the concept indicated in Figure 1. In essence, an equation giving ignition delay times is developed, the vapor concentrations required in the equation being given in terms of the partial pressures of the reactants in the thrust chamber. The partial pressures of each propellant are obtained by the analysis for chamber pressurization due to propellant vaporization (Section III B).

We consider a volume element of vapor-phase reactants in a thrust chamber and assume heat losses from the volume are small. The heat equation, for a bimolecular reaction and no heat losses, becomes (eq. 36):

$$\bar{P}_g \bar{c}_{pg} \frac{dT}{dt} = QW = A Q c_1 c_2 e^{-E_a/RT} \quad (44)$$

Introducing non-dimensional variables

$$\theta = \frac{T}{T_g}, \quad \xi = At \sqrt{c_1 c_2}, \quad \alpha = \frac{E_a}{RT_g}, \quad \lambda = \frac{Q \sqrt{c_1 c_2}}{\bar{P}_g \bar{c}_{pg} T_g}$$

equation (44) becomes

$$\frac{d\theta}{d\xi} = \lambda e^{-\alpha/\theta} \quad (45)$$

In the case where $\alpha > 17$, Todes has shown that the ignition delay is very closely approximated by:

$$\tau_{ign} = \frac{e^{\alpha}}{\alpha \lambda} \quad (46)$$

Although in our case the values of α are between 9 and 12 due to the low activation energies of the ignition reactions, we will use equation (46) in the absence of a better criterion of ignition. Reintroducing the usual variables in equation (46), one obtains:

$$\tau_{\text{ign}} = \frac{RT_g^2}{E_a A Q} \frac{\bar{\rho}_g \bar{C}_{pg}}{c_1 c_2} e^{E_a/RT_g} \quad (47)$$

Expressing the concentrations c_1 and c_2 in terms of reactant partial pressures p_f and p_{ox} , and expressing the density and heat capacity of the reactant mixture in terms of the properties of the individual species, we obtain finally for the ignition delay time:

$$\tau_{\text{ign}} = \frac{R^2 T_g^3}{P_g E_a A Q} \left(1 + \frac{1}{\beta}\right) (C_{pf} + \beta C_{pox}) e^{E_a/RT_g} \quad (48)$$

where $P_g = p_f + p_{ox}$

$$\beta = \frac{p_{ox}}{p_f}$$

and C_{pf} and C_{pox} are molar heat capacities.

The reactant partial pressures, p_f and p_{ox} are obtained individually by the analysis in Section III B for chamber pressurization due to propellant vaporization.

The theoretical ignition delay time in a given engine operating under specified conditions is obtained by determining the point of intersection of the two curves of Figure 1. From the individual partial pressure curves for each reactant (by Sect. III B), the total pressure curve for the chamber can be constructed assuming no reaction, as well as a vapor phase composition curve (β values) and an average gas temperature curve for the vapor mixture. Values of P_g , T_g and β for various vaporization times are substituted into equation (48) until the calculated τ_{ign} agrees with the time associated with the particular values of P_g , T_g and β used.

Obviously, equation (48) applies to a system in which not only the pressure and temperature are constant during the ignition delay period but also the composition of the reactant mixture. Although the gas temperature variation is not too great during chamber pressurization due to propellant vaporization (Fig. 2), the gas pressure varies considerably as it rises toward a steady-state vaporization chamber pressure. Thus, the intersection of the two curves of Figure 1 where the dotted curve is given by eq. (48) would be expected to give ignition delays shorter than corresponding experimentally determined ignition delays.

In addition to the pressure variation, the vapor composition can be expected to vary due to the different vaporization rates of the two reactants. In general, the vapor composition, for usual liquid mixture ratios, is quite lean since the oxidizer is much more volatile. The sensitivity of calculated ignition delays to vapor composition, temperature and pressure is given in the following section.

2. Results of Hypergolic Ignition Model and Comparison with Experiment

a. N₂O₄/UDMH

Several pressure-ignition delay curves, calculated by equation (48), are plotted in Figure 25 for N₂O₄/UDMH. Three β values and two temperatures have been used in calculating the curves. The lower temperature (286°K) is an estimated value for the gas temperature in a typical engine during the ignition time based on the chamber pressurization calculations. The three values of β used with this temperature indicate the effect of vapor composition on ignition delay. The most favorable vapor composition for ignition is the equimolecular mixture for which $\beta = 1$ (Curve 3). The stoichiometric vapor mixture ($\beta = 4$) causes somewhat longer delays, (Curve 2). In a rocket chamber at space conditions, one might expect that the vapor-phase composition (for simultaneous propellant entries) would be roughly proportional to their vapor pressures at the temperature in question. On this basis, a β of about 6 for N₂O₄/UDMH gives the vapor composition. The ignition delays for this case (Curve 1) are seen to be about 40% longer than the delays of the equimolecular mixture at the same pressure.

The effect of temperature is indicated by a comparison of Curves 2 and 4 which are both for the stoichiometric vapor mixture. The ignition delays for the lower temperature case are roughly 50% longer than the delays for the warmer mixture at the same pressure. The temperature difference is 12°C.

The pressure-ignition delay curve based on estimated preignition vapor phase composition and temperature in an engine (Curve 1 of Fig. 25) is given in Figure 26 together with experimental ignition delays reported in Ref. 1. The experimental ignition delay times start when the lagging propellant first emerges as a liquid from the injector face.

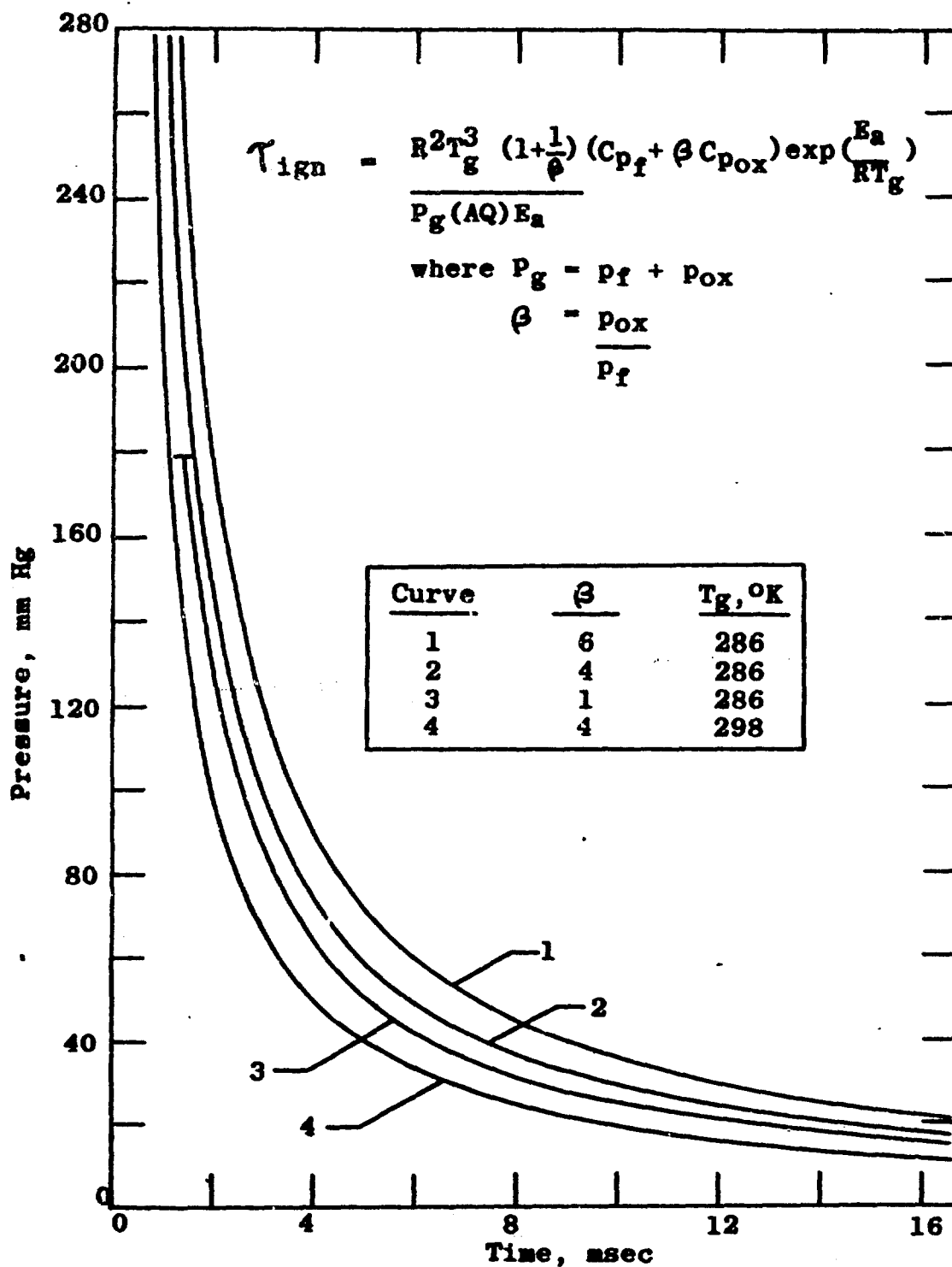


Figure 25. Theoretical Ignition Delay-Pressure Curves for N_2O_4 /UDMH

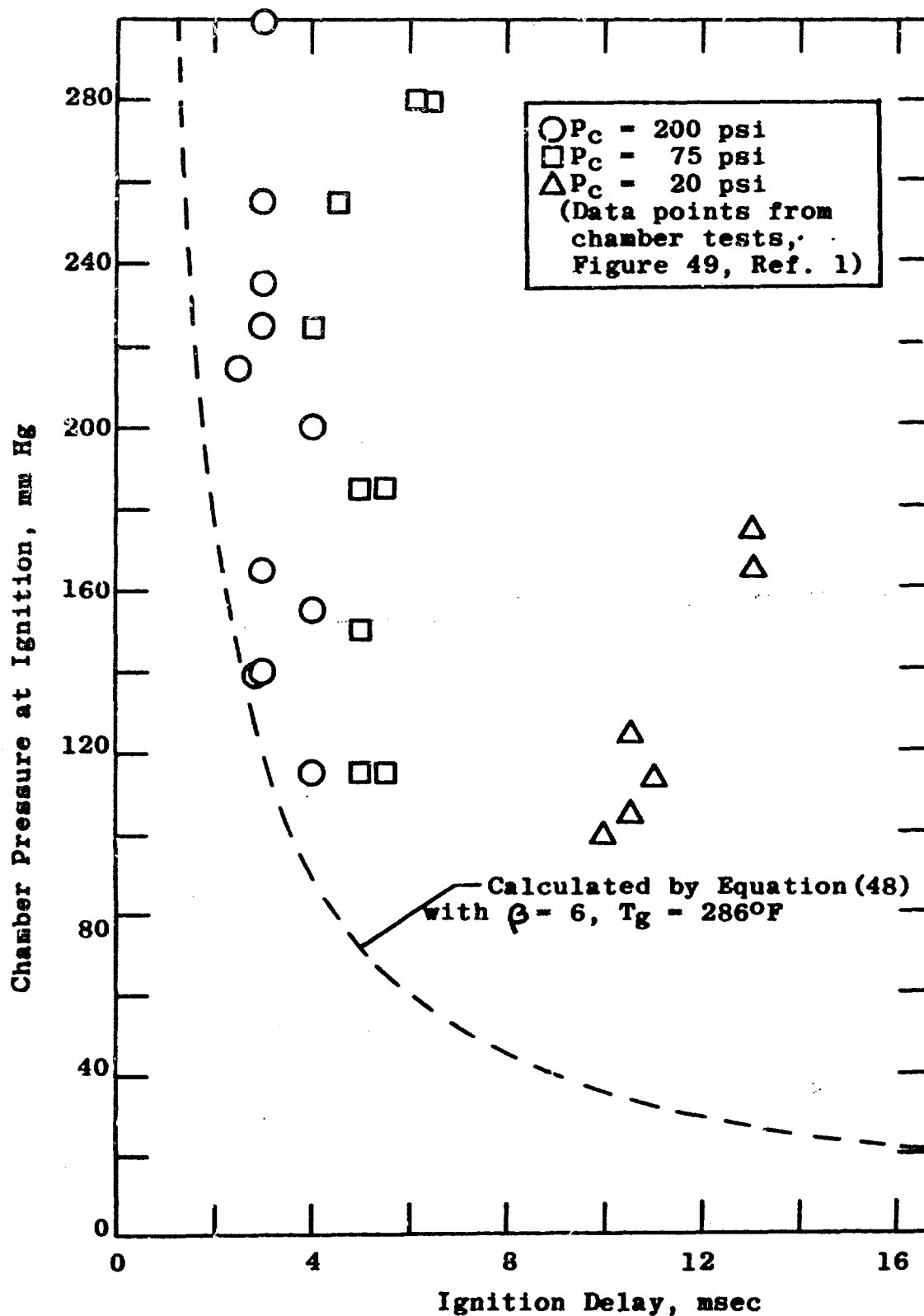


Figure 26. Comparison of Experimental and Theoretical Ignition Delays for Estimated Preignition Vapor Phase Composition and Temperature

These delays are plotted against the pressure in the chamber when ignition occurred. The delays were measured with engines of various thrust chamber configurations (design P_c , L^* , C.R.) operating at 1 mm Hg ambient pressure.

The theoretical curve, calculated for a fixed gas temperature and vapor phase composition, does predict delays shorter than experimental ones as anticipated. One could use some average value of the pressure in the chamber during the ignition delay time in order to get better agreement between experimental and theoretical results. However, this would be of little value until the actual vapor phase composition and temperature can be predicted by the chamber pressurization analysis in Section III B. As stated previously, an accounting of the transient build-up to full flowrate for the very volatile propellants (N_2O_4) must be included in the analysis in order to properly predict chamber pressurization, vapor composition and temperature. Since the less volatile hydrazine fuels undergo no, or only slight, "flashing" inside the injector volume, the analysis predicts their chamber pressurization rates adequately.

b. N_2O_4/MMH

Theoretical pressure-ignition delay curves for N_2O_4/MMH are given in Figure 27. The same two temperatures are used here as in the $N_2O_4/UDMH$ case. Again the equimolecular mixture ($\beta = 1$) gives the shortest delays at a given temperature (Curve 3). The stoichiometric mixture ($\beta = 2.5$) gives only slightly longer delays (Curve 2). Using the same criterion as before for estimating the preignition vapor phase composition, a high β results due to the lower vapor pressure of MMH. The calculated curve for this case indicates exceptionally long delays. The temperature effect on ignition delays for this combination is seen by comparing Curves 2 and 4.

A comparison of Figure 27 for N_2O_4/MMH with Figure 25 for $N_2O_4/UDMH$ shows the latter combination has significantly shorter delays.

3. Pressure Spiking Consideration

Two possible causes of pressure spiking are (1) explosion of the "pre-ignition reaction product" (adduct) at ignition and (2) very fast reaction of accumulated propellants.

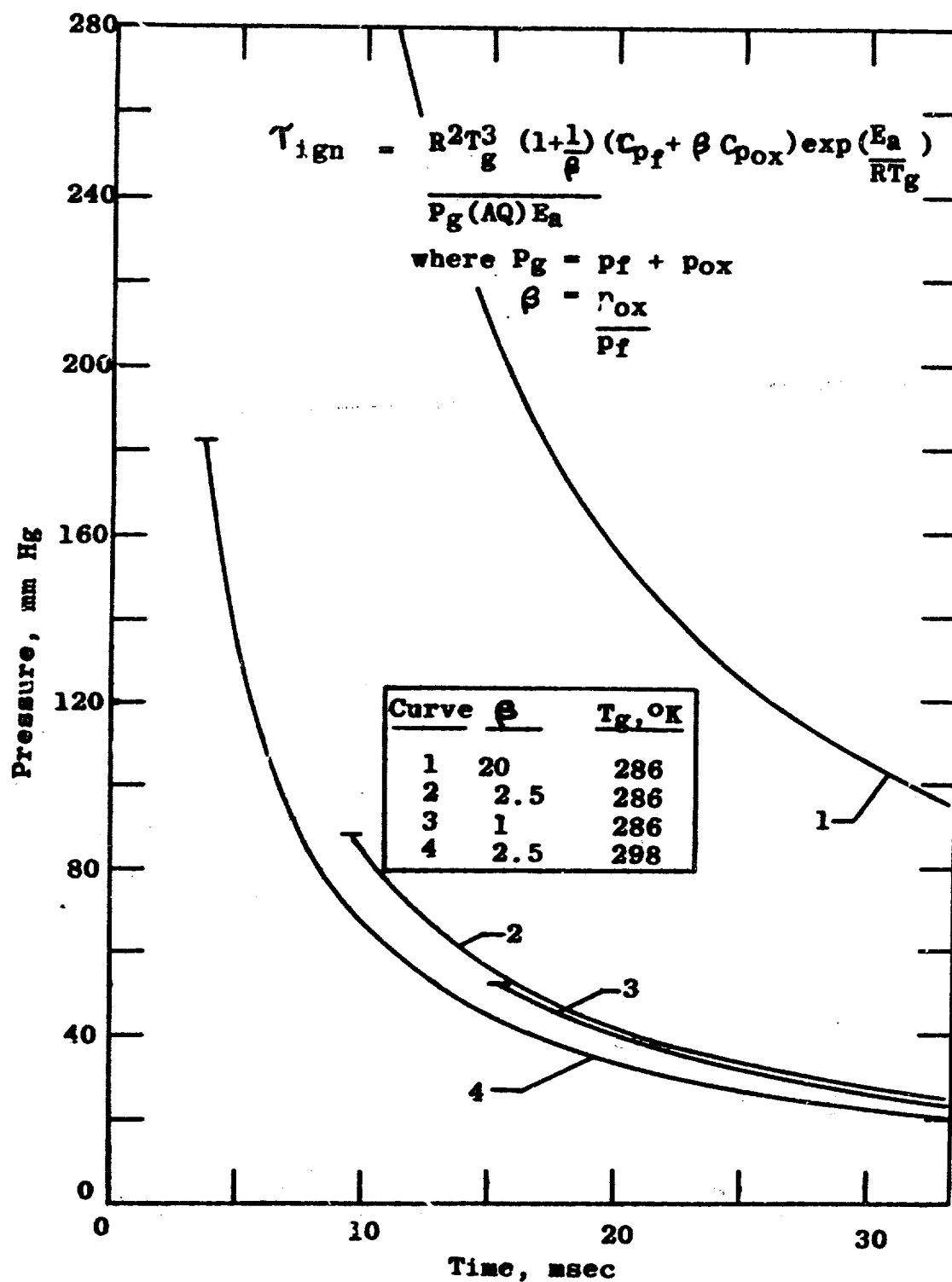


Figure 27. Theoretical Ignition Delay-Pressure Curves for N_2O_4/MMH

a. Pre-ignition Reaction Product

During the course of the experimental determination of the overall kinetic rate factors for ignition, it was found that all four hydrazine-type fuel/ N_2O_4 combinations formed a reaction product under conditions at which ignition did not occur. The "adduct" condensed on the walls of the reactor tubes and generally collected in the annulus at the base of the tubes. The adduct, which formed at pressures below the minimum ignition pressures (Tables V through VIII), is a clear yellow, viscous liquid when it accumulates at the base of the reactor.

With N_2H_4 as fuel, a negligible quantity of the adduct collected in the reactor annulus. Some material did condense on the reactor walls but the droplets "boiled" vigorously. Particularly with N_2H_4 , readily observable smoke was entrained in the flowing gas stream at the sub-ignition pressures.

The liquid adducts that collected with MMH, UDMH, and 50-50 as fuels are stable at room temperatures and pressures and have very low vapor pressures.

Chemical analyses, which were performed mainly on the MMH adduct, show the adduct has the characteristics of a monopropellant and contains considerable energy. Since the adduct forms at pressures which exist during ignition delay periods in attitude control engines, it is reasonable to suspect that the adduct is the cause of the pressure spikes that occur during engine start transients.

A qualitative correlation between the quantity of adduct formed and tendency toward spiking appears to exist. It was found in the case of NO_2 /MMH that the adduct which collected at the base of the reactor annulus was about 20% of the total mass of reactants flowed during the measured time period (9 minutes). Qualitatively, NO_2 /50-50 formed a similar amount of adduct but NO_2 /UDMH formed only about one-tenth as much. Engine tests indicate that spiking tends to be less severe with UDMH as fuel than with either MMH or 50-50 as fuel. The tendency of N_2O_4 / N_2H_4 toward spiking was not investigated in this program.

It is interesting to note that the 50-50 blend of N_2H_4 and UDMH forms an appreciable amount of liquid adduct while neither fuel individually with NO_2 forms more than about 10% as much.

It should be mentioned that the experimental apparatus in which the adducts were formed did not allow rates of formation of the adducts to be determined. The adducts formed well within 100 msec but whether they can form during typical ignition delay times (up to 10 msec or so) cannot be stated at present.

b. Fast Reaction of Accumulated Propellants

A second possible cause of pressure spiking is, of course, very fast reaction of accumulated, unreacted propellants. Once the analysis of chamber pressurization due to propellant vaporization is completed (Section III B.2.h), the mathematical model of hypergolic ignition can give the quantities of fuel and oxidizer in the chamber at ignition, the mass of each in the vapor phase, etc. In essence, the hypergolic ignition model gives not only the ignition delay time but also the conditions in the chamber at ignition from which pressure spikes result. These are then the initial conditions for a pressure spiking model (autoignition/detonation transition concept) which would permit evaluation of chamber geometry and ignition hydraulics from a pressure spiking viewpoint.

CONFIDENTIAL

AFRPL-TR-65-257

IV

TASK II - EVALUATION OF ADDITIVES TO REDUCE ACTIVATION ENERGY

(U) The experimental apparatus used in the chemical kinetics study, Figure 12, is well suited to the screening of additives. Since the fuels are metered in the liquid state and are subsequently vaporized drop-by-drop before entering the reaction chamber, it is assumed that the fuel-additive vapor stream has the same composition as the liquid fuel-additive mixture. Preferential vaporization is eliminated. Also, pressure ignition limits are a sensitive, reliable measure of ignition delays. The pressure limits are quite easily measured, and are obtained much less expensively and more accurately than engine ignition delays. Screening tests of many additives can be accomplished in a relatively short time. Promising additives should then be checked in actual engine tests to ascertain the improvement actually realized.

(U) Five fuel additives and one oxidizer additive were tested in the low pressure, premixed-vapors apparatus to evaluate their effect on hypergolic ignition of NO_2/MMH at low pressures. Generally, tests were made for both the stoichiometric and equimolecular mixtures.

A. Fuel Additives

(U) The five organic fuel additives are miscible with MMH and so mixtures of the liquids were prepared and tested in the same manner as the neat fuels themselves, i.e., liquid phase flow metering followed by drop-wise vaporization in a heated glass spiral.

(U) The results of the tests are given in Table XIV. The minimum ignition pressures for the two "neat" mixtures were measured prior to the additive testing.

(U) The data of the table shows that of the five fuel additives, only furfuryl alcohol had a significant beneficial effect. The minimum ignition pressure of the neat stoichiometric mixture was reduced by about 25% and that of the neat equimolecular mixture by about 17%. The other four additives had no significant effect, one way or the other.

CONFIDENTIAL

AFRPL-TR-65-257

TABLE XIV

EFFECT OF FUEL ADDITIVES ON IGNITION OF NO_2 /MMH MIXTURES

Additive	Minimum Ignition Pressure, mm Hg	
	Stoichiometric $\phi = 1.0$	Equimolecular $\phi = 2.5$
None	6.0	4.4, 4.3
Furfuryl Alcohol	4.4, 4.6, 4.5	4.0, 3.5, 3.3
Phenylether	5.8, 5.3, 5.8	4.5, 4.5
Methylbutynol	6.0, 6.0	4.0, 4.2
Ethylether	6.0, 6.5, 6.0	4.2
Benzene	6.0, 5.8, 6.1	4.6, 4.3, 4.0

4.7 cm burner diameter, $\frac{L}{D} = 10.8$

Total propellant flow rate = 33.6 cc/sec at STP

All additives are in amount of 10% by weight of fuel

B. Oxidizer Additives

(C) The very short ignition delays experienced with Compound A and the hydrazine-type fuels in the unconfined impinging stream tests of the preceeding program (Ref. 1) suggested that delays of N_2O_4 /MMH might be shortened if a fluorine-containing additive were used. Compound R, i.e., $\text{CF}(\text{NF}_2)_3$, looks very attractive on paper as it contains seven atoms of fluorine per molecule, has roughly the same volatility as N_2O_4 , and is miscible with N_2O_4 giving a mixture that is safe to handle at concentrations of the additive to over 20%.

(U) Because N_2O_4 is flowmetered in the vapor state in the experimental system, it was necessary to meter the additive flow separately to ensure a known concentration. The two vapor streams were mixed at the base of the burner, well before the mixing point with the fuel vapor.

CONFIDENTIAL

AFRPL-TR-65-257

(C) The tests with Compound R produced results unlike any others in the system. The minimum ignition pressure was not only increased, but the good reproducibility of the tests observed consistently to this point no longer was obtained.

(C) After a control run with the neat N_2O_4 /MMH combination, two tests with Compound R, at concentrations of 3 wgt. % N_2O_4 and 2 wgt. % N_2O_4 , were made using the stoichiometric mixture. Minimum ignition pressures for the doped system were higher than for the neat system. A repeat test of the neat combination, after purging the additive line, gave minimum ignition pressure of 35% higher than the corresponding pressure measured just prior to the Compound R additive tests. The pressure was even higher than those obtained with the additive. Two subsequent check runs with the neat combination, this time the equimolecular mixture, gave again minimum ignition pressures well above the value obtained prior to the additive tests.

(C) Only after thoroughly washing the burner tubes did results agree with the previously measured values for the neat system. Reproducibility became good once more. Compound R apparently contaminated the system. It was noted that the liquid which slowly collected at the base of the burner tubes during the Compound R tests was darker in color than the usual clear, yellow liquid from the neat N_2O_4 /MMH mixtures.

(U) The Compound R flow system was well suited to testing gaseous additives to the oxidizer. Thus a few tests with air and with oxygen were made. Minimum ignition pressures with both of these additives were higher than for the neat system. The increase in the minimum ignition pressure was found to depend on the amount of gaseous additive added. These two additives apparently act simply as diluents.

CONFIDENTIAL

AFRPL-TR-65-257

V

TASK III - THRUST CHAMBER DESIGN PARAMETER STUDY

A. Test Apparatus and Instrumentation

1. Experimental Facilities

(U) The thrust chamber design parameter studies were performed in a large vacuum tank so that the effect on ambient pressure due to propellant vaporization and combustion would be negligible. The vacuum tank is 7 ft. in diameter and 25 ft. long providing a volume of approximately 1000 cu. ft. It is fabricated of stainless steel for use with corrosive propellants and products. The tank has four 6 in. diameter ports along each side for instrumentation and observation purposes. For the schlieren pictures, 3/4 in. thick plate glass windows which had suitable optical qualities were used.

(U) The vacuum pump system consists of a Roots E 225 pump and a Roots 1000 blower. An adsorption column or trap for removing any residual F_2 and HF from the exhaust products is installed between the vacuum chamber and pumps. The column contains successive sections of activated sodium bifluoride, soda lime, and drierite. The vacuum pumps and adsorption column are shown in Figure 28.

(U) The durations of the thrust chamber tests were approximately 80 msec which was adequate to achieve steady-state chamber pressure to allow determination of the 90% P_c time. At flow rates corresponding to a design thrust level of 50 lb., the pressure rise in the tank after a test at a 10 mm Hg pressure level was less than 0.5 mm Hg because of the short run duration and large tank volume. In most cases the short duration of the tests also prevented damage to the transparent chambers, permitting them to be used for a series of tests without the necessity of entering the tank and replacing the cylinder.

(U) The oxidizer and fuel propellant systems for the liquid Compound A/hydrazine-type propellants and gaseous F_2/H_2 propellants are shown in Figures 29 and 30, respectively. Each liquid system consisted of a 300 cc stainless steel tank, safety valve, propellant solenoid valve, and associated hand valves and tubing. Each set was mounted on a separate plate which contained provisions for all necessary external connections such as pressurization, vents and loading so that a



5801-17

Figure 28. Vacuum Pumps and Adsorption Column for Fluorinated Oxidizer Propellant Combinations

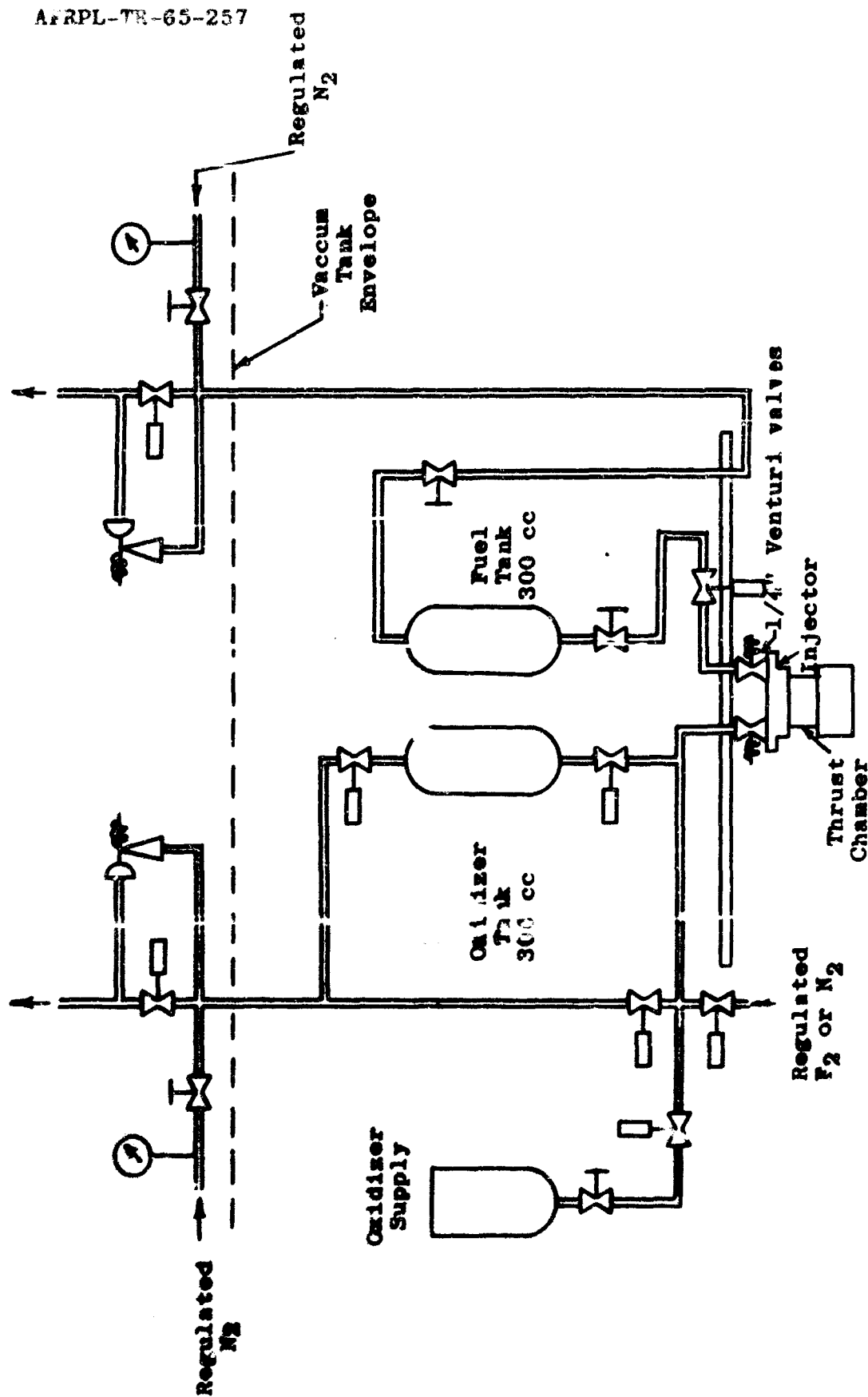


Figure 29. Schematic of Compound A/Hydrazine Propellant Systems

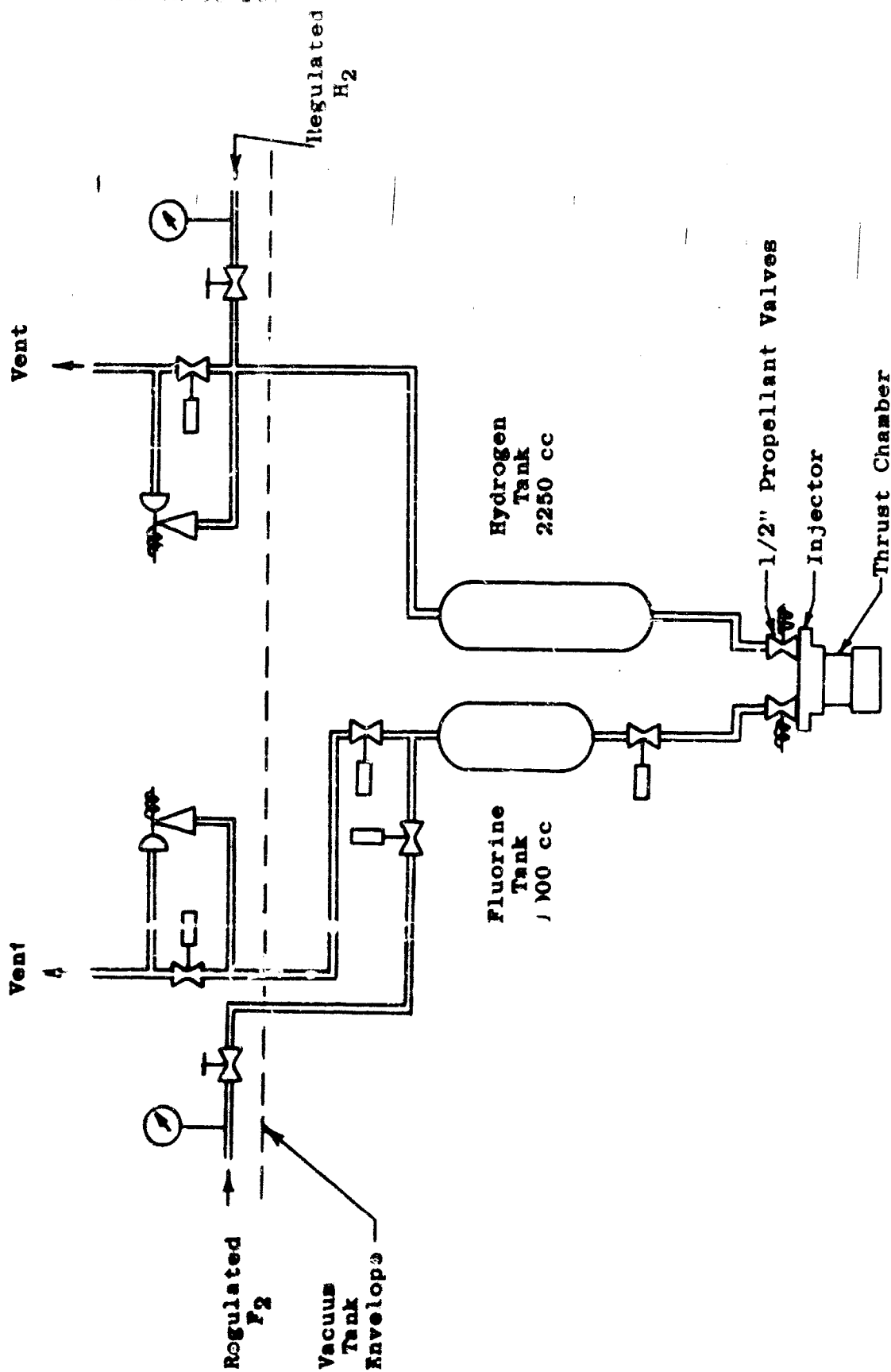


Figure 30. Schematic of Fluorine/Hydrogen Propellant Systems

propellant temperature conditioning bath could be installed, if desired. The tank sizes were increased to 1000 cc for the fluorine and 2250 cc for the hydrogen to minimize pressure decrease during the tests with gaseous propellants.

Special solenoid valves were procured to assure fast response rates and compatibility with both of the oxidizers used. The Compound A tests were made with 1/4 in. venturi valves manufactured by the Fox Valve Development Co., Inc., Hanover, N. J. These valves were fabricated from stainless steel and employed a pintle providing metal-to-metal propellant shutoff in the throat of the oxidizer venturi and Teflon-to-metal shutoff in the fuel valve. As a result, the propellant volume in the valve downstream of the seat was quite small and the valve was mounted directly to the back face of the injector which minimized the time required for the propellant to fill the system. The normal valve opening time was 3-4 msec at 24 volts D.C. Initially, attempts were made to use Teflon poppets in the oxidizer valve also to ensure zero leakage. However, it was found that Teflon could not withstand the high flowrate conditions, necessitating the use of aluminum alloy (6061-T6) poppets.

The gaseous propellant valves were similar in design but were sized for 1/2 in. lines so that flowrates equivalent to 50 lb. thrust could be obtained with gaseous propellants without excessive pressure drop. Orifices also were used in place of the venturi sections. Again, aluminum alloy was used for the oxidizer poppet to ensure suitable compatibility. Teflon was used for the fuel poppet. Both the 1/4 in. and the 1/2 in. sets of propellant valves were powered by a separate 90 VDC power supply to decrease valve response time to about 3 msec with the 1/2 in. valves and somewhat less with the 1/4 in. valves.

Standard 1/4 in. Jamesbury ball valves having Teflon seats were used as safety and vent valves for all propellant systems. The Teflon seats eroded in the F₂ vent valve about half way through the F₂ tests and the Compound A safety valve seats were partially eroded at the end of the test program although the latter was not severe enough to leak and may have occurred during passivation with F₂. The F₂ valve seats were replaced and the valve functioned satisfactorily for the balance of the F₂/H₂ tests.

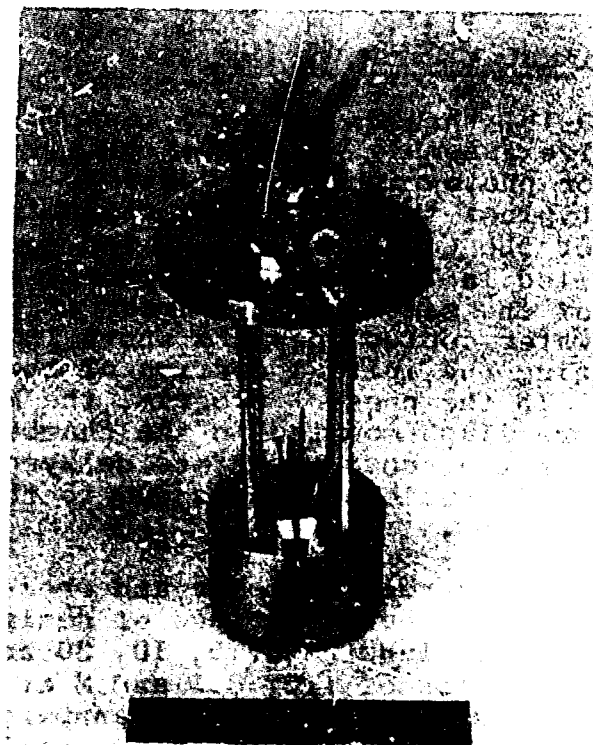
2. Experimental Hardware

The 50-lb. thrust, attitude control chambers consisted of an injector-valve assembly, a chamber flange, a transparent chamber section for photographic observation, and a stainless steel nozzle. A typical thrust chamber assembly, including the Fox valves used for the Compound A tests and two Kistler pressure transducers installed in the nozzle, is shown in Figure 31. An exploded view of the same thrust chamber is shown in Figure 32. The Kistler water cooled adapters shown in the pictures were used only during the initial portion of the original 10-month program. In the present program, the Model 601 and 603 transducers were flush-mounted in the chamber. A thin layer of grease over the sensing surface delayed until after shutdown the onset of spurious signals due to thermal effects from the combustion gases.

The nozzle throat diameter and chamber length and diameter were varied to provide a range of design parameters including characteristic lengths of 5, 10, 30 and 50 in. with nominal contraction ratios of 1.5, 3.5 and 8 at design chamber pressures of 20, 75 and 200 psia. The transparent chamber sections were fabricated from commercially available sizes of acrylic tubing which were simply cut to the desired length. Since standard tube diameters were used, actual contraction ratios ranged from 1.4 to 9.

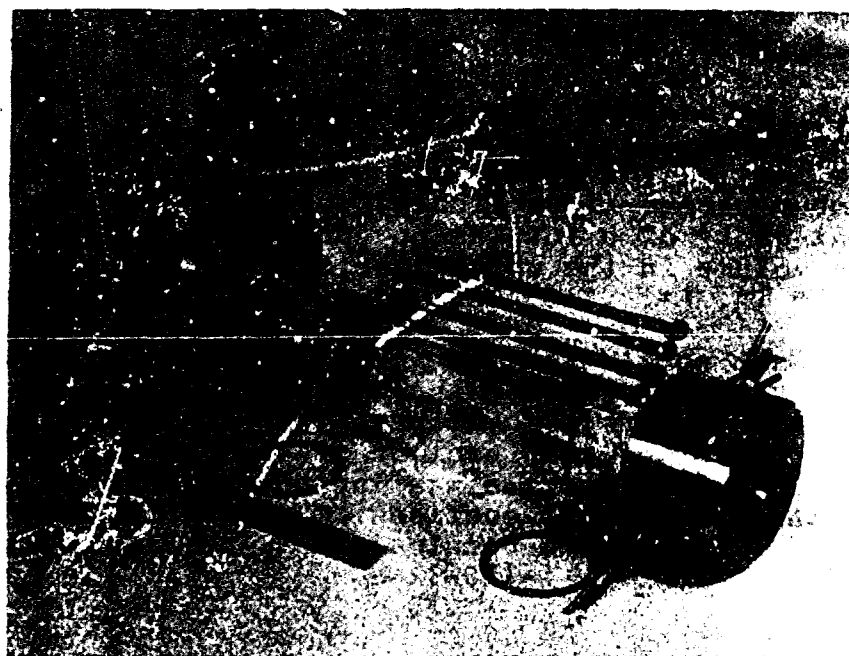
A separate stainless steel nozzle section was fabricated for each of the three contraction ratios at design chamber pressures of 20 and 75 psia and for contraction ratios of 3.5 and 8 at the 200 psia design chamber pressure. Tests were not made at a contraction ratio of 1.5 at 200 psia chamber pressure because the resulting chamber diameter was too small to be used with the desired injector configurations. Tests also were not made with the 1.5 contraction ratio nozzles at an L^* of 50 in. at any of the design chamber pressures because the L/D of the chamber became impractically long. Also, the 8 contraction ratio at an L^* of 5 in. was not physically possible to test because the volume in the nozzle section was more than equivalent to a 5 in. L^* .

Each nozzle section included a $3/4$ in. length with the same internal diameter as the inside of the respective chamber section to permit mounting of the Kistler pressure transducers. The volume of this section as well as that of the convergent portion of the nozzle was included in the L^* calculations for sizing the transparent sections. Typical nozzles are shown in Figures 33 and 34. The nozzles shown in Figure 33 are designed



5801-14

Figure 31. **Transparent Thrust Chamber Assembly**



5801-12

Figure 32. **Exploded View of Transparent Thrust Chamber**



5801-13

Figure 33. Set of Nozzles for Same Design Chamber Pressure (75 psi) and Different Contraction Ratios (1.5-8)



5801-16

Figure 34. Set of Nozzles for Same Contraction Ratio (3.5/1) and Different Design Chamber Pressures (20-200 psi)

for the same nominal chamber pressure (75 psia) but for different contraction ratios. The nozzles in Figure 34 are designed for the same contraction ratio (3.5), but for different nominal chamber pressures.

The entire chamber assembly was assembled with 1/4 in. threaded rods. Buna-N O-rings were used to seal the flanges and the transparent chamber sections with satisfactory results. This type of construction and assembly was used to facilitate rapid changes of chambers and nozzles because of the large number of configurations to be tested. In some tests the chamber flange at the injector end was replaced with a thicker flange to allow room for installation of a Kistler pressure transducer at the injector end of the chamber as well as the nozzle end. In these tests the transparent chamber length was reduced to maintain the design I*.

The twenty-seven thrust chamber configurations tested in the Task III program are shown in Table XV.

The two injectors used in the liquid propellant tests are shown in Figure 35. The majority of the tests were made with the single element doublet injector having 0.052 in. diameter orifices. The impingement angle was 60° , the impingement length was 0.12 in., oxidizer velocity was 75 ft/sec and fuel velocity 80 to 100 ft/sec. The single element triplet injector maintained the 60° angle between the center oxidizer orifice and each outside orifice and the impingement length was also 0.12 in. with the same propellant velocities. In both designs, the Fox valves were mounted directly on the back of the injector with the outlet section of the venturi inside the injector body so the throat was approximately in-line with the back face of the injector. This minimized the volume between the valve poppet at the venturi throat and the injector orifices.

The injector for the gaseous propellant tests, shown in Figure 36, consisted of a single axial orifice for the fluorine surrounded by a concentric annulus for the hydrogen. The orifice was 0.20 in. in diameter and the annulus, angled at 30° to the axis so that the hydrogen sheet impinged on the fluorine stream, was 0.020 in. wide. The larger propellant valves mounted directly on the rear face of the injector to minimize volume downstream of the valve.

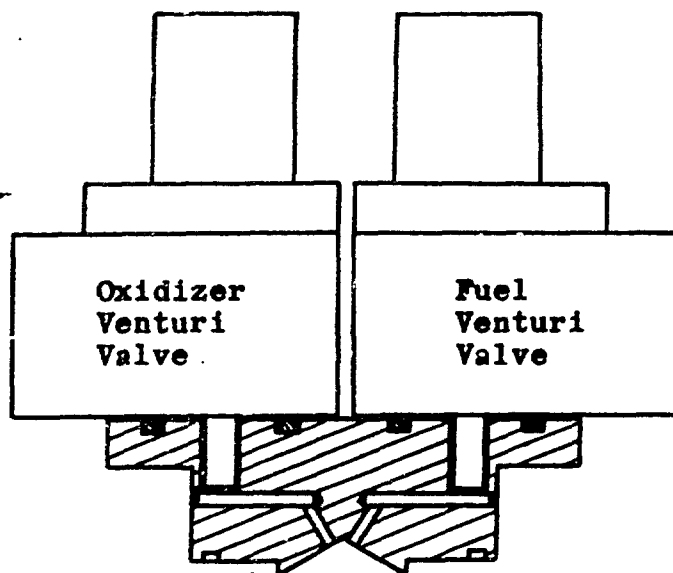
TABLE XV
TASK III - THRUST CHAMBER CONFIGURATIONS

Design P_c psia	D_c in.	A_c/A_t	Chamber Length, in. (a)			
			$L^* = 5$	$L^* = 10$	$L^* = 30$	$L^* = 50$
200	0.75	3.22	0.67	2.21	8.42	14.66
200	1.25	9.00	(c)	0.25	2.45	4.69
75	0.87	1.72	1.84	4.77	16.47	(b)
75	1.25	3.50	0.44	1.87	7.61	13.35
75	1.87	7.90	(c)	0.25	2.69	5.23
20	1.50	1.41	2.81	6.35	20.53	(b)
20	2.37	3.54	0.25	1.37	7.03	12.67
20	3.50	7.68	(c)	0.25	2.46	5.07

(a) Chamber length indicated is for transparent chamber length only. L^* includes additional volume in nozzle including 0.75 in. length equal to chamber diameter (for instrumentation) and nozzle convergent section.

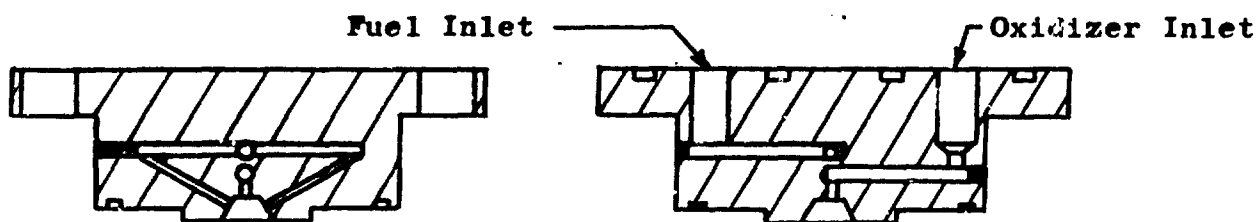
(b) Configurations not tested because of impractically long chamber lengths.

(c) Configurations not feasible because nozzle L^* is greater than 5 in.



Both Orifices = 0.052 in. diameter

(a) Doublet Injector with Valves Assembled



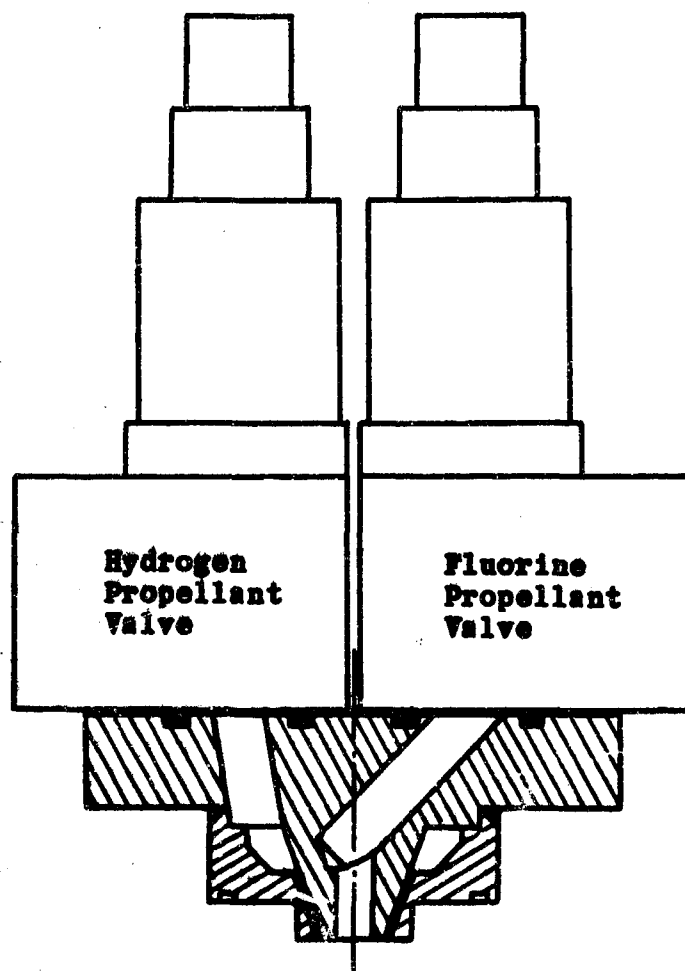
Oxidizer Orifice = 0.052 in. diameter

Fuel Orifice = 0.033 in. diameter

(Two sections taken 90° apart)

(b) Triplet Injector

Figure 35. Injectors for Compound A/ N_2H_4 - Type Propellants



Fluorine Orifice = 0.209 in. diameter

Hydrogen Annulus = 0.020 in. wide

Figure 36. Concentric Injector and Valves for F_2/H_2 Tests

3. Instrumentation

In addition to conventional instrumentation required for propellant pressurization and system monitoring, special instrumentation was employed to determine ignition delays and monitor pressure transients during the ignition process. This instrumentation included high speed schlieren movies of the propellant impingement zone, photomultiplier tube to detect ignition, high speed direct photography, and high response pressure transducer and recording equipment.

a. Schlieren System

The purpose of the schlieren system was to investigate propellant stream characteristics and determine the time at which the propellants impinged. Not only can the initial time of contact be ascertained by this method, but information on vaporization and mixing of the propellants could be obtained. Since it was anticipated that initial injection of the propellants would be in the vapor phase at the ambient pressures below 10 mm Hg, direct photography alone was not adequate for this purpose.

Although the schlieren instrumentation could not be used to detect propellant entry during the actual thrust chamber tests because of the poor optical properties of the plastic chambers, it was used to study the injection characteristics of each injector with each of the propellants that were investigated. Schlieren films were made of each injector without the chamber installed in order to determine the time from valve signal to propellant entry as both vapor and liquid to aid in analysis of the thrust chamber ignition tests. Schlieren films were also made in which both propellants were injected simultaneously in order to determine ignition delay in these unconfined tests for comparison with the thrust chamber tests.

A two-mirror, parallel-path schlieren system was used with a Fastax high-speed camera to obtain suitable time resolutions. The essential components of the system included a Unertl Model BH6 Normal and Color Schlieren Source, a pair of eight-inch front-surface parabolic mirrors of 64 in. focal length, knife-edge, and the Fastax camera capable of up to approximately 16,000 pictures per second using split-frame optics. Time resolution at ignition was approximately 7 frames (14 pictures) per msec.

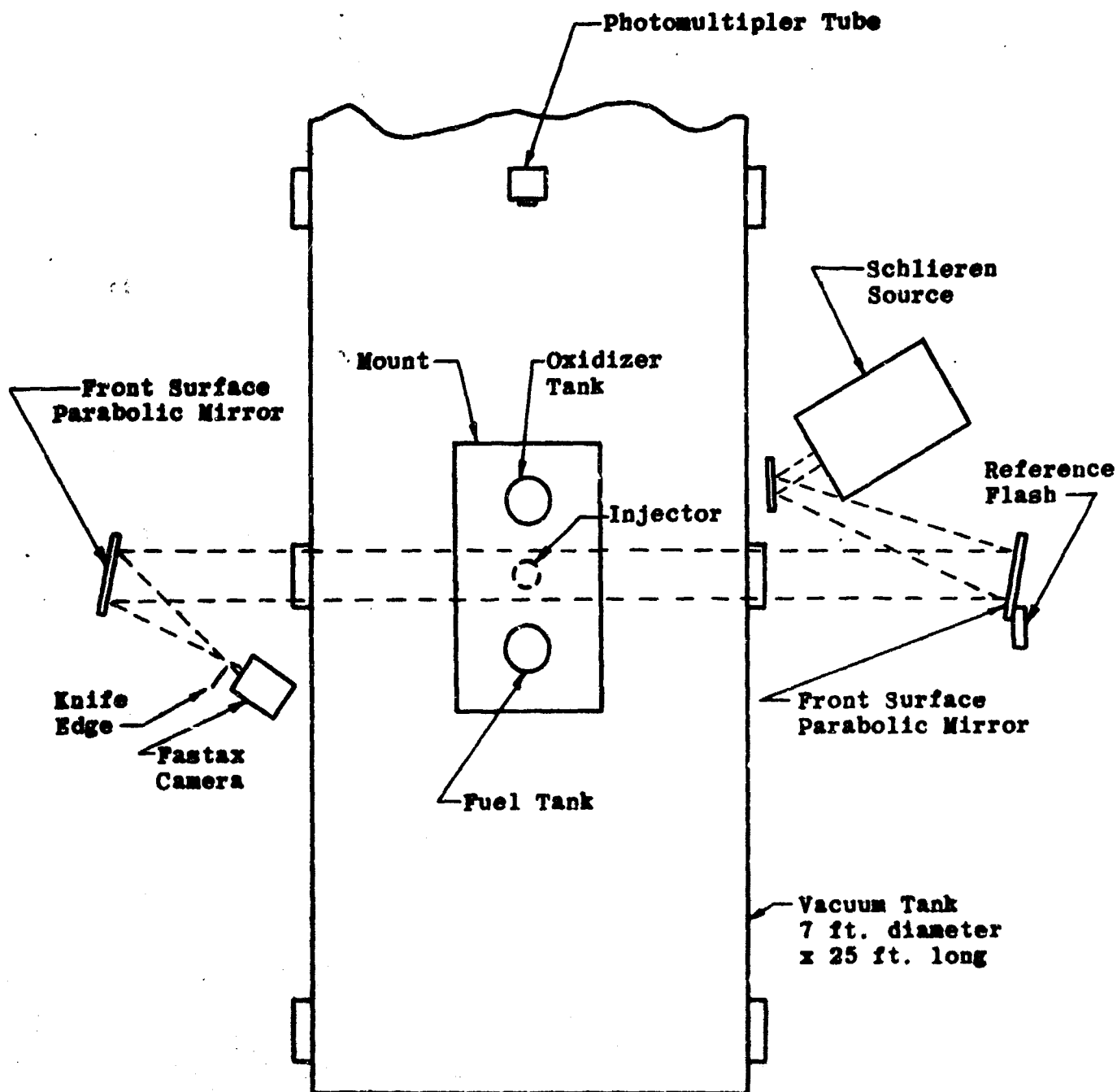


Figure 37. Schematic of Thrust Chamber Test Setup

The schlieren light source and one parabolic mirror are shown in Figure 38. The second mirror and Fastax camera with its controls are shown in Figure 39.

b. Direct Photography

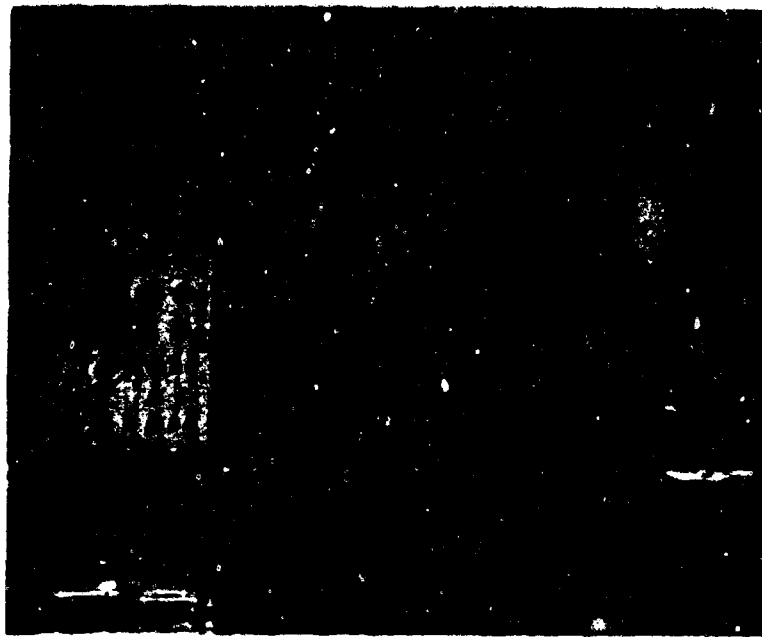
A Kodak camera having a speed of approximately 3000 frames per second and a second full-frame Fastax camera were used for direct photography in selected tests with the complete thrust chamber assembly. They were used to determine the location of ignition in the chamber and the nature of the propagation of the flame. The cameras viewed the chamber through the same tank windows as the schlieren and were located about six feet from the combustion area. Tank lights were not on so ignition location could be detected from the combustion light and therefore propellants could not be seen before ignition in these tests.

c. Ignition Detection

To determine the time at which ignition occurred, a flame detector consisting of an RCA 1P 28 photomultiplier tube was used. The tube is sensitive to wavelengths from about 2200A to 8000A. No filter was required since the tank was not illuminated for the thrust chamber tests. The flame detector was located in the vacuum chamber approximately 6 feet from the injector with an unobstructed view from the injector to the bottom of the tank, a distance of about 3 1/2 feet. It could sense ignition through the plastic chambers in the thrust chamber tests or elsewhere in the tank in the unconfined tests regardless of origin.

d. Pressure Instrumentation

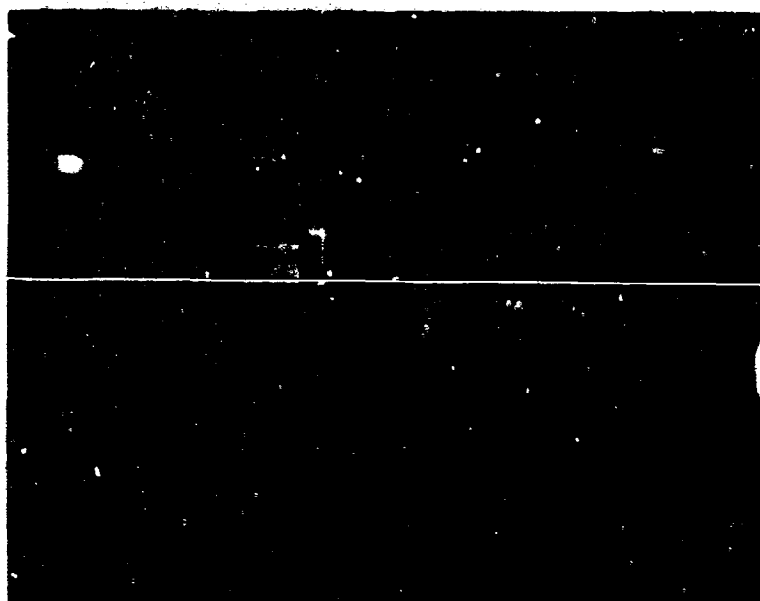
Chamber pressure was measured with Model 601 and 603 Kistler pressure transducers and Model 566 Kistler charge amplifiers. The outputs were read out on an oscilloscope and photographed for analysis. Two transducers were mounted in the same plane at the nozzle end of the thrust chamber, as shown in Figure 31, for all tests. A model 601 transducer having a frequency of 150,000 cps and rise time of 3 microseconds was calibrated for 345 mm Hg pressure at 3 cm deflection to define the preignition chamber pressure rise due to propellant entry and vaporization. A Model 603 transducer with only 1/5 the sensitivity, but with a natural frequency of 200,000 cps and rise time of 1 microsecond, was calibrated for several chamber pressure ranges, depending upon the design chamber pressure, to



5801-6

Figure 38.

Schlieren Light Source and Oscilloscope Setup



5801-4

Figure 39.

Schlieren Camera Setup

record steady-state pressure as well as any possible pressure spikes which might be experienced. A second Model 603 transducer was used at the injector end of the chamber in some tests to compare the chamber pressure at both ends of the chamber. The transducers were uncooled because of the short duration tests, but the diaphragms were protected from overheating with a layer of silicone grease to prevent drift after ignition. Although the grease would melt after several tests, particularly at the highest chamber pressure, and have to be replaced, it did not appear to react with the propellants nor did it affect the response of the transducers as indicated by comparative tests.

e. Recording Equipment

In addition to the schlieren and direct photography films, the primary means of data acquisition was a Tektronix Type 551 Dual-Beam Oscilloscope with suitable amplifiers to permit simultaneous display of four parameters. The output from the photomultiplier tube and the two Kistler transducers at the nozzle end of the chamber were monitored on the oscilloscope and recorded by a Polaroid camera. The fourth channel was used for the third Kistler transducer or for the current from the propellant valve circuit, depending upon the nature of the test.

The oscilloscope and camera are visible in Figure 38. Also shown is the single-flash strobe light attached to the parabolic mirror pedestal. The flash, having a duration of about 2 msec, was detected by the cameras and by the photomultiplier tube and was used as a reference signal to correlate the various instrumentation.

B. Experimental Thrust Chamber Program

The objective of the Task III thrust chamber tests was to evaluate the influence of thrust chamber design parameters on the ignition delay of two advanced propellant combinations, gaseous fluorine/hydrogen and Compound A/hydrazine-based fuels. The specific design parameters of interest were characteristic length, chamber pressure, contraction ratio, and oxidizer lead. The programmed range of these parameters is shown below:

Characteristic Length	5-50 in.
Chamber Pressure	20-200 psia
Contraction Ratio	1.5 - 8

CONFIDENTIAL

AFRPL-TR-65-257

Oxidizer Lead	+ .002 to - .002 sec
Thrust	50 lb
Ambient Pressure	0.2 psia or less

(U) The principal propellant combinations investigated during the program were gaseous fluorine/hydrogen and Compound A/ N_2H_4 . For comparison, tests were also made with Compound A/UDMH and Compound A/MHF-5.

(U) Since unconfined impingement tests, which have been reported in AFRPL-TR-65-105, indicated that injection parameters had no significant influence on ignition characteristics, simplified injectors were used so that injection characteristics (vaporizing, mixing) of the various propellants could be readily determined photographically. No attempt was made to optimize the injectors from a performance standpoint. The majority of the tests were made with a single concentric injector for the F_2/H_2 tests and a single-element doublet for the Compound A tests.

(U) All tests were made with ambient pressure in the large vacuum tank between 7 and 10 mm Hg (0.13 to 0.19 psia). The twenty-seven thrust chamber configurations shown in Table XV were tested with the two principal propellant combinations (F_2/H_2 , Compound A/ N_2H_4) to investigate the effects of characteristic length, chamber pressure, and contraction ratio with simultaneous propellant injection. Duplicate tests were made with most of the configurations to determine reproducibility of the results. Selected combinations of thrust chamber configurations were then used to evaluate the ignition characteristics of the other propellant combinations, the effect of oxidizer lead or lag and the effect of mixture ratio with the Compound A combinations.

(U) Results of the experimental program are discussed in the following sections.

C. Experimental Results - Compound A/Hydrazine-Based Fuel Tests

(C) A complete series of ignition tests was made with Compound A/hydrazine for the range of thrust chamber configurations which are tabulated in Table XV. The design chamber pressures selected for these configurations were 20, 75, and 200 psia for a nominal thrust level of 50 lbs. Comparative

CONFIDENTIAL

AFRPL-65-257

tests were made with Compound A/UDMH and Compound A/MHP-5 at all three chamber pressures in chambers with a 30 in. L* and 3.5 contraction ratio.

1. Schlieren Characterization of Propellants

(C) In order to determine the ignition delays for the various propellant combinations and chamber configurations, the propellant entry times were measured with the schlieren system. Since the schlieren techniques are ineffective with the plastic chambers installed, each propellant and injector was evaluated without the chamber attached and the results are shown in Table XVI. Each propellant was injected individually to determine the time at which vapor and liquid injection first appeared without being masked by the second propellant or ignition. Several additional schlieren tests were made with both propellants injected simultaneously to determine ignition delay and ignition location in the unconfined state. The column labeled "resistance" in Table XVI is the value of the series resistor used in the valve circuit to delay the second propellant valve. In all schlieren tests, a dummy propellant valve was used in place of the first propellant valve to duplicate the electrical conditions in the actual chamber tests.

(C) The physical properties of the propellants greatly affect the state in which the various propellants are first injected, particularly at the low ambient pressure involved. Significant differences between the propellants were detected in the schlieren films. For example, hydrazine does not vaporize sufficiently for the schlieren system to detect any gaseous propellant before entry of the liquid stream. Hydrazine first enters as a thin coherent stream even at low ambient pressure with no indication of vaporization or break-up within the 2 inch length visible in the schlieren field of view as shown in Figure 40. Entry time of the liquid was very easy to detect, but the entry time varied over a range of several milliseconds at low ambient pressure. Three tests with nominal flows of 0.08 lb/sec at 20 mm Hg pressure produced entry times of 10.7, 9.0 and 10.4 msec. These tests were longer than anticipated so additional tests were made at higher ambient pressures to determine if pressure influenced the timing. The flowrate remained constant with the changing back pressure since it was controlled by the pressure upstream of the venturi which remained constant. Entry times at the higher ambient pressures in Table XVI were shorter and more reproducible probably due to less vaporization of the hydrazine.

CONFIDENTIAL

CONFIDENTIAL

AFRPL-TR-65-257

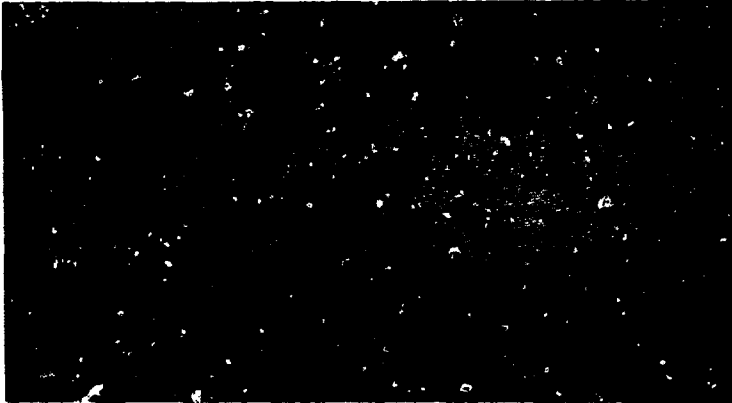
TABLE XVI

SCHLIEREN DATA - UNCONFINED TESTS OF COMPOUND A, N_2H_4 , UDMH,
AND MHF-5 USING DOUBLET INJECTOR

Propellant	Ambient Pressure mm Hg	Resistance ohms	w lb/sec	Valve Signal to		
				Vapor msec	Vapor & Liquid msec	Liquid msec
Compound A	20	0	.120	2.7	6.4	10.2
	20	0	.120	3.2	7.3	10.9
	20	0	.120	2.9	7.3	10.8
	20	10	.120	4.8	8.2	10.1
	20	20	.120	4.9	8.2	11.8
	20	30	.120	4.4	8.7	12.0
	20	0	.128	---	6.8	10.7
	20	0	.108	---	6.7	10.2
N_2H_4	750	0	.060			6.4
	750	0	.060			6.4
	750	0	.060			7.3
	750	0	.060			6.4
	150	0	.060			8.3
	100	0	.060			8.2
	50	0	.060			10.0
	20	0	.060			9.0
	20	0	.060			10.4
	20	0	.060			10.7
	20	5	.060			11.2
	20	10	.060			11.0
	20	20	.060			11.7
	20	30	.060			13.5
	20	40	.060			15.9
	20	0	.072			10.1
	20	0	.052			11.2
UDMH	17	0	.060	3.1	---	
	17	0	.060	3.4	7.1	
	17	0	.060	2.9	7.1	
MHF-5	11	0	.060		7.1	8.0
	11	0	.060		9.1	10.6
	11	0	.060		7.8	9.8
	11	30	.060		11.7	13.9
	11	40	.060		14.2	16.3
	11	0	.072		8.0	9.2
	11	0	.052		9.3	12.3

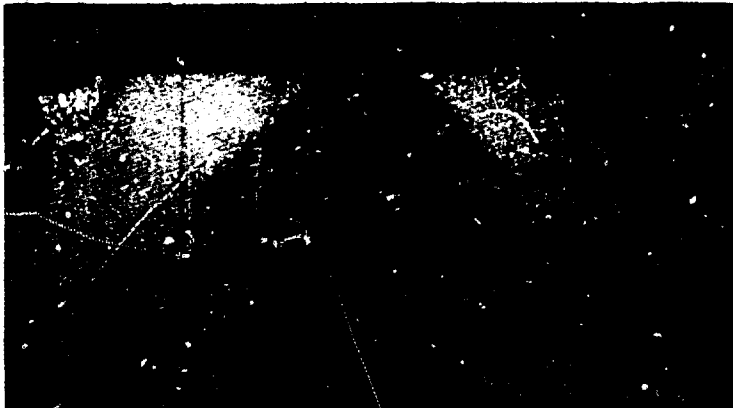
CONFIDENTIAL

AFRPL-TR-65-257



5801-22

**Figure 40. Schlieren of Hydrazine Injection,
Ambient Pressure = 20 mm Hg**



5801-21

**Figure 41. Schlieren of Compound A Injection,
Ambient Pressure = 20 mm Hg**

CONFIDENTIAL

AFRPL-TR-65-257

Varying hydrazine flowrate to obtain other mixture ratios did not change entry time by more than 1/2 msec at the 20 mm Hg pressure. Entry time was shorter for low O/F and longer for high O/F as would be expected for the varying flowrate. Fuel entry could be delayed up to 5 msec by varying the resistor in the propellant valve circuit.

In the other extreme, Compound A vaporized very drastically at low pressure and the precise time of Compound A entry was more difficult to define. At 20 mm Hg ambient pressure, vapor could barely be detected about 3 msec after valve "on" signal which corresponds to expected time of valve opening. A mixture of vapor and liquid appeared at about 7 msec and a definite change to a more dense liquid phase could be seen between 10 and 11 msec. In contrast with the cohesive hydrazine stream, however, the steady-state oxidizer flow appears to vaporize immediately upon injection at low pressure and the stream expands very rapidly as shown in Figure 41. The rapid spread of the oxidizer flow obscures the entrance of the fuel in the ignition tests.

The schlieren tests with UDMH, which has a higher vapor pressure than hydrazine, appear to be similar to the Compound A tests. Vapors first are visible at about 3 msec after valve "on" signal and they appear to become a mixture of liquid and vapor at 7 msec. However, there was no clear-cut transition to all-liquid as with the Compound A.

The initial state of MHF-5 appears to be a mixture of vapor and liquid based on the density of the schliere and the time at which it appears (about 7 msec) which corresponds quite closely with the appearance of the UDMH mixture at the same flowrate. The MHF-5 also vaporized rapidly after injection when steady state flow was established. The steady-state appearance of both UDMH and MHF-5 is quite similar to that of Compound A shown in Figure 41.

The schlieren tests with both propellants are reported in subsequent sections describing the results of the chamber configuration tests for the various fuels with Compound A. In general, ignition times of the unconfined tests were comparable to those for the chamber tests.

CONFIDENTIAL

AFRPL-TR-65-257

2. Thrust Chamber Tests - Compound A/N₂H₄

Table XVII summarizes the results of the thrust chamber tests with Compound A/N₂H₄ for the various thrust chamber configuration parameters with the doublet injector. These tests were made at a mixture ratio of 2.0.

The significance of the various data columns in Table XVII and the subsequent tables is as follows. The ambient pressure, P_a , is the pressure in the vacuum tank. It was measured before the test, but it did not increase more than 0.5 mm Hg during a test. Chamber pressure, P_c , is the steady-state value and 90% P_c is the time from valve "on" signal to 90% of the steady-state chamber pressure. These values were determined from the high-range pressure transducer which was also used to determine the shape of the pressure transient after ignition and the magnitude of any pressure peaks which might occur. The time from electrical signal to the propellant valves to both the first indication of a signal on the photomultiplier tube and the vertical deflection of the photomultiplier signal are designated by "PM_{First}" and "PM_{Vert}", respectively. The P_{ign} or pressures at ignition corresponding to the preceding photomultiplier signals are also included in the table. These pressures were measured by the pressure transducer having the expanded low pressure range for detection of initial pressure rise due to propellant vaporization. The final column in the table is the time at which the low-range pressure transducer rose nearly vertically, indicating a rapid chamber pressure rise due to ignition. The correlation between this indication of ignition and that of the photomultiplier tube is discussed further later in this section.

Tables XVIII and XIX summarize the additional mixture ratio and propellant lead tests made with Compound A/N₂H₄ using the doublet injector. In Table XVIII, the results are shown for tests at mixture ratios of 1.5, 2.0, and 2.5. These tests were made with chambers having a contraction ratio of 3.5 and L^* extremes of 5 and 50 in., at all three chamber pressures. Also included are four unconfined tests which were monitored with both the oscilloscope and the schlieren. In all the mixture ratio tests except test 963, the individual propellant flow rates were adjusted to maintain a constant total flow rate of 0.18 lb/sec. In test 963, the oxidizer flow rate was reduced to extend the low mixture ratio range to 1.0. In this test the total flowrate was reduced from 0.18 lb/sec to 0.144 lb/sec. The tests at a mixture ratio of 2.0 are repeated from Table XVII to provide a direct comparison with the other tests.

CONFIDENTIAL

TABLE XVII
THRUST CHAMBER TESTS - COMPOUND A/N₂H₄, DOUBLET INJECTOR, O/F = 2.0

Run No.	L* in.	Ac/Ac	P _a mm Hg	P _c psig	90% P _c msec	P _W first msec	P _{ign} mm Hg	P _W vert msec	P _{ign} mm Hg	P _W vert msec
876	5	3.22	10	76	14	11.5	170	11.5	170	12
877			10	---	--	8.5	110	10	240	10
878			10	---	--	10	140	12	190	12
943			9.5	80	19	10	90	10	90	10
883	10	3.22	10	86	17	8	67	10	183	10.5
884			10	92	12	10.5	148	11	170	10.5
885			10	92	12	9	125	9	125	9
872	10	9.00	8	86	19	8.5	35	12	>350	11
873			9.5	112	19	9	72	11	>350	9
853	30	3.22	10	152	17	9.5	58	11.5	150	12
854			10	---	--	8.5	58	10	140	11
886	30	9.00	10	105	18	10.5	105	10.5	105	11
887			10	112	17	10.5	120	10.5	120	10.5
911	50	3.22	10	---	--	9.5	45	12.5	150	14
912			10	148	16	12	125	12	125	13
898	50	9.00	10	152	30	11.5	55	11.5	55	12
899			10	160	21	11	55	12.5	170	13
879	5	1.72	9.5	20	19	7.5	43	10	95	10.5
880			10	30	19	10.5	148	10.5	148	11.5
874	5	3.50	10	33	--	11.5	80	11.5	80	11.5
875			10	33	18	10.5	84	10.5	84	10
925			10	21	17	10.5	45	12.5	142	12.5
926			10	32	16	9	45	11	260	11.5
927			10	61	20	12	110	12	110	12

CONFIDENTIAL

CONFIDENTIAL

AFRPL-TR-65-257

TABLE XVII (continued)

Run No.	L* in.	A _c /A _t	P _a mm Hg	P _c psig	90% P _c msec	P _W test msec	P _{ign} mm Hg	P _W test msec	P _{ign} mm Hg	P _c test msec
896	10	1.72	8	43	19	9	33	11	94	11.5
897			9	30	--	11.5	61	12.5	275	12.5
898	10	3.50	10	23	20	10	79	10	79	10.5
899	10		10	43	17	10	79	10	79	10
900	10	7.90	10	30	19	8.5	22	10.5	205	10.5
901	10		10	33	19	11	68	12	68	11
902	30	1.72	10	--	--	14.5	65	14.5	85	15.5
903	10		10	69	20	13.5	--	14	--	--
904	30	3.50	9	--	--	10.5	32	12	85	12
905	10		10	53	20	11.5	44	11.5	44	12
906	30	7.90	10	53	17	12	45	12	45	12.5
907	10		10	50	19	11.5	56	12	85	12
908	50	5.50	9	41	23	9	20	12	55	13
909	10		9.5	46	23	12	45	12	45	13
910	50	7.90	10	34	23	9.5	20	12	39	12.5
911			10	52	19	10	20	11.5	39	12
912			10	53	20	11	45	11	45	11.5
913	5	1.41	10	6	14	11	20	14	50	14
914			10	6	14	12	44	12	44	12.5
915	5	3.54	10	5	14	11.5	20	11.5	20	11.5
916	10	1.41	10	7	17	8.5	10	11	27	11.5
917			10	7	17	10.5	20	10.5	20	11
918	10	3.54	7.5	10	22	13.5	28	13.5	28	14
919			10	11	24	13	25	13.5	31	13.5

CONFIDENTIAL

CONFIDENTIAL

AFRPL-TR-65-257

TABLE XVII (continued)

Run No.	L* in.	A _c /A _t	P _a mm Hg	P _c psig	90% P _c msec	PM _{1/2} msec	P _{ign} mm Hg	PM _{1/2} msec	P _{ign} mm Hg	P _{1/2} msec	P _{cryst} msec
922	10	7.68	9.5	4	18	10	10	13.5	10	33	13.5
923			10	5	17	14	30	14.5	30	33	14.5
915	30	1.41	10	15	23	13	30	13	30	30	14.5
916			10	15	28	13	15	13.5	15	20	14.5
851	30	3.54	10	9	18	10.5	15	10.5	15	15	11
852			10	3	18	11	15	11	15	15	11.5
888	30	7.68	10	7	16	9.5	10	9.5	10	15	11.5
889			10	5	15	9.5	10	9.5	10	9.5	10.5
907	50	3.54	10	12	24	10	10	11.5	10	10	13
908			10	10	27	12	10	13	10	10	14
900	50	7.68	9.5	11	18	10.5	10	13.5	10	15	14
901			10	12	22	11	10	12	10	15	13.5
929	Unconfined		20	---	--	11.1	20	11.1	20	20	---

CONFIDENTIAL

CONFIDENTIAL

TABLE XVIII

THRUST CHAMBER TESTS - COMPOUND A/N₂H₄, DOUBLET INJECTOR, VARIABLE MIXTURE RATIO

O/F	Run No.	L* in.	Ac/At	P _a mm Hg	P _c psig	90% P _c msec	PM first msec	P _{ign} mm Hg	PM vert msec	P _{ign} mm Hg	P _c vert msec
1.5	941	5	3.22	9.5	119	14	8.5	101	11	>350	8.5
2.0	876			10	76	14	11.5	170	11.5	170	12
	877			10	---	--	8.5	110	10	240	10
	878			10	---	--	10	140	12	190	12
	943			9.5	60	19	10	90	10	90	10
2.5	939			9	96	14	12.5	296	12.5	296	12.5
	940			10	83	14	12.5	>350	12.5	>350	12
1.0**	963	5	3.50	10	51	21	10	195	10	195	11
1.5	961			9	46	15	10.5	77	10.5	77	10.5
	962			9.5	51	21	10	126	10	125	9
2.0	874			10	33	--	11.5	80	11.5	80	11.5
	875			10	33	18	10.5	84	10.5	84	10
	925			10	21	17	10.5	46	12.5	142	12.5
	926			10	32	16	9	45	11	280	11.5
	927			10	61	20	12	10	12	110	12
1.5	947	50	3.50	10	63	28	10	10	10	10	11.5
	948			10	63	28	9	10	11	96	9.5
2.0	909			9	41	23	9	20	12	55	13
	910			9.5	46	23	12	45	12	45	13
2.5	949			10	63	32	12.5	55	13.5	55	13.5
	950			10	63	29	13.5	70	13.5	70	14

** Total flow reduced from 0.18 to 0.144 lb/sec for this test.

CONFIDENTIAL

CONFIDENTIAL

TABLE XVIII (continued)

O/F	Run No.	L* in.	Ac/At	Pa mm Hg	Pc psig	90% Pc msec	PMfirst msec	Pign mm Hg	PMvert msec	Pign mm Hg	PMvert msec	Pcvert msec
1.5	951	5	3.54	10	5	12	10.5	30	10.5	30	10.5	10
	952			10	7	16	9.5	30	9.5	30	9.5	9.5
2.0	953			10	5	14	11.5	20	11.5	20	11.5	11.5
2.5	954			10	5	14	12.5	30	12.5	30	12.5	12.5
	955			10	6	14	12.5	39	12.5	39	12.5	12.5
1.5	934	50	3.54	10	14	18	8	10	9	10	9	9
	935			10	14	22	9	10	9	10	9	10
	936			10	17	17	9	10	9	10	9	10
2.0	907			10	12	24	10	10	11.5	10	11.5	13
	908			10	10	27	12	10	13	10	13	14
2.5	932			10	11	27	12	30	12	30	12	12.5
	933			10	14	27	11.5	25	11.5	25	11.5	12.5
1.5	928	Unconfined		20	---	--	9.4	20	9.4	20	9.4	---
	931			20	---	--	8.8	20	9.2	20	9.2	---
2.0	929			20	---	--	11.1	20	11.1	20	11.1	---
2.5	930			20	---	--	9.4	20	12.0	20	12.0	---

CONFIDENTIAL

TABLE XIX
THRUST CHAMBER TESTS - COMPOUND A/N₂H₄, DOUBLET INJECTOR, VARIABLE LEADS

Lead Prop.	Lead msec	Run No.	L* in.	A _c /A _t	P _a mm Hg	P _c psig	90% P _c msec	P _{st} first msec	P _{ign} mm Hg	P _{st} second msec	P _{ign} mm Hg	P _{st} second msec
Fuel	.5	945	5	3.23	10	75	15	10.5	375	12	>350	9.5
	0	976			10	76	14	11.5	170	11.5	170	12
		977			10	--	--	8.5	110	10	210	10
		978			10	--	--	10	140	12	190	12
		943			9.5	80	19	10	90	10	90	10
Ox.	.5	944			9.5	85	14	11	135	12.5	>350	11
Ox.	3	946			10	--	16	14	>350	14.5	>350	13.5
Fuel	5	955	5	3.54	9.5	7	16	11	10	11	10	11
Fuel	3	957			9	7	15	10.5	9	10.5	9	10
Fuel	1	956			9	5	14	11.5	34	11.5	34	11
	0	953			10	5	14	11.5	20	11.5	20	11.5
Ox.	3	960			10	5	17	12.5	30	13	105	12
Ox.	5	959			9.5	5	18	15.5	35	15.5	35	15.5
Fuel	1	918	30	1.41	9.5	17	21	11.5	10	13	20	14
	0	915			10	15	23	13	30	13	30	14.5
		916			10	15	26	13	15	13.5	20	14.5
Ox.	1	917			9	10	32	15.5	39	15.5	39	17
Ox.	2	919			10	10	23	13	15	15	33	15
Fuel	3	937	50	3.54	10	15	27	9	10	11	15	11.5
	0	907			10	12	24	10	10	11.5	10	13
		908			10	10	27	12	10	13	10	14
Ox.	3	938			10	13.5	21	13	20	13	20	14.5

CONFIDENTIAL

AFRPL-TR-65-257

Table XIX contains the oxidizer lead/lag tests. These tests were made by delaying the lagging propellant valve by adjusting the appropriate resistor in the valve circuit. The lead time was computed from the previously discussed schlieren tests (Table XVI) of the individual propellants. Most of these tests were performed at the lowest design chamber pressure to more readily detect differences in ignition time.

a. Ignition Characteristics

Although the photomultiplier tube is used to detect ignition in the thrust chamber tests, ignition also is indicated in each test by a sharp increase in the rate of pressure rise measured by the Kistler pressure transducer calibrated for the low pressure range to detect vaporization and ignition. Generally, both of these indications of ignition coincide although there may be up to a 0.75 msec lag in the ignition time indicated by the pressure transducer installed in the nozzle section. This lag is due to the finite time required for propagation of the flame front from the injector to the nozzle and is discussed in more detail in the discussion of the Compound A/MHF-5 tests.

In some tests, however, there were slight fluctuations in the photomultiplier trace on the oscilloscope up to 3-4 msec in advance of the vertical deflection associated with ignition. These fluctuations were small in amplitude and even returned to zero deflection for one or more milliseconds in some tests before the final strong deflection occurred. Both the time from valve signal to these initial small fluctuations (when they occurred) and the vertical deflection are reported under the "PM_{first}" and "PM_{vert}" columns, respectively, in Tables XVII, XVIII and XIX. The pressure in the chamber at each of these times is also reported. In the tests in which the small fluctuations did not occur the time indicated in the "PM_{first}" column is the same as in the "PM_{vert}" column.

Schlieren tests were made without the chamber and nozzle installed to determine ignition delay in an unconfined condition and to investigate these fluctuations to determine which signal from the photomultiplier tube should be considered as the indication of ignition. These tests are reported in Table XVIII as Tests 928-931 and are summarized below:

CONFIDENTIAL

A7RPL-TR-65-257

Test	Ignition Time, msec		
	Photomultiplier		Schlieren
	Initial Signal	Vert. Defl.	
928	9.4	9.4	9.8
929	11.1	11.1	11.2
930	9.4	12.0	12.1
931	8.8	9.2	9.2

The time resolution of the schlieren system was approximately 0.07 msec per picture. As indicated in the table, the schlieren indication of ignition and the vertical deflection of the photomultiplier tube agreed very closely in each of the tests. In test 930, however, the photomultiplier detected slight light output at 9.4 msec and again at 9.7 msec but returned to zero before the strong deflection at 12.0 msec. The schlieren pictures indicate that liquid oxidizer entered at 9.2 msec but that there was no evidence of ignition until 12.1 msec. Ignition occurred at the impingement point of the two propellants, well within the field of view of the camera. Similar photomultiplier fluctuations were experienced in Test 931 although the time between the initial fluctuations and the vertical rise was much shorter.

On the basis of these tests it appears that the small fluctuations in the photomultiplier trace are the result of very small localized and discontinuous reactions and should not be considered as a true indication of ignition. This is also indicated by the relatively small increase in chamber pressure during the period in which these fluctuations occur prior to the vertical deflection of the photomultiplier tube output.

Ignition in a chamber was also studied photographically with high-speed motion pictures at about 4000 frames per second. In tests 947 to 950, reported in Table XVIII, the first visible sign of ignition was a small flame, 1 to 2 inches long, at the injector end of the chamber. In the two lower mixture ratio tests (947-948), the first visible light was detected at 9 and 10 msec after valve opening while chamber pressure was still at the original ambient pressure of 10 mm Hg. The flame filled most of the chamber cross-sectional area and required 11 to 13 frames (about 3 msec)

CONFIDENTIAL

CONFIDENTIAL

AFRPL-TR-65-257

to reach the nozzle end of the chamber. During this period, the chamber pressure increased to 300 mm Hg and continued to rise slowly and smoothly thereafter.

By contrast, the higher mixture ratio tests (949-950) did not show any visible light until 12.5 and 13.5 msec by which time the chamber pressure had increased to 55 and 70 mm Hg due to propellant vaporization and possibly some low order reaction. The flame initially was visible only in the center of the chamber and reached the nozzle within 1 msec. Chamber pressure increased rapidly during the 1 msec period and the low pressure trace rapidly rose off scale during this period. The high pressure trace also rose abruptly with a series of small oscillations of about 10-15 psi amplitude. In all four tests, the photomultiplier indication of ignition preceded the abrupt pressure rise by 0.5 to 1.5 msec.

From analysis of the motion pictures, it is evident that ignition is initiated at the impingement point of the liquid propellants and proceeds to fill the chamber over a period of 1 or more milliseconds. The time difference between chamber pressure rise and photomultiplier output is due to the finite time required for ignition to travel the length of the chamber. The time delay will be discussed in more detail in the Compound A/MHF-5 tests where pressure transducers were located at both ends of the chamber. As the result of the schlieren and direct photography tests, it was concluded that the vertical deflection of the photomultiplier tube should be taken as the true indication of ignition and subsequent discussions will be based on this time.

As discussed at the beginning of this section, the schlieren tests indicated some variation in the determination of propellant entry time. Both Compound A and N_2H_4 entered as a liquid between 9 and 11 msec at nominal flowrates. The ignition times from valve signal in Table XVII range from 9 to 14.5 msec. Thus, the uncertainty in propellant entry time represents a large fraction of any calculated ignition delay. In any event, ignition delays are certainly less than 5 msec from entry of the second liquid propellant and are more probably less than 2 msec even at the low ambient pressures used for these tests.

b. Effect of Thrust Chamber Configuration on Ignition and Rise Time

The effects of thrust chamber configuration on ignition and rise time to 90% of steady-state chamber are shown

CONFIDENTIAL

CONFIDENTIAL

AFRPL-TR-65-257

in Figures 42 and 43, respectively, for the tests reported in Table XVII. The times shown in Figure 42 are from electrical signal to the valve so that the times required for propellants to reach the chamber (9-11 msec) are included. From Figure 42 it is evident that the thrust chamber configuration effects on ignition time are not significant. The range of ignition delays are quite similar for all configurations except for the 50 in. L^* tests. Although the average ignition times are approximately the same, the shortest ignition time with 50 in. L^* chamber was 11 msec compared with 9-10 msec for the other L^* configurations, indicating the possibility of a slight L^* effect at large L^* s. Also, close examination of the data indicates that the ignition times for the 200 psia design chamber pressure configurations were less than 12.5 msec, while the ignition times for the other design chamber pressure configurations were up to 14.5 msec. Although it appears that the average ignition times are longer for the 30 in. L^* tests having a contraction ratio of 1.5, similar tests with this contraction ratio at other L^* s do not indicate any significant effect of this parameter.

Similarly, there are no significant effects of thrust chamber configuration on rise time as indicated in Figure 43. Rise times shown in the figure are measured from ignition to 90% of steady-state chamber pressure. As might be expected, however, the rise times appear to increase as the L^* of the thrust chamber is increased due to the larger volumes involved, although the effect is small over the wide range of configurations actually tested.

Contrary to the results of thrust chamber tests performed previously with N_2O_4 and hydrazine-type propellants (Ref. 1), it is apparent that the influence of thrust chamber configuration on ignition and rise time is small with Compound A and N_2H_4 . These results are not contradictory however, because it also has been demonstrated in unconfined tests that ignition of Compound A and hydrazine is not influenced significantly by ambient pressure. The ignition characteristics of N_2O_4 /hydrazine-type propellants are a strong function of ambient pressure and depend upon vaporization of the propellants to increase the pressure in the chamber to a level at which ignition can occur. Although pressure also may rise in the chamber in tests with Compound A/hydrazine-type fuels due to vaporization prior to ignition, ignition does not depend on pressure rise and there is no direct correlation between ignition delay and pressure in the chamber at ignition.

CONFIDENTIAL

CONFIDENTIAL

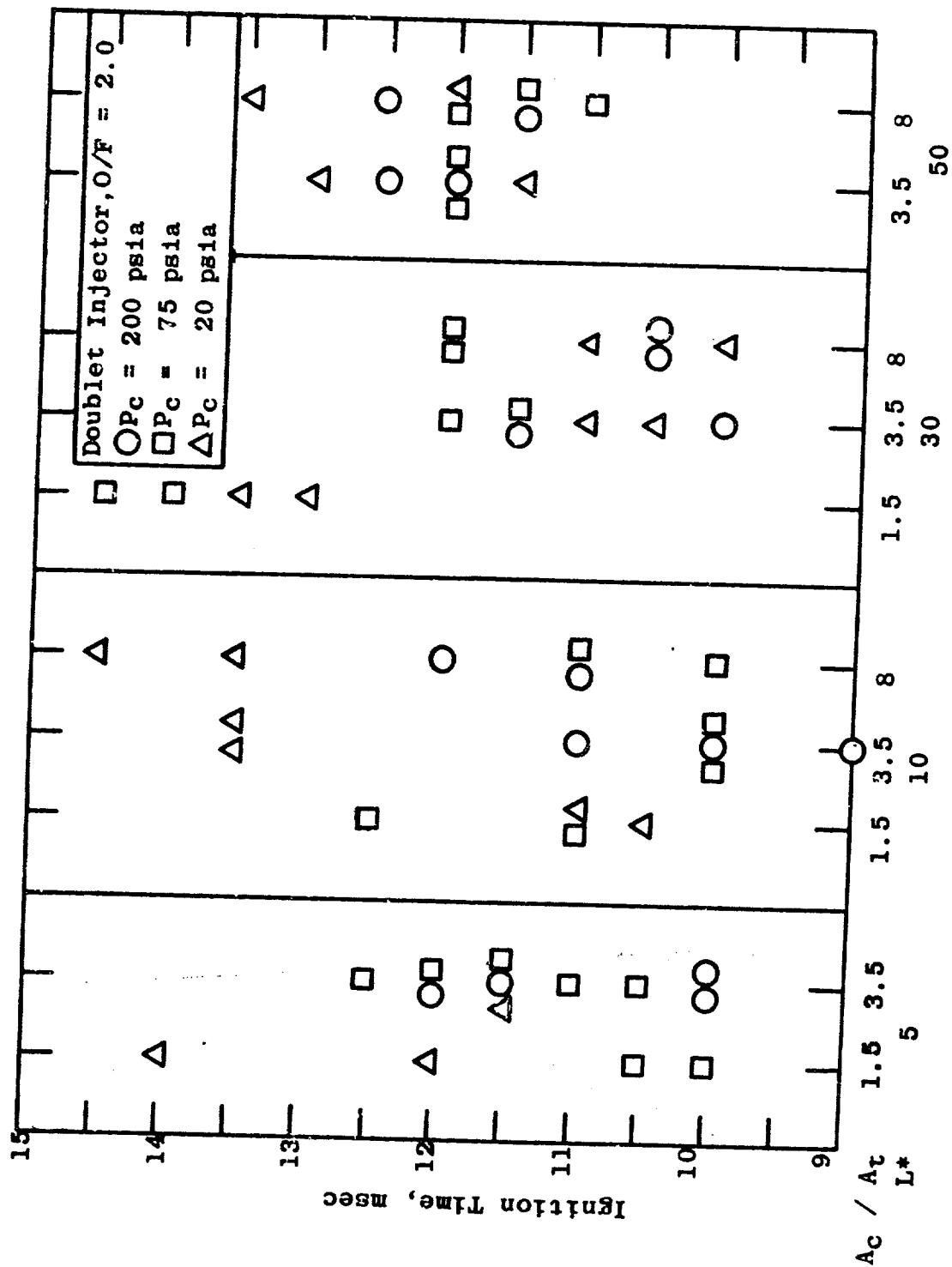


Figure 42. Effect of Chamber Configuration on Ignition Time - Compound A/Hydrazine

CONFIDENTIAL

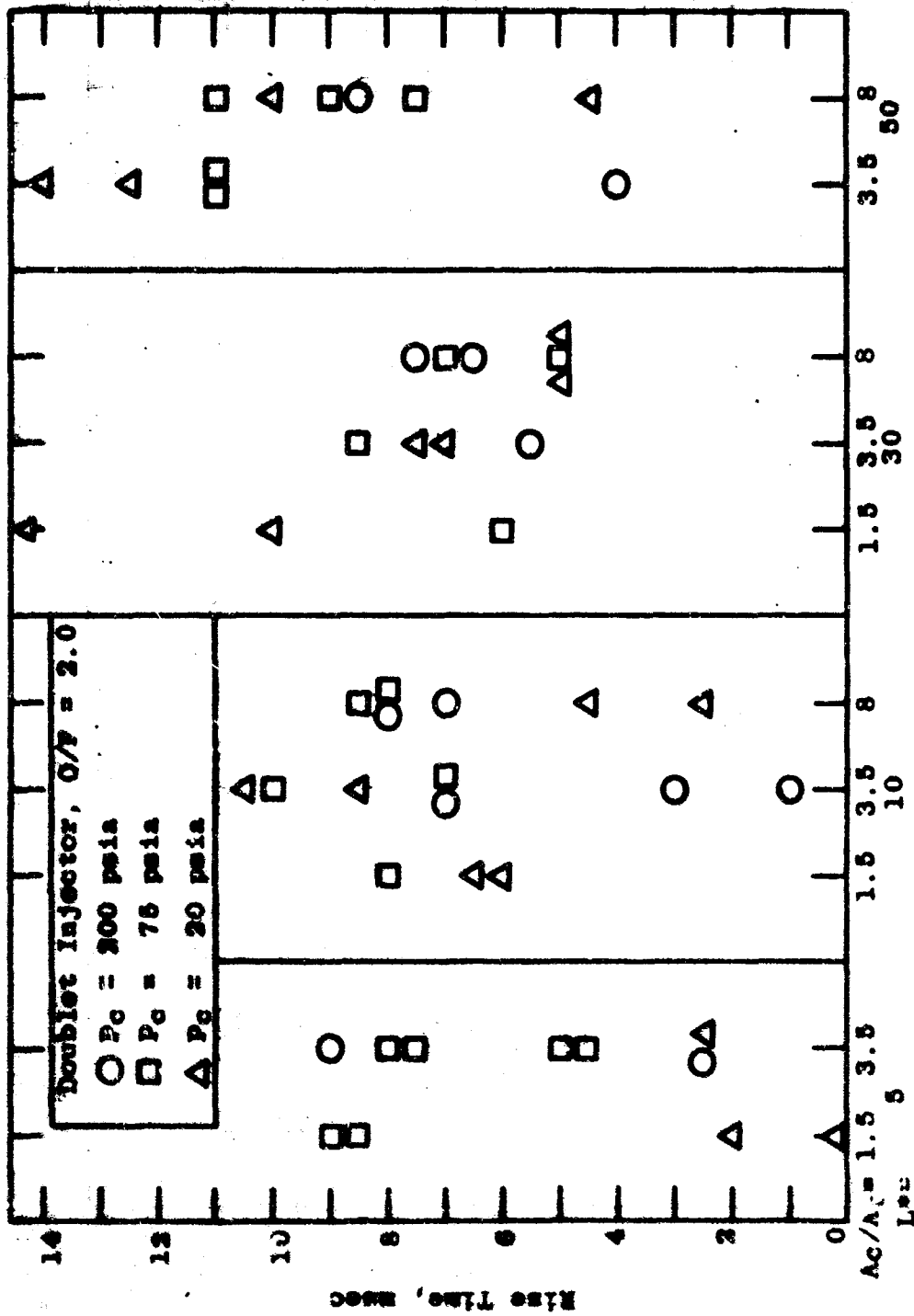


Figure 43. Effect of Chamber Configuration on Rise Time -
Compound A/Hydrazine

CONFIDENTIAL

AFRPL-TR-65-257

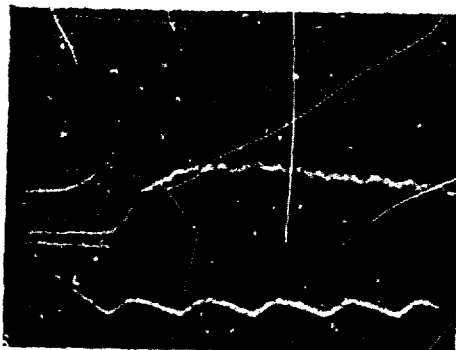
The short ignition delays obtained with Compound A and the hydrazine fuels also resulted in smooth ignition transients in most cases. No pressure spikes of the very short duration, high amplitude type associated with H_2O_4 and hydrazine fuels were encountered. Only Tests 851, 852, 915 and 916 had any indications of pressure peaks during the starting transient and these were less than steady-state chamber pressure.

Three Compound A/ H_2N_2 oscillograph traces are reproduced in Figure 44. Tests 886, 893, and 889 were made at nominal chamber pressures of 200, 75, and 20 psia, respectively, with a contraction ratio of 9.0 and an L^* of 30 in. These traces are typical of the smooth transients experienced with most of the Compound A tests. The upper trace in each record is the low pressure Kistler transducer showing the pressure before ignition. The next trace is the high pressure Kistler which is calibrated for 36, 33, and 16.5 psi/cm in the three records. The third trace is the photomultiplier which deflects downward at ignition and the lowest trace is the valve current.

c. Effect of Mixture Ratio on Ignition

The effect of mixture ratio on ignition time is shown in Figure 45. Ignition times are compared for Compound A/ H_2N_2 (Table XVIII) and Compound A/NEF-5 (Table XXI) at mixture ratios of 1.5, 2.0 and 2.5 with thrust chambers having design chamber pressures of 20, 75 and 200 psia and L^* s of 5 in., 30 in. and 50 in. As indicated in the figure, average ignition times increased about 1 msec as the mixture ratio was increased to 2.5 from the nominal 2.0 value and decreased about 1.5 msec as the mixture ratio was decreased to 1.5. These results are mitigated somewhat by the effect of varying propellant flowrates upon entry time into the chamber. As previously discussed in Section VCI, varying hydrazine flowrate to obtain other mixture ratios changed entry time up to about 0.5 msec at 20 mm Hg pressure. Entry time was shorter at the lower mixture ratios and longer at the higher mixture ratios due to the varying flowrates through the fixed manifold and injector volumes. In view of these effects on propellant entry, however, it still appears that ignition times are somewhat shorter with lower mixture ratios. Both H_2N_2 and NEF-5 showed the same trend. As in the tests at the nominal 2.0 mixture ratio, thrust chamber configuration has no significant effect on ignition time.

CONFIDENTIAL



$P_c = 105$ psig

$A_c/A_t = 9.00$

$L^* = 30$

Test 886



$P_c = 50$ psig

$A_c/A_t = 7.90$

$L^* = 30$

Test 893



$P_c = 5$ psig

$A_c/A_t = 7.68$

$L^* = 30$

Test 889

(sweep = 5 msec/cm)

Figure 44. Oscillograph Records of Compound A/ N_2H_4

CONFIDENTIAL

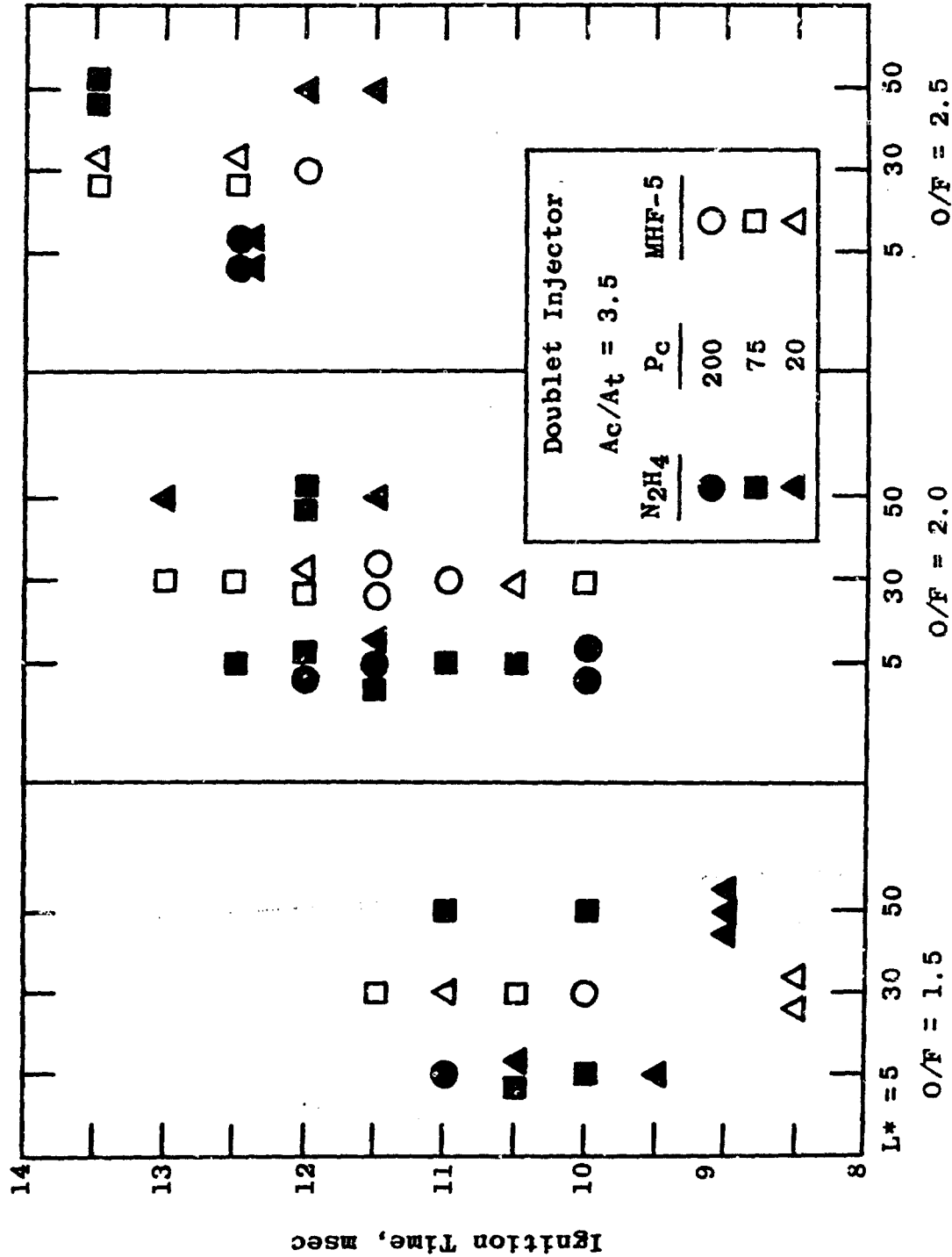


Figure 45. Effect of Mixture Ratio on Ignition Time -
Compound A/N₂H₄ and Compound A/MHF-5

CONFIDENTIAL

AFRPL-TR-65-257

The apparent effect of mixture ratio on ignition time was also observed in the previous tests with N_2O_4 /hydrazine fuels and is discussed further in Reference 1.

d. Effect of Propellant Leads on Ignition

The effect of propellant leads on the ignition of Compound A/ N_2H_4 is shown in Figure 46. The center point of the abscissa represents simultaneous application of power to both propellant valves. Under these conditions the schlieren characterization of the injector discussed in Section VCI indicates that fuel first enters as a liquid at 10-11 msec while Compound A first enters as a vapor at 3 msec, a mixture of vapor and liquid at 7 msec, and finally as a liquid at 10-11 msec. For the tests with simultaneous energization of both propellant valves, it is apparent that ignition occurs at or just after both propellants arrive in the chamber in the liquid phase. Since a vapor phase of N_2H_4 is not detectable in the schlieren films, this time also corresponds to the initial entry of N_2H_4 .

A fuel lead was created by delaying the oxidizer valve with the variable delay rheostat in the control system. Under these conditions, the fuel entry time was not affected as indicated by the horizontal band in Figure 46 corresponding to a fuel entry time of 10-11 msec to the left of center of the figure. If, for example, a fuel lead of 3 msec were desired, energization of the oxidizer valve would be delayed 3 msec and, as indicated in the figure for a 3 msec fuel lead, oxidizer vapor first appears at 6 msec, the mixture at 10 msec and liquid at 13-14 msec. Conversely, an oxidizer lead was obtained by delaying energization of the fuel valve. Note that entry times of the various oxidizer phases under these conditions are represented by horizontal lines or bands to the right of the figure.

Data points for the three design pressure configurations shown in the legend have been superimposed on the propellant entry times. It is evident that with an oxidizer lead, ignition does not occur until entry of the liquid fuel. Also, with a fuel lead, ignition again occurs when liquid fuel first enters regardless of the physical state of the oxidizer. With a 3 msec fuel lead the oxidizer is a mixture of vapor and liquid at ignition and with a 5 msec fuel lead the oxidizer is in the vapor state. The hydrazine is the controlling propellant and ignition occurs upon its injection in the liquid state. If a vapor phase preceeds liquid injection it cannot be detected by the schlieren system and is too small to cause ignition.

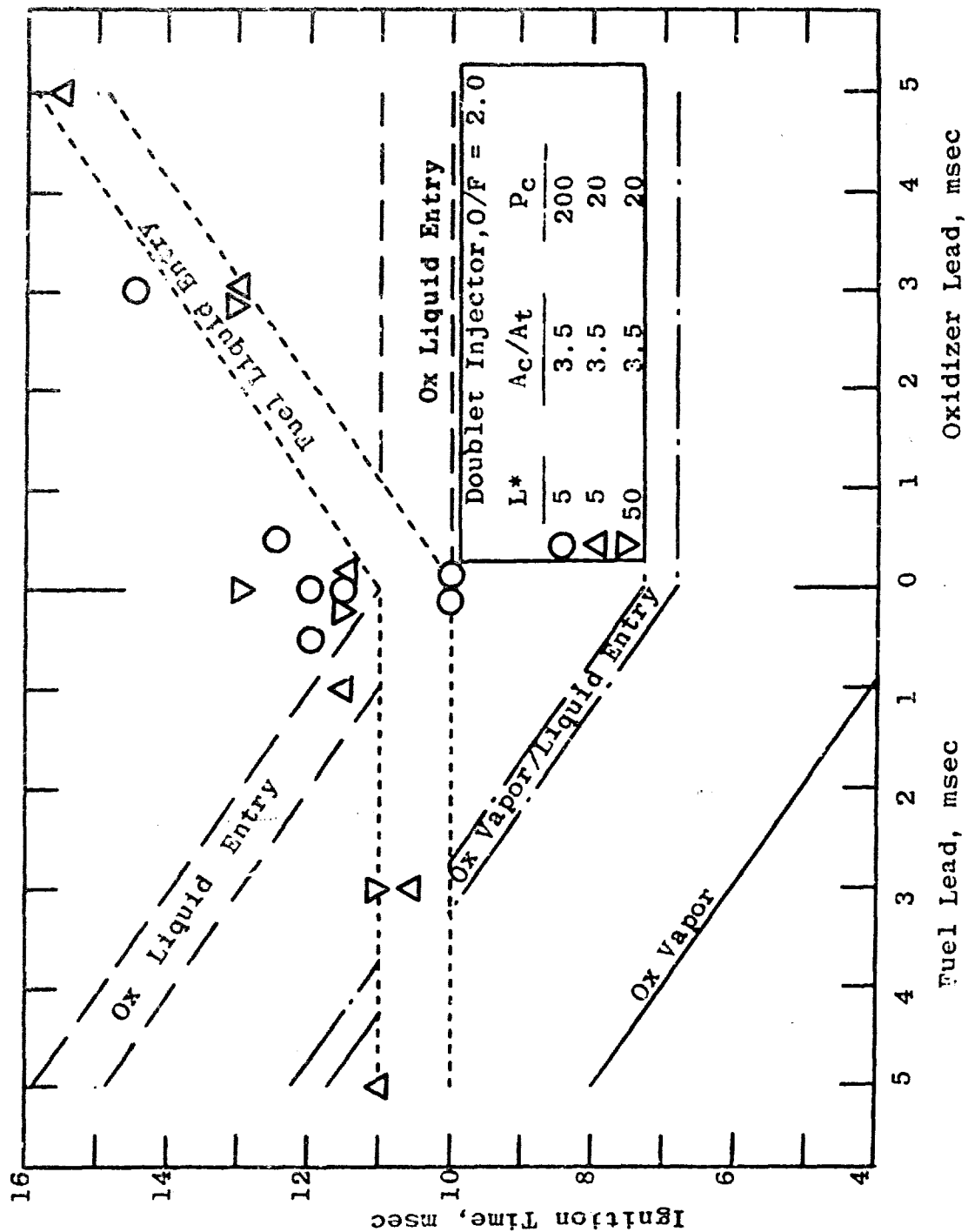


Figure 46. Effect of Propellant Leads On Ignition Time-
Compound A/Hydrazine

CONFIDENTIAL

AFRPL-TR-65-257

e. Triplet Injector Tests

Three chamber configurations were tested with Compound A/hydrazine using the triplet injector shown in Figure 35. The results of these tests are summarized in Table XX. In this injector, the oxidizer passages were similar to those in the doublet injector, but the fuel passages were necessarily longer due to the orifice pattern. As could be expected from the results with the doublet injector, the ignition times were about 4 msec longer with the triplet injector due to the later fuel entry associated with the longer manifold. The pressure at ignition was higher due to the longer oxidizer lead but times to 90% P_c were comparable to those with the doublet injector.

3. Thrust Chamber Tests - Compound A/UDMH, Compound A/MHF-5

Thrust chamber tests were also made with Compound A/UDMH and Compound A/MHF-5 for comparison with the Compound A/ N_2H_4 tests previously discussed. These tests were made with the same thrust chamber configurations using the doublet injector shown in Figure 35. The data for the Compound A/UDMH and Compound A/MHF-5 tests are tabulated in Tables XXI and XXII, respectively. Individual characteristics of these combinations first will be discussed and then comparisons with Compound A/ N_2H_4 will be made.

a. Compound A/UDMH Tests

In tests 855, 856, 857 and 863 with Compound A/UDMH, the initial photomultiplier indication of ignition was an almost vertical deflection at approximately 7 msec which left the oscilloscope face in a small fraction of a millisecond. The ignition times in these four tests correspond to the entry time of the mixture of vapor and liquid fuel as determined by the schlieren tests reported in Table XVI. In the other five tests, one or more weaker photomultiplier signals, with a return to or near zero between pips, preceded the stronger signal. The weak signals correspond to the period of gaseous injection from 3 to 7 msec as indicated by the schlieren films and the stronger signal at 7 msec corresponds to entry of the fuel as a vapor/liquid mixture.

The occurrence of the weak reactions during fuel vapor injection appears to be influenced by thrust chamber

CONFIDENTIAL

AFRPL-TR-65-257

TABLE XX

THRUST CHAMBER TESTS - COMPOUND A/N₂H₄, TRIPLET INJECTOR, O/F = 2.0

Run No.	L* in.	A _c /A _t	P _a mm Hg	P _c psig	90% P _c msec	P _M first msec	P _{ign} mm Hg	P _M vert msec	P _{ign} mm Hg	P _{vert} msec
844	30	3.22	8.5	152	21	13.5	123	14.5	155	13.5
845			10	158	22	15	147	15.5	177	16
846	30	3.50	10	53	26	15.5	60	15.5	60	16
847			10	56	22	16	66	16	66	17.5
841	30	3.54	8	15	24	12.5	19	12.5	19	13.5
842			9.5	16	24	15.5	26	15.5	26	16
843			10	16	24	16.5	32	16.5	32	18

TABLE XXI

THRUST CHAMBER TESTS - COMPOUND A/UDNH, DOUBLET INJECTOR, O/F = 2.0

Run No.	L* in.	A _c /A _t	P _a mm Hg	P _c psig	90% P _c msec	P _M first msec	P _{ign} mm Hg	P _M vert msec	P _{ign} mm Hg	P _{vert} msec
855	30	3.22	10	---	---	9.5	49	9.5	49	10.5
856			10	---	---	7	33	7	33	7.5
857			11	---	---	6	35	6.5	62	7
862	30	3.50	10	26	16.5	4	10	8	35	8
863			10	33	15	7	25	7	25	7.5
858	30	3.54	9	7	17	5	9	9	15	9.5
859			10	4	17	3	10	7	10	7.5
860			10	7	16	4	10	8	10	8.5
861			10	7	16	4	10	8	15	8.5
864	Unconfined		17	---	---	3.5	---	7	---	---

CONFIDENTIAL

CONFIDENTIAL

TABLE XXII
THRUST CHAMBER TESTS - COMPOUND A/MHF-5, DOUBLET INJECTOR

O/F	Run No.	L* in.	A ₀ /A _t	P _a mm Hg	P _c PSIA	90% P ₀ mm Hg	Exhaust mm Hg	P _{ign} mm Hg	Exhaust mm Hg	P _{ign} mm Hg	Exhaust mm Hg	Exhaust mm Hg	Exhaust mm Hg
1.5	945	30	3.33	10	--	--	10	35	10	35	10	10.5	--
2.0	941			10	104	23	--	--	--	--	--	13	--
	942			10	--	--	10	35	11.5	35	11.5	11.5	--
	943			10	--	--	10	35	11	35	11	11.5	--
2.5	944			10	--	--	13	100	13	100	13	13	--
1.5	971	30	3.30	10	26	19	10.5	30	10.5	30	11	10.5	10.5
	972			10	33	13	11.5	30	11.5	30	13	11.5	11.5
2.0	965			10	33	23	10	29	10	29	10	10	10
	966			10	34	21	12	2	13	43	13.5	13.5	13
	967			10	33	19	13	40	13	40	13	13.5	11
	968			10	36	18	12.5	45	13.5	45	13	13.5	13
2.5	969			10	33	27	12.5	55	12.5	55	13	13.5	13.5
	970			10	33	23	13.5	55	13.5	55	14	13.5	13.5
1.5	975	30	3.24	10	7	31	12	10	11	10	11.5	11.5	11
	973			10	7	28	3.5	10	8.5	10	9	9	8.5
	974			10	7	30	8.5	10	8.5	10	9	9	--
2.0	973			10	6	22	9.5	10	11.5	10	12	12	12
	974			10	6	23	10.5	10	13	10	13	13	13.5
	975			10	6	21	10.5	10	10.5	10	11	11	10.5
2.5	976			10	6	21	13.5	20	13.5	20	14	14	13.5
	977			10	6	20	10	20	13.2	20	13	13	13

CONFIDENTIAL

CONFIDENTIAL

AFRPL-TR-35-257

TABLE XII (continued)

Q/T	Run No.	L ₀ in.	A ₀ /A _c	P ₀ mm Hg	P ₀ psig	90% P ₀ msec	FWfirst msec	Pign mm Hg	FWfirst msec	Pign mm Hg	FWfirst msec	Module Port msec	Injector Port msec
2.0	906	Unconfined		10	---	---	13.4	---	24.0	---	---	---	---
	907			10	---	---	10.1	---	10.1	---	---	---	---
	908			9.5	---	---	11.3	---	11.3	---	---	---	---
	909			7.5	---	---	11.3	---	11.3	---	---	---	---
2.0	900	Unconfined		9	---	---	<3	---	<3	---	---	---	---
	901			5	---	---	9.1	---	8.7	---	---	---	---
	902			7.5	---	---	8.8	---	8.4	---	---	---	---

corrine from valve "on" signal of lagging propellant

CONFIDENTIAL

CONFIDENTIAL

AFRPL-TR-65-257

configuration. The thrust chambers in which the vapor phase reactions were detected (tests 858 to 861) were designed for low chamber pressure and had relatively large chamber volumes and diameters. The tests with thrust chambers designed for high chamber pressure which had small volumes and diameters (for the same L^* and A_c/A_t) by comparison, however, did not indicate a vapor phase reaction and ignition did not occur until the UDMH was injected as a vapor/liquid mixture.

The schlieren test shown in Table XXI with both propellants injected simultaneously showed oxidizer vapor appearing at 3.0 msec, fuel vapor at 3.1 msec, and ignition occurring at 3.3 msec. In the same test, the photomultiplier tube also indicated ignition at 3.3 msec by slight deflection of the trace. A stronger signal occurred at 7 msec when the liquid fuel entered.

The times from signal to 90% of steady state chamber pressure in the chamber tests were about 2 msec shorter with UDMH than with hydrazine due to the 2 msec shorter ignition times obtained with UDMH. The shorter ignition times in turn were due to the shorter time required for UDMH to enter the chamber compared with N_2H_4 . Rise times from ignition to 90% P_c , however, were comparable for hydrazine and UDMH.

b. Compound A/MHF-5 Tests

The tests made with Compound A/MHF-5 are summarized in Table XXII. The minimum volume, doublet injector was used with three chamber configurations at mixture ratios of 1.5, 2.0 and 2.5. Several tests (986 - 992) were made without the chamber installed in order to obtain ignition characteristics with the schlieren system.

In tests 987, 988, and 989, ignition occurred 10.1 to 11.3 msec after valve signal, corresponding to the liquid entry time of liquid MHF-5 (10-11 msec). The ignition times also corresponded to the entry time of liquid Compound A (10-11 msec) as also determined in previous schlieren films. Since ignition times corresponded to the liquid entry times of both propellants, Tests 989 to 991 were made with long propellant leads (about 1/4 sec) to determine if ignition would occur with either propellant in the vapor phase. In Test 989 with a long fuel lead in order to establish liquid fuel injection before entry of the oxidizer, ignition occurred less than 3 msec after the "on" signal to the Compound A valve. Ignition, therefore, coincided with initial

CONFIDENTIAL

CONFIDENTIAL

AFRPL-TR-65-257

gaseous injection of the Compound A. In Tests 990 and 991 with long oxidizer leads, to establish liquid oxidizer injection, the ignition times, measured from "on" signal to the fuel valve, were 8.1 and 8.8 msec, which correspond very closely to the vapor/liquid mixture times for MHF-5. It appears therefore that if either the Compound A or the MHF-5 is present as a liquid, ignition will occur with the other propellant in the liquid or vapor phase (vapor/liquid mixture for MHF-5) with ignition delays of less than 1 msec.

The other tests in Table XXII with the three chamber configurations have ignition delays within 2 msec of the delays obtained in the unconfined tests for the same mixture ratio. As in the hydrazine tests, chamber configuration does not affect ignition time and the delay in the unconfined tests are comparable to the shortest delays in the chambers. The variation in ignition time with mixture ratio has already been shown in Figure 45.

In Tests 965-980, a third Kistler transducer was installed at the injector end of the chambers which were about 8 in. long in this series of tests. In the 8 tests with the 75 psia design chamber pressure nozzle (965 - 972), there was no indication of ignition from the photomultiplier tube until the strong vertical deflection corresponding to liquid entry of the propellants. In all of these tests, the pressure transducer at the injector end of the chamber showed a sharp rise at the same time as the photomultiplier trace deflected. The two transducers at the nozzle end of the chamber, however, did not start to rise until 1/2 msec later. The transducer outputs were interchanged on the oscilloscope in two tests to be sure the 1/2 msec difference was not a result of a time lag in the dual beams of the oscilloscope. The same time lag was obtained in each case indicating that the delay in pressure rise between the injector end and the nozzle end of the chamber was real. Once ignition occurred, however, there was no detectable phase shift in the oscillations of the transducer at either end of the chamber.

Three of the 8 tests with the 20 psia design chamber pressure nozzle (Tests 973, 974, 977) had an indication of the preignition reactions discussed previously on the photomultiplier trace. These reactions, however, were not detectable in the pressure traces. In these three tests, the injector pressure rise was delayed 1/2 msec after the stronger photomultiplier signal although the reason for the delay is not evident. The remaining tests were similar to the 75 psia chamber pressure tests in which injector pressure rise corresponded to the strong deflection of the photomultiplier trace, and up to

CONFIDENTIAL

CONFIDENTIAL

AFRPL-TR-65-257

1/2 msec delay in the pressure rise at the nozzle end was observed. These data corroborate the photographic evidence previously noted that ignition of Compound A/ N_2H_4 occurs at the injector and takes a finite time to progress to the nozzle end of the chamber.

c. Comparison of Compound A/Hydrazine Fuels Test

The ignition times and the times to 90% of steady-state chamber pressure are compared for Compound A and the three hydrazine-type fuels in Figure 47 and 48. The data are for thrust chamber configurations having an L^* of 30 in. and a contraction ratio of 3.5 for each of the three design chamber pressures. The tests were made at a mixture ratio of 2.0.

As indicated above, inspection of Figure 47 shows that UDMH has the shortest ignition time of the three fuels. Ignition occurs at about 7 msec corresponding to the entry of a liquid/vapor mixture of UDMH. With N_2H_4 and MHF-5, ignition does not occur until after 10 msec at which time both propellants are being injected in the liquid phase. As indicated in the figure, design chamber pressure has no significant effect on the ignition times of the respective combinations. Although not shown in this figure, previous discussions have also shown that the other thrust chamber configurations (L^* , A_c/A_t) have little effect on ignition time.

As shown in Figure 48, 90% of steady-state chamber pressure is also reached faster with UDMH than the other fuels by virtue of the earlier ignition obtained with UDMH. Rise times from ignition to 90% of steady-state chamber pressure, however, are similar for all three fuels. As might be expected, the rise times associated with the low design chamber pressure configurations are slightly longer than with the high design chamber pressure configurations because of the larger chamber volumes involved.

The ignition transients with both UDMH and MHF-5 were smooth and there was no indication of pressure peaks or spikes in any of the tests.

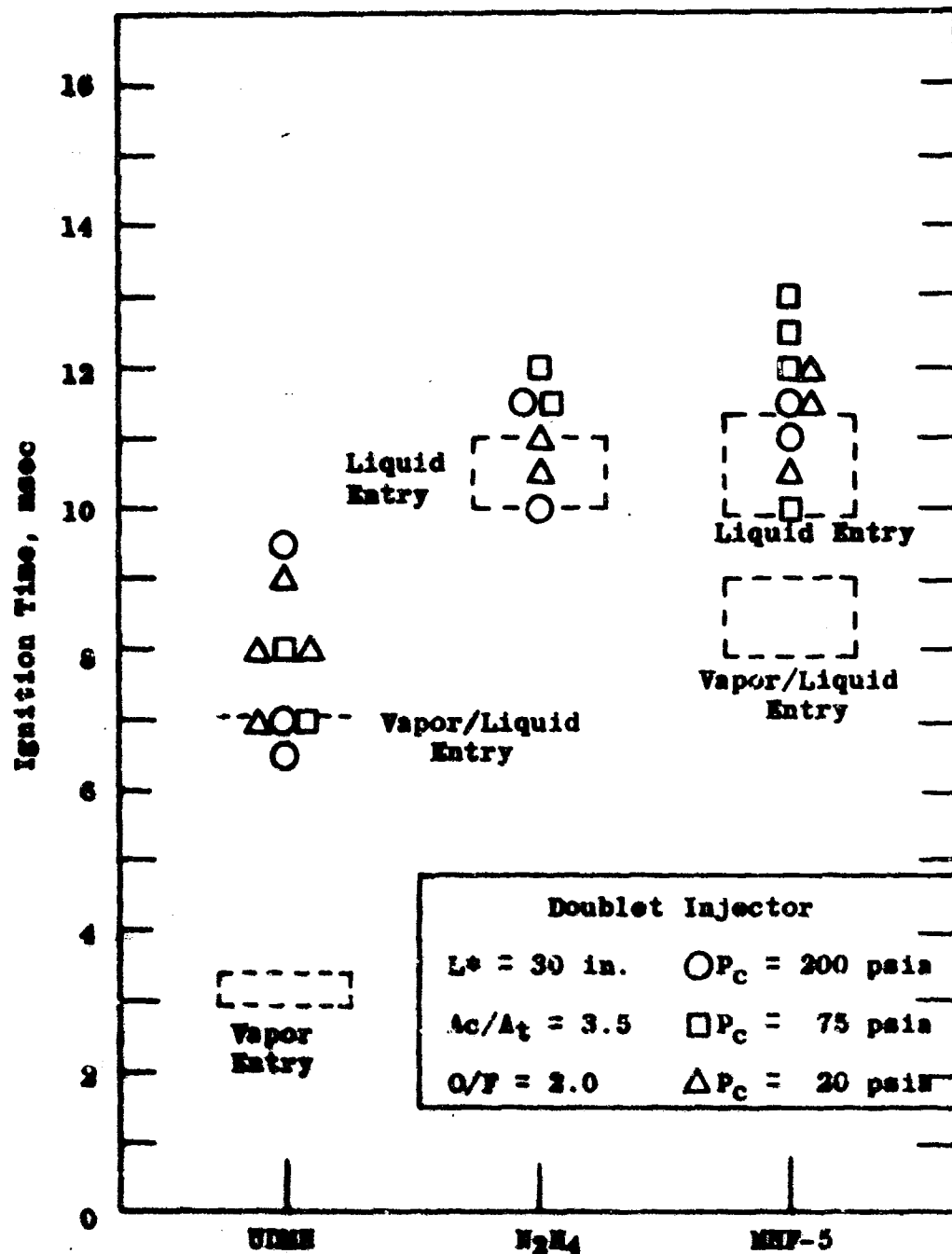


Figure 47. Ignition Times - Compound A/Hydrazine Fuels

CONFIDENTIAL

AFRPL-TR-65-257

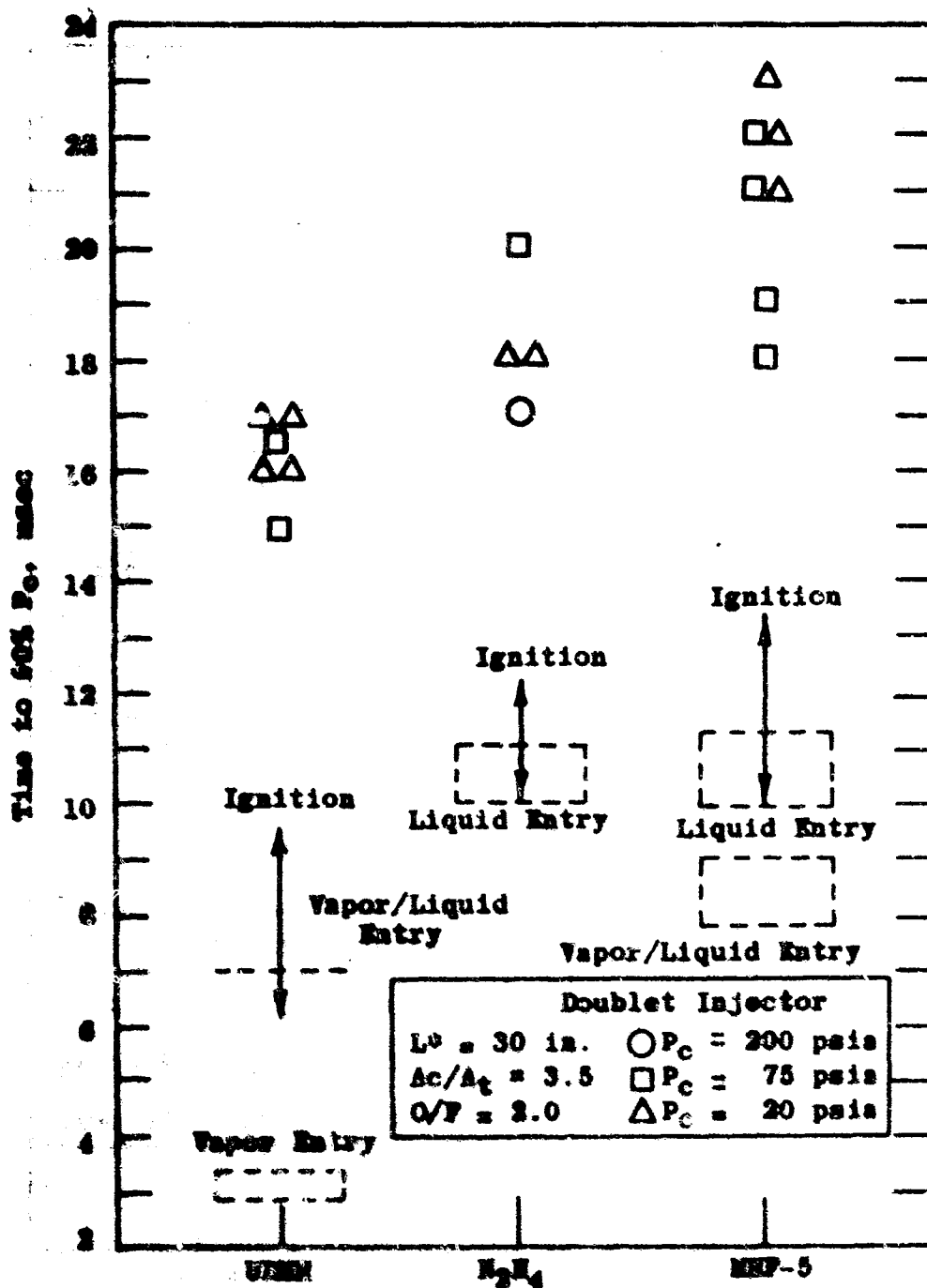


Figure 43. Time to 90% P_c - Compound A/
Hydrazine Fuels

CONFIDENTIAL

D. Experimental Results - Fluorine/Hydrogen Tests

A complete series of ignition tests was also made with gaseous fluorine and hydrogen using the thrust chamber configurations shown in Table XV. The chambers and nozzles were identical to those used for the Compound A tests, but the concentric injector shown in Figure 36 was used with the larger propellant valves previously discussed in order to obtain the desired flowrates with gaseous propellants. The fluorine was injected axially through a single orifice and the hydrogen was injected through a concentric annulus so that it impinged on the fluorine stream at a 20° angle.

Data from the twenty-seven chamber configurations tested are summarized in Table XXIII. The tabulated parameters are defined as they were for the Compound A tests. Ignition time shown in the table is based on the photomultiplier output. No preignition reactions were noted with this propellant combination. The shorter ignition and rise times experienced with this combination permitted a faster oscilloscope sweep which resulted in ignition time resolution of 0.1 msec compared with 0.5 msec for the Compound A/ N_2H_4 tests. The "valve current" column in the table is the time from valve "on" signal to the first minimum in the valve current trace. Six tests were made with the fuel valve delayed 2-3 msec as indicated in the table.

Early in the test program it was found that a 2-3 msec spread in ignition time was being experienced which could not be correlated with thrust chamber configuration. The ignition time, which is defined as the time from valve "on" signal to ignition, varied from 2.8 to 6.0 for tests with simultaneous propellant valve energization. A spread of up to 2.3 msec was noted for successive tests with the same chamber configuration. In order to determine the cause of these small but unexplained variations in the results, the various components of the test system were examined. It was found that the DC power supply used for these tests had a 120 cps ripple when drawing the 12 amps required to operate the larger propellant valves. This ripple was visible on the valve current trace. The effect of the ripple was somewhat accentuated by the fact that the tank pressures required to obtain the desired gaseous propellant flowrates were approaching the limiting pressure at which the large, direct-acting solenoid valves would open consistently. The variation in power due to the ripple at the critical opening point could affect actual opening time by several msec. It is evident, therefore, that the apparent variation in ignition times

TABLE XXIII
THRUST CHAMBER TESTS - FLUORINE/HYDROGEN, CONCENTRIC INJECTOR, O/F = 8

Run No.	L* in.	Ac/At	P _a mmHg	P _c psig	90% P _c msec	Ignition msec	P _{ign.} mmHg	Rise Time msec	Valve Current msec
***1061	5	3.22	8.5	99	11.6	3.4	8.5	8.2	4.4
1062			9	92	7.2	3.4	9	3.8	7.6
1063			9	92	8.2	3.0	9	5.2	5.6
1065	10	3.22	10	119	8.4	3.0	10	5.4	6.0
1066			9.5	119	7.6	3.4	9.5	4.2	7.8
1067			9.5	---	---	5.6	9.5	---	3.9
**1068			9	---	---	6.3	124	---	---
1057	10	9.00	9.5	---	---	5.2	9.5	---	2.3
1058			9.5	109	10.6	4.7	9.5	5.9	2.3
1059			10	109	7.6	2.9	10	4.7	6.1
1060			10	109	9.8	4.7	10	5.1	2.5
1086	30	3.22	9.5	132	10.4	3.7	9.5	6.7	7.6
1087			9.5	132	9.7	3.3	9.5	6.4	8.0
1088			10	132	9.4	3.0	10	6.4	6.8
1036	30	9.00	9.5	119	8.7	4.0	9.5	4.7	0.9
1037			10	125	8.8	2.9	10	5.9	5.2
1038			10	125	9.8	4.5	10	5.3	2.1
1009	50	3.22	10	132	9.7	3.6	10	6.1	---
1010			10	139	9.6	3.1	10	6.5	---
**1011			9	132	12.0	6.8	32	5.2	---
1070	50	9.00	9	119	10.9	3.5	9	7.4	6.6
1071			9.5	122	9.8	3.5	9.5	6.3	8.3
1072			9.5	132	11.8	4.7	9.5	7.1	2.6

** Fuel propellant valve delayed 2-3 msec
***Oxidizer valve full open delayed

TABLE XXIII (continued)

Run No.	L* in.	Ac/At	P _a mmHg	P _c psig	90% P _c msec	Ignition msec	P _{ign.} mmHg	Rise Time msec	Valve Current msec
1064	5	1.72	9.5	40	9.3	4.0	9.5	5.3	0.3
1065			9.5	43	8.8	3.1	9.5	5.7	6.5
1066			10	43	10.0	3.0	10	7.0	7.2
1054	5	3.50	9	26	7.9	3.2	9	4.7	7.3
1055			9.5	25	8.0	3.2	9.5	4.8	6.4
1056			9.5	19	7.2	4.6	9.5	2.4	2.4
1067	10	1.72	9.5	50	6.8	2.0	9.5	3.9	6.5
1068			10	50	7.8	3.9	10	3.9	1.2
1069			10	50	8.8	4.6	10	4.2	2.4
999	10	3.50	8.5	43	9.0	4.8	8.5	4.2	2.5
1000			0	43	6.8	3.3	9	3.5	7.7
1001			9	43	5.8	2.9	9	2.9	6.2
**1002			9.5	43	10.0	7.0	73	3.0	---
1051	10	7.90	10	20	7.2	3.6	10	3.4	6.9
1052			9.5	19	9.1	3.0	9.5	6.1	5.5
1053			9.5	19	7.2	4.5	9.5	2.7	1.8
1079	30	1.72	9	56	10.2	4.1	9	6.1	0.8
1083	30	3.50	9.5	50	8.5	4.0	9.5	4.5	8.0
1084			9.5	53	8.2	3.2	9.5	5.0	8.0
1085			10	53	8.2	3.1	10	5.1	7.6
1039	30	7.90	9.5	53	9.7	3.6	9.5	6.1	6.7
1040			10	53	9.0	3.1	10	5.9	7.3
1041			10	53	11.2	4.6	10	6.4	2.2

** Fuel propellant valve delayed 2.3msec

TABLE XXIII (continued)

Run No.	L* in.	Ac/At	P _a mmHg	P _c psig	50% P _c msec	Ignition msec	P _{ign.} mmHg	Rise Time msec	Valve Current msec
1018	50	3.50	9	46	11.2	5.0	8	6.2	---
1020			9.5	51	10.9	5.1	9.5	5.8	---
1021			9.5	53	10.2	4.8	9.5	5.4	---
**1022			10	53	9.7	5.5	10	4.2	---
1073	50	7.90	9.5	56	10.1	4.0	9.5	6.1	0.3
1074			9.5	54	10.8	4.8	9.5	6.0	2.8
***1075			9.5	54	12.7	3.6	9.5	9.1	4.0
1033	5	1.41	9.5	6	6.3	4.9	9.5	3.4	2.0
1034			10	6	6.4	2.9	10	3.5	5.8
1035			10	6	7.4	4.4	10	3.0	1.6
1048	5	3.54	9.5	3	8.6	5.4	9.5	3.2	2.2
1049			9.5	3	7.6	4.7	9.5	2.9	1.6
1050			10	3	9.0	6.0	10	3.0	3.4
1030	10	1.41	8	7	7.3	4.4	8	2.9	1.2
1031			8	7	5.6	2.8	8	2.6	6.9
1032			9	7	6.8	3.1	9	3.7	7.0
993	10	3.54	7.5	6	8.0	4.2	7.5	3.8	---
994			7.5	6	6.9	3.2	7.5	3.7	7.6
995			8	6	7.4	4.7	8	3.0	2.5
** 998			8.5	6	9.3	6.0	8.5	3.3	---
1045	10	7.68	9	5	8.8	5.3	9	3.5	2.0
1046			9	5	8.6	5.2	9	3.4	3.1
1047			9.5	5	8.4	5.0	9.5	3.4	2.8

** Fuel propellant valve delayed 2-3 msec

*** Oxidizer valve full open delayed

TABLE XXIII (continued)

Run No.	L* in.	Ac/At	P _a mmHg	P _c psig	90% P _c msec	Ignition msec	Pign. mmHg	Rise Time msec	Valve Current msec
1027	30	1.41	9	12	10.1	4.0	9	6.1	1.0
1028			8	13	10.4	4.0	8	6.4	1.0
1029			8.5	13	10.4	4.4	8.5	6.0	1.8
1080	30	3.54	9.5	9	9.0	3.6	9.5	5.4	6.6
1081			9.5	10	7.4	2.8	9.5	4.6	6.6
1082			10	10	9.0	3.7	10	5.3	0.6
1042	30	7.68	9.5	7	10.2	5.2	9.5	5.0	3.6
1043			9.5	7	7.8	3.2	9.5	4.6	7.6
1044			10	7	8.0	3.0	10	5.0	6.2
1014	50	3.54	10	14	11.9	5.1	10	6.8	---
1015			9.5	14	11.6	4.6	9.5	7.0	---
1016			9.5	14	10.8	4.1	9.5	6.7	---
**1017			8.5	13	12.6	7.2	8.5	5.4	---
1076	50	7.68	9	14	15.4	3.6	9	11.8	6.6
1077			9.5	14	16.8	4.5	9.5	12.3	2.1
1078			9.5	14	14.3	3.2	9.5	11.1	7.4

** Fuel propellant valve delayed 2-3 msec

encountered is due to the ripple rather than the result of any propellant or chamber characteristics. In Figure 49, the ignition time is plotted as a function of the minimum point on the valve current trace. It is apparent that all ignition times can be included in a 1 msec wide band irrespective of chamber configuration and that with a more stable power supply, all chamber configurations would have had equal ignition times within $\pm 1/2$ msec.

Schlieren films also were taken of the injection and ignition of the unconfined gaseous propellants. Both the fluorine and hydrogen gases were difficult to detect in the schlieren pictures at ambient pressures below 10 mm Hg. Because of the low density of the gases it is possible that some vapors may have entered for a short period before the flowrate was sufficient to detect propellant entry at the low ambient pressure. The propellant entry times in the four F_2 tests, three H_2 tests, and three F_2/H_2 schlieren ignition tests are included in Figure 49 and are all within $1/4$ msec of the center of the 1 msec spread. All three ignition times of these unconfined tests are within the 1 msec band also. In the unconfined tests with both propellants being injected, the leading propellant obscured entry of the second propellant because of the concentric design. However, ignition delays from the leading propellant were only 0.70 msec at 100 mm Hg ambient pressure, 0.29 at 50 mm, and 0.24 at 7 mm. The apparently longer delay at 100 mm may have been due to more accurate detection of the first gas at the higher pressure rather than a truly longer delay. Ignition was clearly visible near the injector in the films at 50 and 100 mm Hg. At 7 mm Hg, however, the origin of ignition could not be determined and it may have occurred out of the field of view of the schlieren system which is limited to about 2 inches from the impingement point.

Several thrust chamber tests were made with the third Kistler transducer at the injector end of the chamber. As in the Compound A tests, the initial rise in chamber pressure at the injector end coincided with the initial visible light. No delay in chamber pressure rise at the nozzle end was experienced with the shorter (1 - 4 in.) chambers. However, delays in pressure rise at the nozzle end with longer chambers ranged from 0.4 to 0.6 msec for chambers about 12 in. long to a maximum of 0.8 msec for the 22 in. long chamber.

The rise times from ignition to 90% P_c were less than 7.5 msec except for one configuration (Tests 1076-1078) which

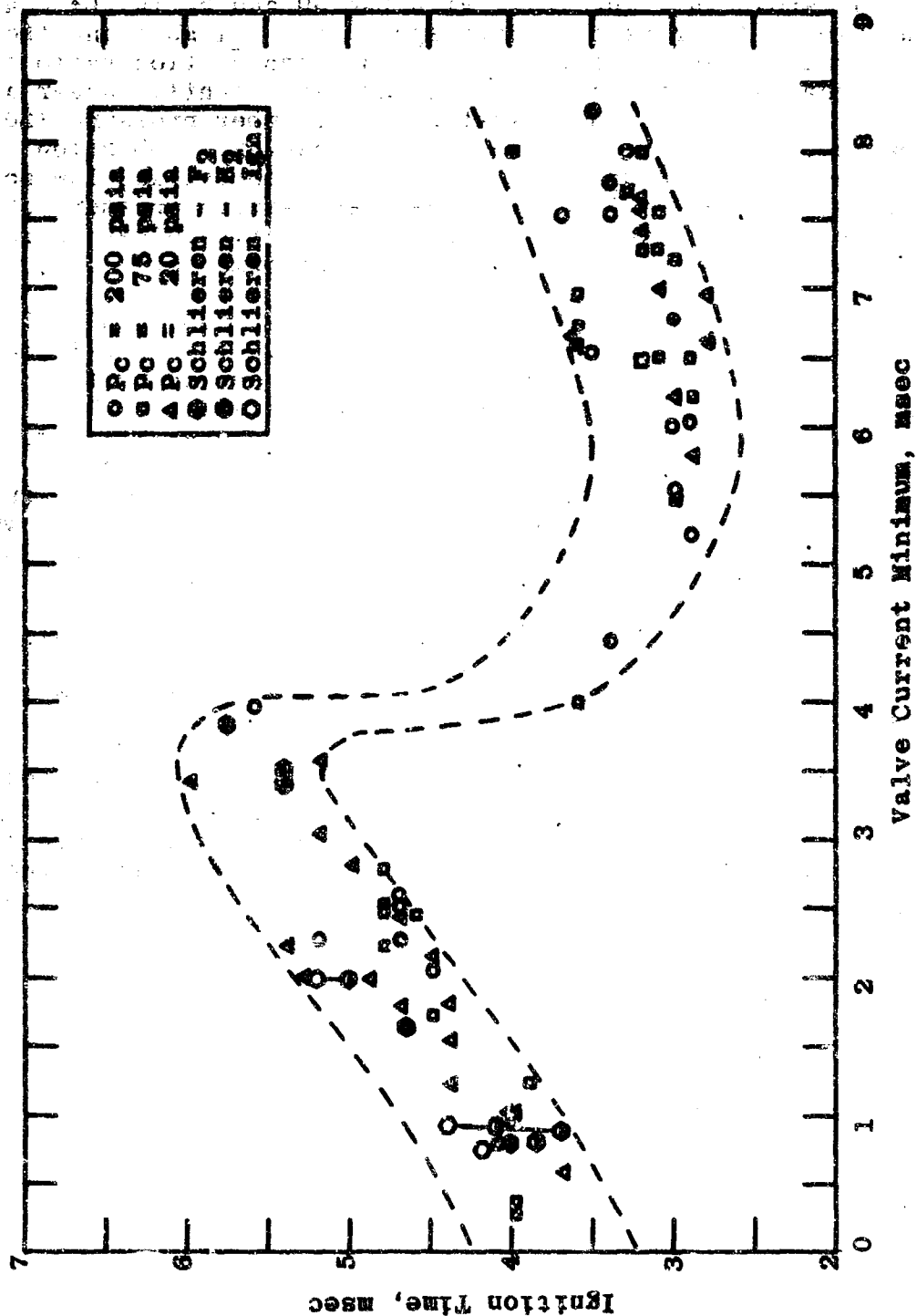


Figure 49. Effect of Valve Current on Ignition Time - F_2/H_2 Chamber Tests

does not seem to fit the other data. Rise times for these three tests were unusually long for no apparent reason. Except for these tests, rise times were proportional to chamber volume or L^* as shown in Figure 50. With the 30 and 50 in. L^* configurations, the rise time data spread was ± 1 msec and there was no significant effect due to either contraction ratio or design chamber pressure. Data spread was slightly larger at the smaller L^* 's and the lowest design chamber pressure (20 psia) appeared to have shorter rise times. However, combustion efficiency with the smaller L^* , 20 psia chambers was low and the time required to reach the low steady-state pressure obtained in these tests is undoubtedly less than that required to reach higher pressures consistent with good performance.

Six tests (Nos. 1008, 1011, 1002, 1022, 998, and 1017) are included in Table XXIII in which the fuel valve was delayed for 2-3 msec. Ignition times were delayed corresponding to the delay in fuel entry. Rise times were comparable to the rise times in the tests with simultaneous valve energization for the 10 in. L^* chambers and 1-2 msec shorter for the 50 in. L^* chambers. Some pressure rise due to the fluorine could be detected in the higher design pressure, shorter L^* chamber configurations when the fuel valve was delayed. In all the other tests ignition preceded any detectable rise in chamber pressure.

There was no indication of any pressure spikes during the rise time with the F_2/H_2 combination in any of these tests. Ignition delays were short as indicated and the pressure transients were smooth.

The oscillograph traces from Tests 1086, 1084, and 1081 are shown in Figure 51. The trace positions are the same as for the Compound A tests in Figure 44, but the sweep is increased from 5 to 2 msec/cm. As in the case of the Compound A/hydrazine-propellant tests the short delays and smooth pressure transients should be noted.

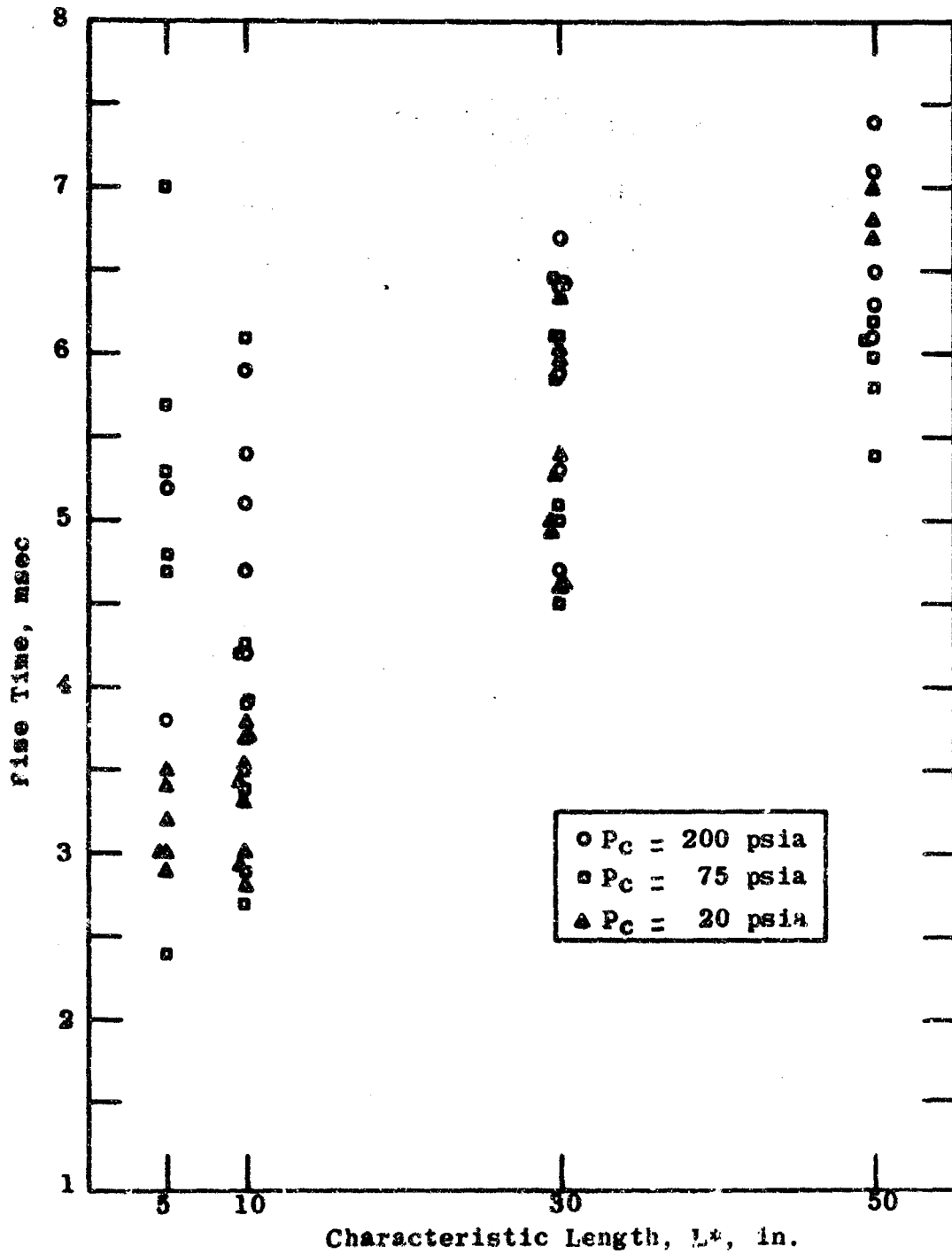


Figure 50. Effect of Chamber L^* on Rise Time - F_2/H_2 Chamber Tests



$P_c = 132$ psig

$A_c/A_t = 3.22$

$L^* = 30$ in.

Test 1086

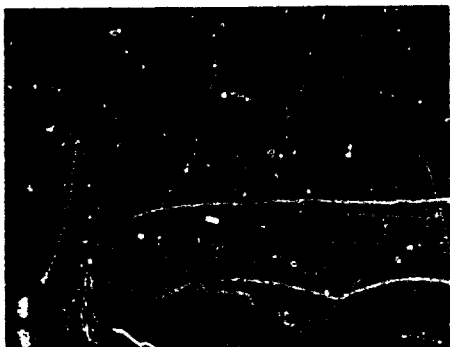


$P_c = 53$ psig

$A_c/A_t = 3.50$

$L^* = 30$ in.

Test 1084



$P_c = 10$ psig

$A_c/A_t = 3.54$

$L^* = 30$ in.

Test 1081

(sweep = 2 msec/cm)

Figure 51. Oscillograph Records of F_2/H_2 Tests

CONFIDENTIAL

AFRPL-TR-65-257

VI

CONCLUSIONS

(U) Significant progress has been made in obtaining a fundamental understanding of hypergolic ignition under vacuum conditions. Although further refinement incorporating additional effects such as propellant "flashing" in injector manifolds is desired to optimize the model, a working mathematical model which predicts the ignition delay of N_2O_4 /hydrazine-type propellants with reasonable accuracy has been developed. Further, the ignition model forms the basis for, and can be extended to, a mathematical model which considers the pressure spiking phenomenon.

(U) Based on the results of the experimental and analytical investigations performed under Part II of Contract AF04(611)-9946 the following conclusions are drawn with regard to the various tasks and phases of the program.

A. Task I - Measurement of Reaction Rate

(U) 1. At sub-ignition pressures, a pre-ignition reaction product (adduct) is formed by each of the NO_2 /hydrazine fuel combinations tested. Chemical analyses of the clear, yellow, viscous liquid adduct formed in appreciable quantities by MMH and NO_2 vapors indicate the adduct is an associative product of the reactants, has the characteristics of a monopropellant, and contains considerable energy. Its relation to pressure spiking during engine start transients is not as yet determined.

(U) 2. The initial rate of pressure rise in a thrust chamber is retarded in the case of very volatile propellants such as N_2O_4 and Compound A by substantial propellant "flashing" within the injector volume upon propellant valve opening. A significant time elapses before the mass flowrate into the thrust chamber reaches its full, nominal value.

(U) 3. Although sufficiently accurate chamber pressurization histories for N_2O_4 cannot be calculated at present due to its transient flowrate behavior upon propellant-valve opening, the chemical kinetics part of the hypergolic ignition model can be compared with experiment. Theoretically calculated ignition delay times in an engine, based on estimated vapor-phase composition and temperature, agree reasonably with experimentally determined engine ignition delays.

CONFIDENTIAL

AFRPL-TR-65-257

(U) 4. In agreement with experimental results, the theoretically derived hypergolic ignition model indicates that the optimum vapor-phase composition for shortest ignition delays is the equimolecular mixture which, for UDMH, MMH and 50-50 with N_2O_4 , are markedly more fuel rich than typical operational mixture ratios. Advantage of this fact to obtain shorter ignition delays may be taken through suitable injector designs coupled with propellant leads and lags.

(U) 5. Dominant ignition reactions of N_2O_4 /hydrazine-type fuels at low pressures are thermal, gas phase reactions which are bimolecular and have low activation energies (less than 10 kcal/mole) and low pre-exponential factors.

(U) 6. Propellant vaporization in a thrust chamber prior to ignition is non-adiabatic due to heat addition to the vapor-drop system from the thrust chamber walls.

B. Task II - Evaluation of Additives to Reduce Activation Energy

(U) 1. The low pressure, premixed vapor stream apparatus is well suited to screening of additives. The measured variable ignition pressure limit is a sensitive, reliable measure of ignition delay. Additives may be evaluated relatively easily with good accuracy and less expensively than in engine firings at low ambient pressure.

(U) 2. Of the five organic fuel additives tested in the apparatus, furfuryl alcohol was found to have a significant beneficial effect on the ignition characteristics of N_2O_4 /MMH.

(C) 3. The one principal oxidizer additive tested, Compound R-FC(NF_2)₃, not only worsened ignition characteristics but also reduced reproducibility considerably. Only after thoroughly washing the apparatus were the normal, repeatable results obtained again with the next propellants.

C. Task III - Thrust Chamber Design Parameter Study

1. Compound A/Hydrazine-type Fuels

(C) a. Ignition delays in the thrust chamber tests with the Compound A/hydrazine-type fuels were very short. Ignition delays with UDMH are somewhat shorter than those with N_2H_4 or MMH-5, although rise times (ignition to 90% P_c) are comparable.

CONFIDENTIAL

AFRPL-TR-65-257

(C) b. Because of the short ignition delay, the pressure transients were smooth with no indication of the very short duration, high amplitude, random pressure spikes characteristic of the N_2O_4 /hydrazine-type fuels.

(C) c. Ignition occurs at the injector and proceeds rapidly and smoothly through the chamber.

(C) d. Ignition in a thrust chamber is independent of pressure rise due to propellant vaporization. Ignition delays in the chamber tests with each propellant were comparable with the delays measured in the unconfined schlieren tests. By contrast, previous thrust chamber tests with N_2O_4 /hydrazine-type fuels (Ref. 1) indicated an extreme pressure dependency.

(C) e. Ignition characteristics are not significantly influenced by thrust chamber configuration parameters because of the lack of pressure dependency.

(C) f. Although the influence of thrust chamber geometry on rise time to 90% of the steady-state chamber pressure was small, the configurations with the smaller volumes generally produced slightly shorter rise times.

(C) g. Mixture ratio tests indicated somewhat shorter ignition delays with fuel-rich mixture ratios than with oxidizer-rich mixture ratios.

(C) h. Propellant lead tests with Compound A/ N_2H_4 indicate that ignition occurs rapidly upon entry of hydrazine regardless of the state (vapor, mixture, or liquid) of Compound A.

2. F_2/H_2

(U) a. Ignition delays were very short (within 1 msec) in the thrust chamber and unconfined schlieren tests.

(U) b. As with Compound A/hydrazine-type fuels, ignition does not depend upon pressure rise in the chamber. In most tests ignition occurred before any detectable rise in pressure due to propellant entry.

(U) c. Ignition delay was not influenced by thrust chamber design parameters.

CONFIDENTIAL

AFRPL-TE-65-257

(U) d. Ignition occurred at the injector and pressure transients were smooth with no indication of pressure spikes in any of the tests.

(U) e. Rise time to 90% of steady-state chamber pressure was very rapid. Rise time was somewhat shorter with smaller L^* 's than with larger L^* 's as might be expected.

VII

RECOMMENDATIONS

Several factors pertinent to hypergolic ignition in reaction control systems that were either outside the scope of the present program or require further study beyond that which time permitted in this six-month effort are enumerated below:

1. The pre-ignition reaction product (adduct) appears, at present, to be a likely candidate for the cause of the pressure spikes experienced during engine start transients. It should be determined whether, in fact, the adduct is the cause. Properties of the adducts formed by the hydrazine fuels with N_2O_4 are required, including their rates of formation and decomposition. It should also be determined whether the adducts are necessary intermediates in the reaction mechanisms for ignition or whether they are side products which tend to impede ignition.

If the adducts do prove to be the major cause of pressure spikes, methods should be investigated to (1) avoid its formation if it is not a necessary intermediate, (2) minimize its accumulation on thrust chamber walls, during ignition delay times (and during tail-off too) and/or (3) retard its decomposition rate in order to lengthen the time over which the accumulated energy is released.

2. To be made general, the analysis for chamber pressurization due to propellant vaporization requires inclusion of expressions to account for the initial transient flowrate behavior of very volatile propellants upon propellant valve opening. Also required is a general expression for the heat addition to the vapor-drop system from the thrust chamber walls.

3. Then, the complete mathematical model for hypergolic ignition in reaction control systems should be further verified by comparisons with experimental ignition delays in engines of various chamber configurations, thrust levels, etc.

4. A mathematical model of pressure spiking during start transients should be developed to permit evaluation of chamber geometry and ignition hydraulics from a pressure spiking viewpoint. The hypergolic ignition model developed in the present program is a major part of the pressure spiking model and is readily extended to include the pressure transient.

AFRPL-TR-65-257

5. Since a reliable, low cost method is now available, extensive screening of chemical additives to shorten ignition delays is recommended. The more costly testing in engines at low ambient pressures can then be limited to only the most promising additives.

6. As indicated above, thrust chamber tests to verify the results of the experiments and to determine the significance of the results under actual operating conditions are required. It is recommended, therefore, that a concurrent fundamental investigation and thrust chamber verification program be undertaken to accomplish the above goals.

~~CONFIDENTIAL~~
Security Classification

DOCUMENT CONTROL DATA - R&D		
(Security classification of title, body of abstract and indexing annotation must be entered when the overall report is classified)		
1. ORIGINATING ACTIVITY (Corporate author) THIOKOL CHEMICAL CORPORATION Reaction Motors Division Denville, New Jersey		2a. REPORT SECURITY CLASSIFICATION CONFIDENTIAL
		2b. GROUP 3
3. REPORT TITLE (U) HYPERGOLIC IGNITION AT REDUCED PRESSURES		
4. DESCRIPTIVE NOTES (Type of report and inclusive dates) Final Report - April 1965 to October 1965		
5. AUTHOR(S) (Last name, first name, initial) Corbett, Albert D.; Dawson, Bruce E.; Seamans, Thomas, F.; Vanpee, Marcel M.		
6. REPORT DATE February 1966	7a. TOTAL NO. OF PAGES 178	7b. NO. OF REFS 12
8a. CONTRACT OR GRANT NO. AF04(611)-9946	8a. ORIGINATOR'S REPORT NUMBER(S) AFRPL-TR-65-257	
A. PROJECT NO. 3058		
C. Task 3058560	8b. OTHER REPORT NO(S) (Any other numbers that may be assigned this report) RMD Project 5801-F Part II	
10. AVAILABILITY/LIMITATION NOTICES DDC release to CFSTI not authorized; qualified requestors may obtain copies of this report from the Defense Documentation Center (DDC), (formerly ASTIA) Cameron Station, Bldg. 5, 5010 Duke Street,*		
11. SUPPLEMENTARY NOTES Report on Hypergolic Ignition of Rocket Propellants	12. SPONSORING MILITARY ACTIVITY Air Force Rocket Propulsion Laboratory Research and Technology Div. Air Force Systems Command	
13. ABSTRACT (U) By theoretical and experimental means, a mathematical model of hypergolic ignition in reaction control systems has been developed based on physical kinetics of droplet evaporation and chemical kinetics of ignition reactions. Reasonable agreement between theoretical and experimental ignition delays are obtained. The dominant ignition reactions of N ₂ O ₄ with the hydrazine fuels at reduced pressures are found to be thermal, gas phase reactions which are bimolecular and have low activation energies and pre-exponential factors. A pre-ignition reaction product was found which is a clear, yellow, viscous liquid with a very low vapor pressure. The "adduct" has the characteristics of a monopropellant and contains considerable energy. Its relation to pressure spiking during engine start transients is as yet undetermined. Of six additives tested, only furfuryl alcohol had a significant beneficial effect on the ignition characteristics of N ₂ O ₄ /MMH. The influence of thrust chamber design parameters on the ignition delay and pressure transients of Compound A with N ₂ H ₄ , UDMH and MHF-5 and also gaseous F ₂ /H ₂ was investigated. ----- *Item 10 (con't) Alexandria, Virginia; Dissemination outside the Department of Defense (or to recipients other than Government Defense Contractors) is prohibited.		

DD FORM 1 JAN 64 1473

~~CONFIDENTIAL~~
Security Classification

CONFIDENTIAL

Security Classification

14. KEY WORDS	LINK A		LINK B		LINK C	
	ROLE	WT	ROLE	WT	ROLE	WT
(1) Fuel and Rocket Propellants						
(2) Space Propulsion						
(3) Injectors						
(4) Combustion Chambers						
(5) Ignition-Hypergolic, Space						

INSTRUCTIONS

1. **ORIGINATING ACTIVITY:** Enter the name and address of the contractor, subcontractor, grantee, Department of Defense activity or other organization (corporate author) issuing the report.

2a. **REPORT SECURITY CLASSIFICATION:** Enter the overall security classification of the report. Indicate whether "Restricted Data" is included. Marking is to be in accordance with appropriate security regulations.

2b. **GROUP:** Automatic downgrading is specified in DoD Directive 5200.10 and Armed Forces Industrial Manual. Enter the group number. Also, when applicable, show that optional markings have been used for Group 3 and Group 4 as authorized.

3. **REPORT TITLE:** Enter the complete report title in all capital letters. Titles in all cases should be unclassified. If a meaningful title cannot be selected without classification, show title classification in all capitals in parenthesis immediately following the title.

4. **DESCRIPTIVE NOTES:** If appropriate, enter the type of report, e.g., interim, progress, summary, annual, or final. Give the inclusive dates when a specific reporting period is covered.

5. **AUTHOR(S):** Enter the name(s) of author(s) as shown on or in the report. Enter last name, first name, middle initial. If military, show rank and branch of service. The name of the principal author is an absolute minimum requirement.

6. **REPORT DATE:** Enter the date of the report as day, month, year; or month, year. If more than one date appears on the report, use date of publication.

7a. **TOTAL NUMBER OF PAGES:** The total page count should follow normal pagination procedures, i.e., enter the number of pages containing information.

7b. **NUMBER OF REFERENCES:** Enter the total number of references cited in the report.

8a. **CONTRACT OR GRANT NUMBER:** If appropriate, enter the applicable number of the contract or grant under which the report was written.

8b, 8c, & 8d. **PROJECT NUMBER:** Enter the appropriate military department identification, such as project number, subproject number, system numbers, task number, etc.

9a. **ORIGINATOR'S REPORT NUMBER(S):** Enter the official report number by which the document will be identified and controlled by the originating activity. This number must be unique to this report.

9b. **OTHER REPORT NUMBER(S):** If the report has been assigned any other report numbers (either by the originator or by the sponsor), also enter this number(s).

10. **AVAILABILITY/LIMITATION NOTICES:** Enter any limitations on further dissemination of the report, other than those

imposed by security classification, using standard statements such as:

- (1) "Qualified requesters may obtain copies of this report from DDC."
- (2) "Foreign announcement and dissemination of this report by DDC is not authorized."
- (3) "U. S. Government agencies may obtain copies of this report directly from DDC. Other qualified DDC users shall request through _____."
- (4) "U. S. military agencies may obtain copies of this report directly from DDC. Other qualified users shall request through _____."
- (5) "All distribution of this report is controlled. Qualified DDC users shall request through _____."

If the report has been furnished to the Office of Technical Services, Department of Commerce, for sale to the public, indicate this fact and enter the price, if known.

11. **SUPPLEMENTARY NOTES:** Use for additional explanatory notes.

12. **SPONSORING MILITARY ACTIVITY:** Enter the name of the departmental project office or laboratory sponsoring (paying for) the research and development. Include address.

13. **ABSTRACT:** Enter an abstract giving a brief and factual summary of the document indicative of the report, even though it may also appear elsewhere in the body of the technical report. If additional space is required, a continuation sheet shall be attached.

It is highly desirable that the abstract of classified reports be unclassified. Each paragraph of the abstract shall end with an indication of the military security classification of the information in the paragraph, represented as (TS), (S), (C), or (U).

There is no limitation on the length of the abstract. However, the suggested length is from 150 to 225 words.

14. **KEY WORDS:** Key words are technically meaningful terms or short phrases that characterize a report and may be used as index entries for cataloging the report. Key words must be selected so that no security classification is required. Identifiers, such as equipment model designation, trade name, military project code name, geographic location, may be used as key words but will be followed by an indication of technical context. The assignment of links, rules, and weights is optional.

CONFIDENTIAL

Security Classification